RISK-BASED DESIGN OF A PROCESS COMPONENT

SIKDER MAINUL HASAN

RISK-BASED DESIGN OF A PROCESS COMPONENT

by

© SIKDER MAINUL HASAN

A Thesis submitted to the

School of Graduate Studies

in partial fulfillment of the requirements for the degree of

Doctor of Philosophy

Faculty of Engineering & Applied Science

Memorial University of Newfoundland

September, 2012

St. John's Newfoundland Canada

بِسْمِ اللَّهِ الرَّحْمَٰنِ الرَّحِيمِ

In the name of Allah, the most Gracious, the most Compassionate

Abstract

The production and transportation of hydrocarbon from a facilities involves complex process system. The components in such a process system are exposed to extreme operating and environmental conditions. To ensure safe and continuous operation, it is important to identify potential risk sources, and incorporate the risk factors in the designing of the process components.

The present work develops a novel integrated methodology for the risk-based design of process components. It may be noted that there are lots of process component but specific consideration is given for oil and gas pipeline. Hence, the scope of the work is comprised of time dependent failure scenarios. The failure mechanisms considered here are: internal corrosion, external corrosion, stress corrosion cracking, fatigue failure due to corrosion fatigue and start up/shut down loading for a specific process component. The time independent failure mechanisms i.e. third party damage, earth movement, and material defects are not considered in this study.

This research considered uncertainties associated with operational characteristics of the process component and included them in the risk-based design framework. The study reviewed different design codes/standards for a transportation system. In the internal corrosion analysis the defect depth was calculated from corrosion rate equations and failure probability was assessed considering the first order reliability method. A

similar procedure was considered for external corrosion analysis. In the internal corrosion analysis, the study compared the performance of different codes and standards and listed comparative advantages of one over other. The external corrosion analysis identified the causes of the variability of probability of failure for recommended codes/standards. It is identified that the difference in parameter contribution in the bulging factor are responsible for variability in the bursting formulas. In the stress corrosion cracking (SCC) failure analysis, the stress based failure assessment diagram (FAD) was considered. The authors also proposed a strain based approach for the same analysis. The stress/strain based approach closely calculates the failure probability of the SCC defects. The corrosion fatigue analysis mainly considered the effect of variable amplitude loading (pressure fluctuation) on small weld defects. The Miners rule and Paris law are simultaneously considered for failure assessment. The Rainflow counting method is considered in the analysis for stress block and cycles counting. The failure probability is calculated from the the damage caused by the pressure fluctuation.

The failure probability obtained for an individual event is integrated using fault tree analysis to obtain the overall risk of the system.

The unified risk is minimized to design individual components to achieve the target safety level of the system.

Acknowledgements

I am grateful to Allah S.W.T, the most gracious, the most merciful, for giving me the strength to complete this thesis. It is with His will, that I have completed this thesis after years of struggle and hard work.

I would like to thank my supervisors Dr. Faisal Khan and Dr. Shawn Kenny for relentless support for my PhD work. All the advice and assistance they gave, academically and non-academically, are really supportive and will never be forgotten. I must remember Dr. Khan for his amazing ability to apprehend problem and provide the necessary guidance throughout the research work. My sincere thanks goes to Dr. Khan for keeping me on the right track in this long voyage. I must remember Dr. Kenny for his amazing technical expertise in pipeline engineering. The structural engineering guidelines provided by Dr. Kenny strengthen the reliability work on the pipeline. I am grateful because I have learnt from them to conduct research without violating the basic laws or principles of science.

I appreciate and acknowledge the financial support of PRAC and NSERC Strategic project. I also thank the School of Graduate Studies and Faculty of Engineering and Applied Science, Memorial University of Newfoundland, for their financial and relevant support.

I would also like to thank to my colleagues in the group at the Bruneau Center for Research and Innovation at Memorial University of Newfoundland. I must mention the names of Dr. Refaul Ferdous and Dr. Premkumar Thodi for their help and assistance.

My heartfelt thanks are given to my parents and my brothers, Dr. Rakib Uddin and Dr. Mahiuddin Ahmed, for educating and encouraging me to pursue higher studies. Last, but not least, I would like to convey my thanks and appreciation to my wife, Asma, for her patience, sacrifices and support during my study.

Table of Contents

List of Tables

Table No. **Page**

List of Figures

Figure No. **Page**

List of Abbreviations

API	American Petroleum Institute
ASD	Allowable Stress Design
ASME	American Society of Mechanical Engineers
ASTM	American Society of Testing Material
BOEMRE	Bureau of Ocean Energy Management, Regulation and Enforcement
BS	British Standard
CEPA	Canadian Energy Pipeline Association
CF	Corrosion Fatigue
CoV	Coefficient of Variation
Cp	Cathodic Protection
CSA	Canadian Standards Association
DFF	Design Fatigue Factor
DNV	Det Norske Veritas
EPFM	Elastic-Plastic Fracture Mechanics
FAD	Failure Assessment Diagram
FEM	Finite Element Method
FORM	First Order Reliability Method
FOSM	First Order Second Moment
FMA	Failure Mode Approach
FTA	Fault tree analysis
HIC	Hydrogen Induced Cracking

HSLA	High Strength Low Alloy
IGSCC	Intergranular Stress Corrosion Cracking
LEFM	Linear Elastic Fracture Mechanics
LRFD	Load and Resistance Factored Design
LSD	Limit State Design
MC	Monte Carlo
MOP	Maximum Operating Pressure
MPP	Most Probable Point
NEB	National Energy Board
PRAISE	Piping Reliability Analysis Including Seismic Events
SCADA	Supervisory Control and Data Acquisition
SCC	Stress Corrosion Cracking
SLS	Serviceability Limit State
SMYS	Specified Minimum Yield Strength
SMTS	Specified Minimum Tensile Strength
SORM	Second Order Reliability Method
SSRT	Slow Strain Rate Technique
TGSCC	Transgranular Stress Corrosion Cracking
ULS	Ultimate Limit State
VIV	Vortex Induces Vibration
WSD	Working Stress Design

Chapter 1

Introduction and Overview

1.1 General

Pipeline systems are integral parts of the offshore or onshore oil and gas industry for gathering, distribution and transportion of hydrocarbon products. At present there are 3,500,000 km of such pipelines around the world [1]. In general, pipelines can be classified into three categories depending on the purpose:

Gathering pipelines: These are small interconnected pipelines with complex networks to bring crude oil or natural gas from several nearby wells to a treatment plant or processing facility. The pipelines in this group are usually short with small diameters.

Transportation pipelines: These are large diameter, long distance pipelines that serve as the main conduit for oil and gas transportation between cities, countries and even continents. The transportation networks of pipelines include several compressor stations in gas lines or pump stations for crude and multi-products pipelines. *Transportation pipelines* as shown in Figure 1.1 are considered the main topic of interest for this study.

Distribution pipelines: These are composed of several interconnected pipelines with small diameters to take the products to the end user.

The pipeline network is comprised of several components to move products from one location to another. The main elements of a pipeline system are [2]:

Figure 1.1: Transportation Pipeline [3]

Inlet station: This is the beginning of the system, where the product is injected into the main line. Storage facilities, pumps or compressors are usually found at these locations.

Compressor/pump stations: Pumps or Compressors (based on oil or gas) are located along the line to move the product through the *transportation pipelines*. The locations of these stations are defined by the topography of the terrain, the type of product being transported, and the operational conditions of the network.

Partial delivery station: These facilities allow the pipeline operator to deliver part of the product being transported.

Block valve station: These are the first line of control for pipelines. With these valves the operator can isolate any segment of the line for maintenance work or isolate a rupture or leak. Block valve stations are usually located every 32 to 48 kilometers, depending on the type of the pipeline.

Regulator station: These are safety valve stations, where the operator can release some of the pressure from the line. Regulators are usually located at the downhill side of a peak.

Final delivery station: These are outlets from which the product is distributed to the consumer.

Oil and gas are highly volatile, flammable and explosive. The safe production and transportation of oil and gas is of extreme importance. Many countries have enacted legislative requirements to ensure safe and reliable transportation of hydrocarbon by pipeline [4]. In the US, onshore and offshore pipelines are regulated by the Pipeline and Hazardous Materials Safety Administration (PHMSA). Certain offshore pipelines are regulated by the Bureau of Ocean Energy Management, Regulation and Enforcement (BOEMRE), formerly Minerals Management Service (MMS). In Canada, pipelines are regulated by either provincial regulators or, if they cross provincial boundaries or the Canada/US border, by the National Energy Board (NEB).

1.2 Design and Operation

Design: Ttransportation pipelines are designed according to the guidelines of ASME B31.8 for gas pipelines and ASME B31.4 for oil pipelines. The design and operation of pipelines is usually regulated through national and local regulations.

Pipelines may experience a variety of loads, including the loads during laying them offshore. However, the major load is assumed to come from internal operating

pressure. Consequently hoop stress as given in Figure 1.2a is the major design factor which most design codes consider in the following equation:

$$\text{Hoop stress} = \sigma_h = \frac{PD}{2t} = \phi\sigma_y \qquad (1.1)$$

where

P = pipeline operating pressure load,

D = outside pipe diameter,

t = pipe wall thickness,

ϕ = design factor

σ_y = yield stress

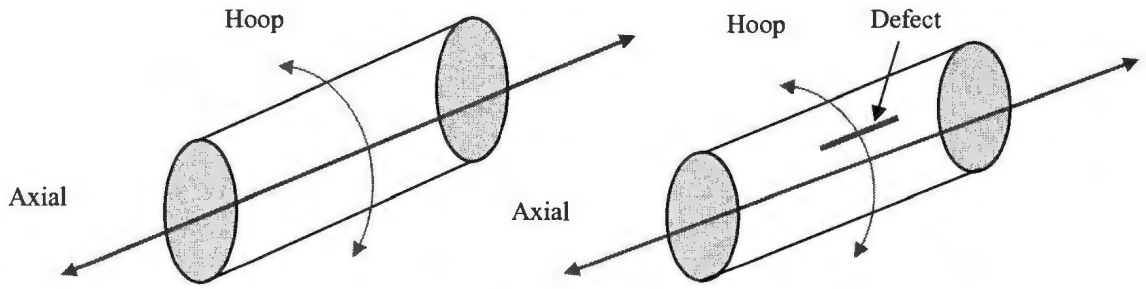

Figure 1.2: Hoop stress of a) Intact Pipe b) Defected Pipe

Equation (1.1) is a burst expression for an intact pipe. If a defected pipe as shown in Figure 1.2b is considered, the burst equation needs to be modified with a reduction factor. The reduction factor (*RF*) in equation (1.2) is suggested by different codes and standards following different approaches.

$$\text{Hoop stress} = \sigma_h = \frac{PD}{2t} * RF = \phi\sigma_y * RF \qquad (1.2)$$

One important point that may be noted for the safe operational limit of the pipeline is that the maximum hoop stress should never exceed 72%-80% of specified minimum yield strength (SMYS) or 10% overpressures of 79% SMYS.

Operation: The field instruments (flow, pressure, temperature gauges) are installed along the pipeline at specific locations, such as injection, delivery, pump (liquid), compressor (gas), or block valve stations. The instruments measure the relevant data of flowing oil or gas. The information measured by the field instruments is then gathered in a local Remote Terminal Unit (RTU) that transfers the field data to a central location using real time communication systems, such as satellite channels and microwave links.

Pipelines are controlled and operated from a remotely located *Main Control Room*. The field data is consolidated in a central database through SCADA (supervisory control and data acquisition). The SCADA as given in Figure 1.3 at the Main Control Room receives the field data, processes and present it to the pipeline operator showing the operational conditions of the pipeline. The operator can monitor the hydraulic conditions and can send operational commands (open/close valves, turn on/off compressors or pumps, change set points) through the SCADA system to the pipeline.

Some pipelines use *Advanced Pipeline Applications* software coupled with SCADA to secure and optimize the operation of the pipeline. These help to perform leak detection, leak location, batch tracking (liquid lines), pig tracking, composition tracking, predictive modeling and look ahead modeling.

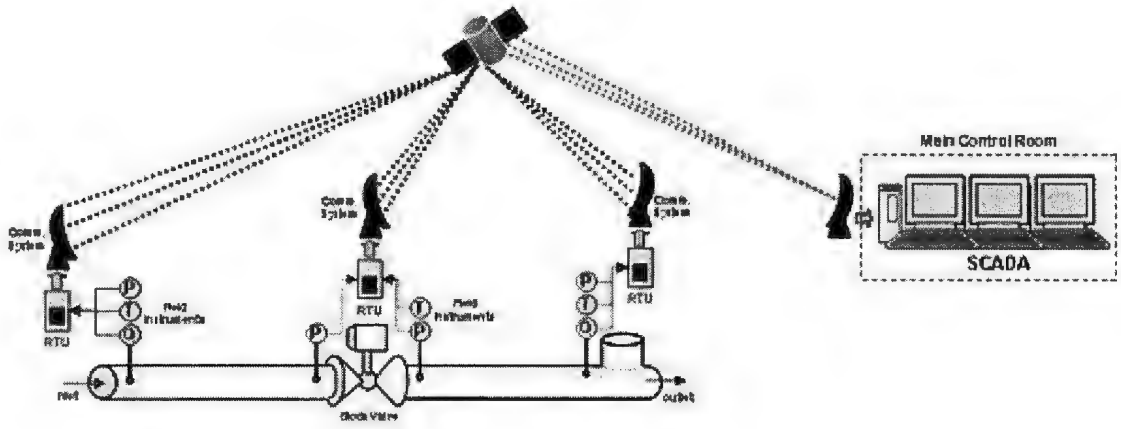

Figure 1.3: The SCADA System for pipelines [2].

1.3 Pipeline Inspection

Pipeline operators use a variety of methods to ensure that pipelines are not damaged, or to detect damage before it poses a problem. Hopkins [3] summarized the methods of detection as in Table 1.1.

Table 1.1: Pipeline Inspection and monitoring methods [3]

Defect/Damage	Surveillance Or Inspection Method						
	Aerial Ground Patrol	Intelligent Pig	Product Quality	Leak Survey	Geo-Tech Survey And Strain Gauges	Cp And Coating Survey	Hydro-Test
3rd Party Damage	P	R					R
Ext. Corrosion		R				P	R
Int. Corrosion		R	P				R
Fatigue/Cracks		R					R
Coating						P	
Material/ Const. Defct.		R					R
Ground Movement		R			R		
Leakage	R	P		R			R
Sabotage	P						

where 'P' is 'proactive' means the pipelines do not become defective or damaged. 'R' is 'reactive'

and it mean that the damage or defects are detected before they cause serious problems

Pipelines can be inspected with intelligent 'pigs' as shown in Figure 1.4. The 'pigs' are sophisticated machines that travel inside the pipe and record the data on the condition of the pipe. These pigs can measure metal loss (e.g. corrosion), and geometry abnormalities (e.g. dents). Sophisticated pigs can map the pipeline or detect the dimensions of defects or cracks which is useful to characterize the defect. Defect characterization is important for subsequent pipeline failure probability estimation.

Figure 1.4: Pig- a pipeline inspection tool [3] used for defect or crack inspection

1.4 Pipeline Failure Statistics

Pipelines are a safe mode of transportation for oil and gas. However, like any other structure, they do fail. The major causes of failure are [3, 5]:

- outside force (sometimes called third party damage, mechanical damage or external interference)

- corrosion of the pipe wall, either internally or externally by the surrounding environment

Figure 1.5 shows the major causes of pipeline failures [3]. Outside force and corrosion are the dominant failure causes, followed by construction or material defects, equipment or operator error, and 'other' failure causes (e.g. leaking valves). These failures have caused tragic casualties in recent years on both oil and gas pipelines [6]. In the present study the corrosion related defects or cracks will be investigated.

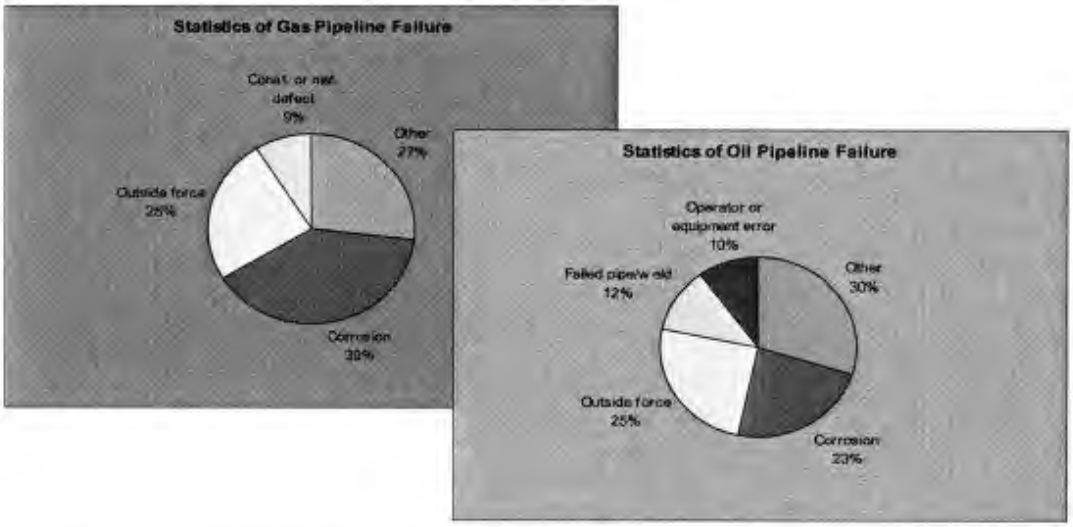

Figure 1.5: Statistics of onshore pipeline failures, data taken from referred sources [2, 4]

1.5 Type and Orientation Defects in Pipeline

The pipeline fails due to a defect, created by a reduction of wall thickness, or the propagation of an initiated crack. A classification of blunt corrosion defects is given in Figure 1.6. The pipe wall thereby loses its capacity or strength [7]. It may be noted that the orientation and type of defect affect the bursting pressure of a pipeline.

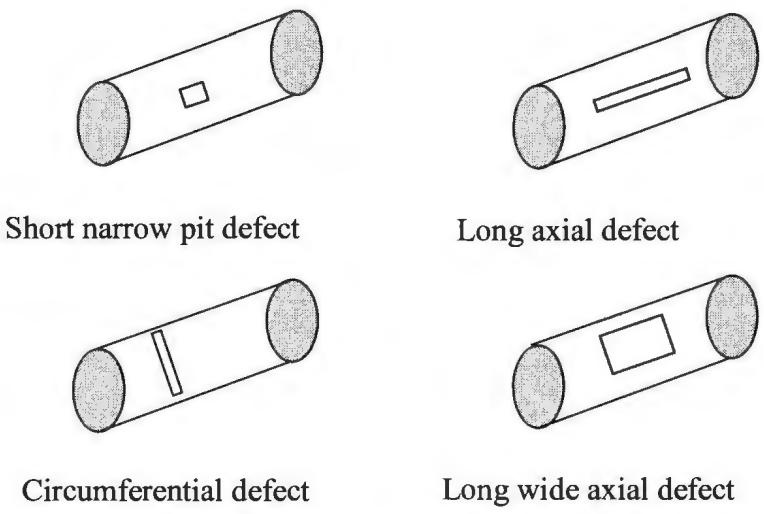

Figure 1.6: Classes of blunt corrosion defects [8-10]

Again the defects may be a single defect or interacting defects as given in Figure 1.7. This study focused on the single defect. The interacting defect is beyond the scope of the present study. Interested readers may consult DNV RP F101 [11].

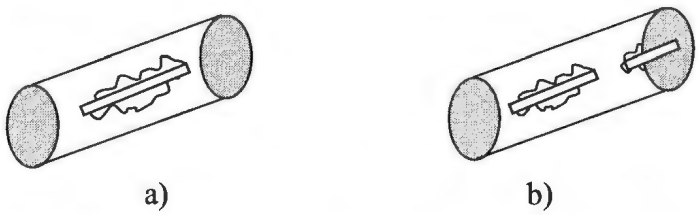

Figure 1.7: Defect type a) single defect b) interacting defects [11]

The pipeline may fail either by hoop or axial stress. If the defect is longitudinally oriented it is likely to fail by hoop stress. The failure mode is given in Figure 1.8. The present study will focus on longitudinal defects or cracks due to internal corrosion,

external corrosion, and Stress Corrosion Cracking (SCC), but the circumferentially oriented crack will be considered for Corrosion Fatigue cracking.

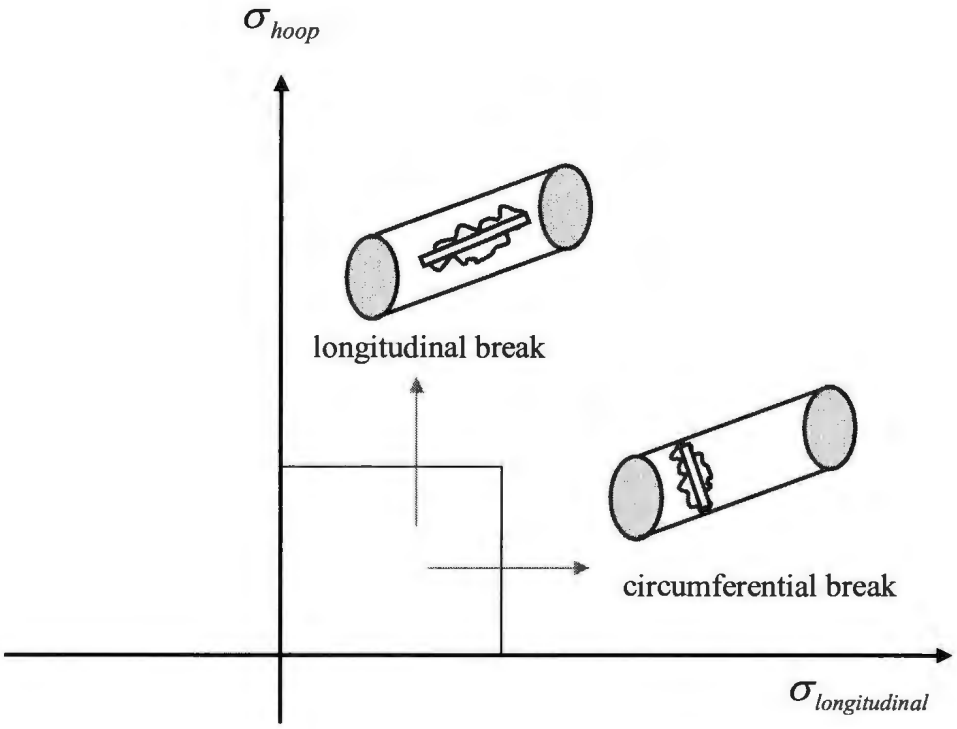

Figure 1.8: Influence of Applied Load on the Failure Mode of Corrosion Defect

1.6 Failure Modes of Pipeline

The failure may happen in the following ways:- burst, leak or puncture, overload, structural collapse (buckling), fatigue, and fracture. The pipeline generally don't become 'unserviceable' due to ovalisation, blockages, distortions, and displacements [3]. The failures considered in this study are burst, leak, fatigue or fracture failures.

1.7 Problem Statement

The existing methods of pipeline design consider pressure containment of defect free pipe with the usual addition of corrosion allowance in the pipeline wall thickness. At the beginning of the design life the pipeline is good in terms of safety record; however, the problem starts as the pipeline ages. As the corrosion defects or cracks develop in aged pipeline, the integrity of the pipeline becomes a major challenge.

The guidance 'fitness for purpose' or 'fitness for service' is considered for the assessment of the integrity of the pipeline. The assessment itself is a complex, time consuming and expensive effort which sometimes require excavation. The repair may require the complete shut-down of the transportation system.

To avoid catastrophic failure in the transportation system, to avoid frequent shut downs or to reduce the frequency of repairs, the time dependent failure sources may be identified and quantified in advance and incorporated in the early design. Hence, the study will focus particularly on the risk-based design of pipelines considering the time dependent degradation mechanism.

In contrast to reliability-based design, risk-based design gives a complete picture of damage by simultaneous consideration of consequence and failure probability. In risk-based design a couple of iterations may be required to find the minimal risk.

1.8 Scope of the Present Work

The scope of pipeline failure is categorized according to the behavior of the failure rate over time. While the failure rate tends to vary with the changing environment,

the underlying mechanism is usually random and exhibits a constant failure rate as long as the environment stays constant. For example, the third party damage rate depends on the location of the pipeline. While the failure rate tends to increase with time and is logically linked with the aging effect, the underlying mechanism is time dependent. In this condition the surrounding environment is the governing factor for failure rate determination. Some failure mechanisms and their respective categories are shown in Table 1.2 for a typical pipeline system.

Table 1.2: Scope of the work: typical failure mechanism of process system [12-14]

Failure mechanism	Nature of mechanism	Failure rate tendency
Corrosion	*Time dependent*	*Increases*
Cracking	*Time dependent*	*Increases*
Third Party Damage	Random	Constant
Earth movement	Random	Constant
Material Degradation	*Time dependent*	*Increases*
Corrosion Fatigue	*Time dependent*	*Increases*

Figure 1.9 shows the pipeline failure rate curve. Pipeline that survive the burn-in phase tend to fail at a constant failure rate. Third-party damages or land movements constitute this part of the failure rate curve. After the burn-in and useful life phase, the failure rate may begin to increase. This is the zone where pipeline begin to wear-out as they reach the end of their useful service life. The effect of time dependent failure mechanism (corrosion or fatigue) is observed in this *wear-out phase* of the curve.

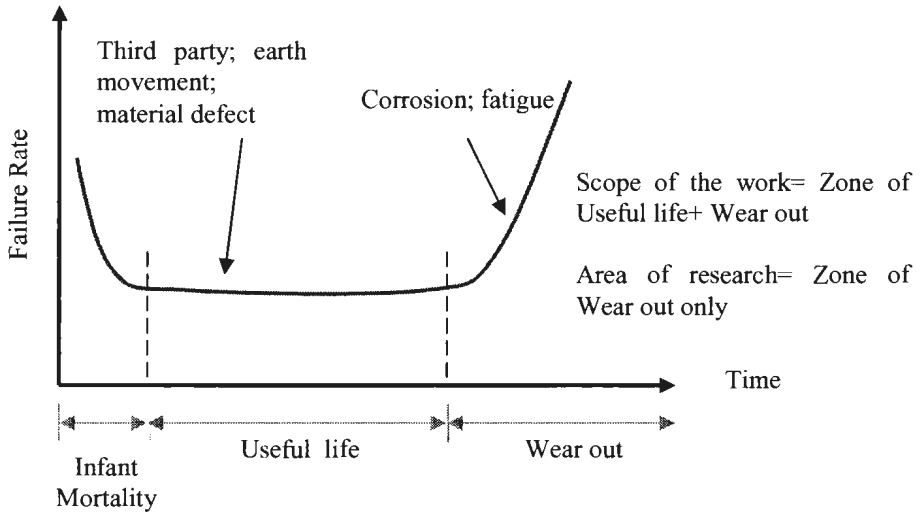

Figure 1.9: Failure rate curve of a process system

The time dependent degradation mechanisms are the focus of this work. The main degradations studied here are:

1. Internal corrosion
2. External Corrosion
3. Stress Corrosion Cracking (SCC)
4. Fatigue failure due to pressure fluctuation and start up/shut down

These degradation mechanisms are considered as major sources of failure and these are discussed in detail in Chapter 4, Chapter 5, Chapter 6 and Chapter 7. The risk-based design is studied for the failure modes listed above.

1.9 Objectives

The main objective of this study is to develop a risk-based design methodology for pipelines considering time dependent degradation mechanisms. This objective is accomplished through the following sub-objectives:

- to develop a risk-based design methodology for pipelines considering probabilistic failures and consequences. *Chapter 3* described risk-based design methodology.
- to assess the failure probabilities for individual failure mechanism considering recommended burst models and to revise the existing burst models where applicable. *Chapter 4-7* describe failure probabilities for individual failure mechanism.
- to develop an algorithm to integrate different failure modes. *Chapter 8* integrates individual failure probabilities considering the algorithm stated in *section 3.4* and the result obtained from *Chapter 4-7*
- to define pipeline design parameters based on allowable maximum risk. *Chapter 8* suggests the revision of the pipeline design parameters.

1.10 Outline of Thesis

Chapter 1 provides a brief introduction to pipeline components, design, construction, operation, inspection, defects and failures. *Chapter 2* discusses literature review related to design evolution, reliability methods and defect or crack failure assessment techniques. *Chapter 3* describes risk-based design methodology. *Chapter 4*

outlines failure assessment due to internal corrosion considering different standards and models. *Chapter 5* discusses failure assessment for external corrosion. *Chapter 6* examines Stress Corrosion Cracking (SCC) failure probability and *Chapter 7* examines weld crack failure due to cyclic loading. *Chapter 8* provides integration of failure probabilities obtained in *Chapter 4-7*; and determine pipeline design parameters based on allowable maximum risk. *Chapter 9* outlines major contributions and future research topics.

1.11 References

[1] Hopkins P. (2007). PIPELINES: Past, Present, and Future. *Keynote Paper. The 5th Asian Pacific IIW International Congress*, Sydney, Australia

[2] *Pipeline Transport,* (2008, August). Retrieved from http://en.wikipedia.org/wiki/Pipeline_transport

[3] Hopkins P. (2002). *The Structural Integrity of Oil and Gas Transmission Pipelines, Comprehensive Structural Integrity*. Volume 1, UK: Elsevier.

[4] *Oil and Gas Occupational Safety and Health Regulations,* (2011). SOR/87-612, Ministry of Justice, Canada

[5] Cosham A., & Hopkins P. (2003). The effect of dents in pipelines – guidance in the pipeline defect assessment manual. *Proceedings ICPVT-10*, Austria.

[6] Anon (2002). Office of Pipeline Safety, Retrieved from www.ntsb.gov and www.ops.dot.gov.

[7] Dillon, C.P. (1995). *Corrosion Resistant of Stainless Steel.* New York: Marcel Dekker, Inc.

[8] Xu, T., & Bee, R. (1997). Development of Guidelines for Acceptance of Corroded Pipe. *Proceeding of the 7th International Offshore and Polar Engineering Conference*, Honolulu, USA.

[9] Hosseini S. A. (2010). *Assessment of Crack in Corrosion Defects in Natural Gas Transmission Pipelines*. University of Ontario, Canada.

[10] Stephens D. R., Bubenik T. A., & Francini R. B. (1995). *Residual strength of pipeline corrosion defects under combined pressure and axial loads.* Battelle Memorial Institute

[11] Recommended Practice DNV RP-F101, (2004). *Corroded Pipelines.* DET NORSKE VERITAS

[12] Muhlbauer, W. K. (2004). *Pipeline Risk Management Manual: Ideas, Techniques, and Resources*. USA: Gulf Professional Publishing

[13] Kiefner, J. F., & Maxey, W. A. (2000). Periodic Hydrostatic Testing or In-line Inspection to Prevent Failures from Pressure-Cycle-Induced Fatigue. *API's 51st Annual Pipeline Conference & Cybernetics Symposium*, New Orleans, Louisiana

[14] Kiefner, J. F., Kolovich, C. E., Zelenak P. A., & Wahjudi T. (2004). Estimating fatigue life for pipeline integrity management. *International Pipeline Conference*, Calgary, Alberta.

Chapter 2

Background Literature Review

This chapter provides a background literature review of the work as a whole. The literature review for internal corrosion, external corrosion, stress corrosion cracking, and weld defect crack assessment are provided in chapters 4, 5, 6 and 7 respectively.

2.1 Design Evolution

2.1.1 Overview

Allowable Stress Design (ASD) is a design philosophy that ensures that the developed stress in a structure does not exceed the elastic limit. This limit is usually restricted by the use of a safety factor. It is also commonly referred to as Working Stress Design (WSD) or permissible stress design.

In contrast to WSD, a new concept, Limit State Design (LSD) is introduced in structural design. A limit state is a condition of a structure beyond which it no longer satisfies relevant design criteria. Limit state design requires that the structure must satisfy either of the design criteria: the ultimate limit state (ULS) or the serviceability limit state (SLS). LSD is also well known as Load and Resistance Factored Design (LRFD). The evolution of limist state design is given in Figure 2.1.

Ultimate Limit State: ULS design criteria satisfy that the structure doesn't collapse when subjected to a peak load. A structure satisfies ULS criteria if all factored stresses remain below the factored resistances. The factored stress is a magnified stress where the magnification factor is multiplied with the stress. The reduction factor is multiplied with the resistances of the structural section of interest.

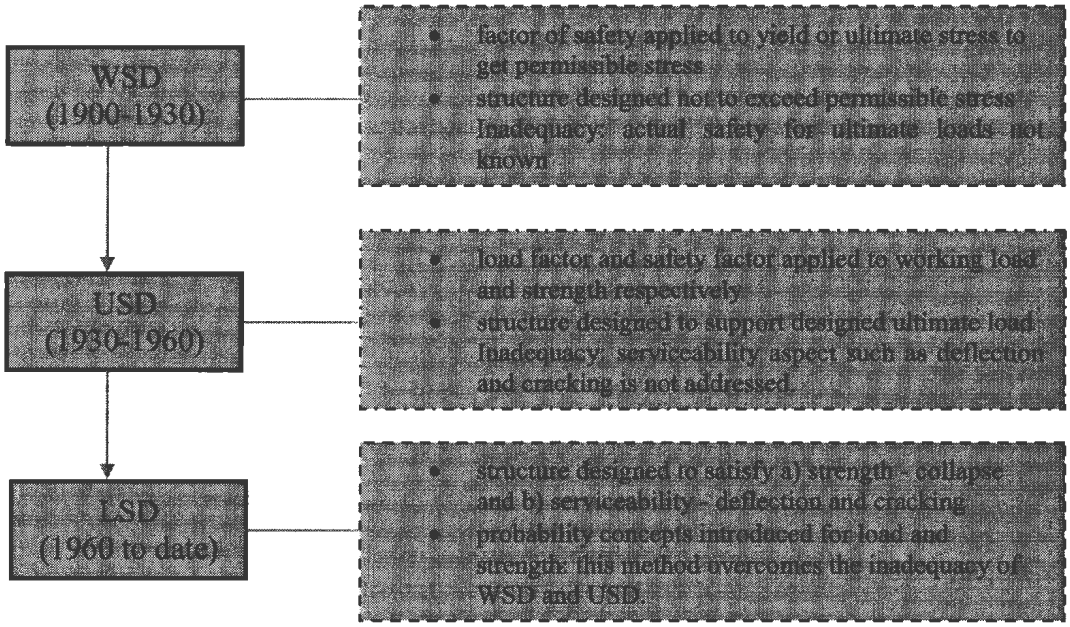

Figure 2.1: Evolution of Limit State Design (LSD)

Serviceability Limit State: The serviceability limit state criterion satisfies that a structure remains functional for its intended use subjected to a routine loading condition. A structure is deemed to satisfy the serviceability limit state when the constituent elements do not deflect by more than certain limits. The example of serviceability limit criterion for a cracked specimen is that the crack width must remain below the maximum specified dimension. The purpose of SLS requirements in a structure is to ensure that the users are

not frightened by certain deflections of the floor, or vibrations by walking, or sickened by certain swaying of the structure during high winds.

2.1.2 Limit States Design

It is well known that the reliability theory got momentum after World War II for modeling uncertainties related to the performance of structures [1-2]. The reliability theory embodied in the limit states design has been used as a basis for many structural design codes for the last two decades. The limit states codes are now used almost exclusively in North America for designing steel and reinforced concrete structures [3-5].

The evolution of the first and second order reliability methods [6-7] is a significant breakthrough since it resulted in huge reductions of computational effort of probability calculation. Hence, the limit states codes have been evolved for many types of structures, such as offshore structures [8], bridges [9], and nuclear containment structures [10].

The application of reliability concepts to the design of pipelines is noted in a different study. Henderson and Nessim [11] developed a reliability-based design approach for pipelines subject to thaw settlement; Sotberg [12] dealt with submarine pipeline applications; Gresnigt [13] looked at plastic design of buried pipelines; and Row *et al.* [14] addressed extreme loading scenarios for Arctic offshore pipelines. Reliability-based design for conventional pipelines has also been advocated by Zimmerman et. al [15].

2.1.3 Rationale for Limit States Design

The structural design ensures that a structure sustains an adequate level of safety during its design life; and that the performance of the structure does not conflict with the functional and operational requirements. To retain the design objective the pipeline must be designed so that the probabilities of excessive deformations or burst should be sufficiently low.

The existing Canadian and American pipeline codes [16-18] are based on allowable stress design for flexible pipeline systems. Using this method, failure is prevented by limiting stresses determined from an elastic analysis to some fraction of the specified minimum yield strength (SMYS). It may be noted that the application of existing standards to high-strength or corrosion resistant steels, high-pressure designs, or other deviations from conventional practice, could lead to either un-conservative or over-conservative designs.

Limit state design criteria, however, provide greater flexibility to pipeline engineers to use non-linear characteristics of the structure in the design.

2.2 Failure Analysis

There are essentially three ways of assessing pipeline failure analysis: *Deterministic Method*, *Numerical Method* and *Probabilistic Method*

Deterministic Method: the deterministic approach considers only lower bound data (e.g. maximum corrosion rate, minimum wall thickness, peak depth of corrosion, minimum material property data) and does not include the uncertainties [19].

Numerical Method: The finite element method (FEM) may be employed to reduce baseless rejection of defective pipelines' sections by properly characterizing the defect and forces acting on the specimen of interest. Safian [20] numbered the steps to be followed for strength analysis of pipelines sections by the finite element method.

Probabilistic Method: Failure analysis by probabilistic method is a method of probability analysis resulting from the various sources of uncertainty to produce an assessment for a particular engineering design. Sections 2.2.1 to 2.2.2 discuss the details of probabilistic methods.

2.2.1 Reliability-Based Method

The probability of failure defines the measure of performance function $g(\mathbf{X})$ smaller than zero, i.e. $P\{g(\mathbf{X}) < 0\}$ where the random variables, $\mathbf{X}= (X_1, X_2, ..., X_n)$, remain in the failure region. The opposite characteristics are observed for reliability. The integral form of the probability of failure or reliability can be evaluated with the joint *pdf* of **X,** i.e $f_{\mathbf{x}}(\mathbf{x})$ as given in equations (2.1) and (2.2)

$$p_f = P\{g(\mathbf{x}) < 0\} = \int_{g(\mathbf{x})<0} f_{\mathbf{x}}(\mathbf{x})d\mathbf{x} \tag{2.1}$$

$$R = 1 - p_f = P\{g(\mathbf{x}) > 0\} = \int_{g(\mathbf{x})>0} f_{\mathbf{x}}(\mathbf{x})d\mathbf{x} \tag{2.2}$$

The close form integral solution of equations (2.1) and (2.2) is complex but by simplification and approximation the solution may be obtained easily. The First Order Reliability Method (FORM) and the Second Order Reliability Method (SORM) are the

two most commonly used reliability methods. The FORM and SORM methods simplify the integrand $f_{\mathbf{x}}(\mathbf{x})$ and approximate the performance function $g(\mathbf{X})$ and solve the equations (2.1) and (2.2) . It may be noted that the random variables in **X** are assumed to be mutually independent, but if the random variables are correlated they need to be converted to independent variables before simplification and approximation.

2.2.1.1 First Order Reliability Method (FORM)

The name 'First Order Reliability Method' comes from first-order Taylor series approximation of the performance function $g(\mathbf{X})$.

Figure 2.2 depicts the visualized three-dimensional case of the probability integrations of equations (2.1) and (2.2). It shows the joint *pdf* $f_{\mathbf{x}}(\mathbf{x})$ and its contours which are projections of the surface of $f_{\mathbf{x}}(\mathbf{x})$ on $X1$ - $X2$ plane in the figure. All the points on the contours have the same values of $f_{\mathbf{x}}(\mathbf{x})$ or the same probability density. The limit function $g(\mathbf{X}) = 0$ is also plotted on $X1$ - $X2$ plane in Figure 2.2.

The volume underneath the surface $f_{\mathbf{x}}(\mathbf{x})$ in Figure 2.2 represents the probability integration of equations (2.2). It could be imagined that the surface of the integrand $f_{\mathbf{x}}(\mathbf{x})$ forms a 'hill', and can be cut by flexible knife ($g(\mathbf{X}) = 0$) and be parted into $g(\mathbf{X}) < 0$ and $g(\mathbf{X}) > 0$. The part $g(\mathbf{X}) < 0$ is removed, and the part $g(\mathbf{X}) > 0$ remains as it is in Figure 2.2. The remaining volume, the volume underneath $f_{\mathbf{x}}(\mathbf{x})$ on the side of the safe region $g(\mathbf{X}) > 0$, is the probability integration of equation (2.2), which represents the

reliability. The removed part, the volume underneath $f_x(\mathbf{x})$ on the side of failure region $g(\mathbf{X}) < 0$, is the probability of failure.

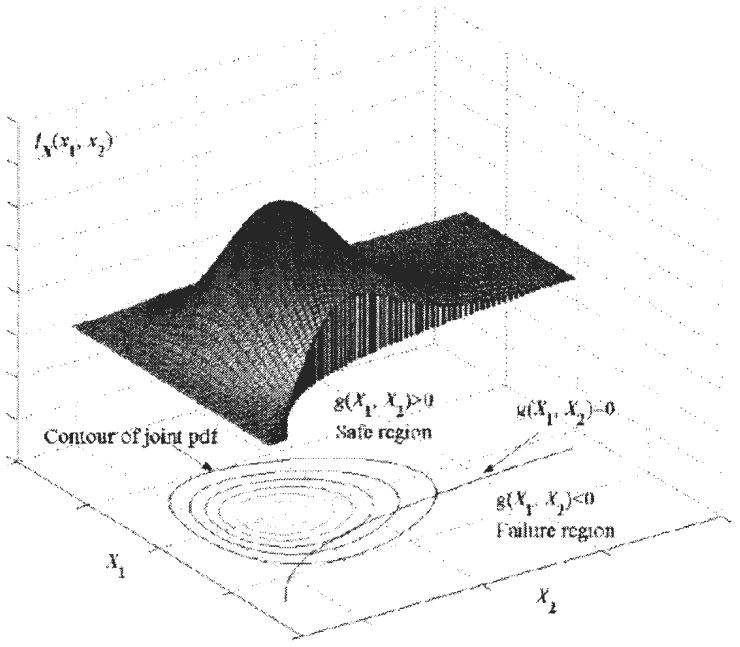

Figure 2.2: Probability Integration in 3-D [20a, 20b]

The contours of integrand $f_x(\mathbf{x})$ and the integration boundary $g(\mathbf{X}) = 0$, in the $X1$-$X2$ plane are evident in Figure 2.3. The contours are also parted by $g(\mathbf{X}) = 0$ and the reliability is obtained by integrating $f_x(\mathbf{x})$ with $g(\mathbf{X}) > 0$ while the failure probability is obtained by integrating $f_x(\mathbf{x})$ with $g(\mathbf{X}) < 0$.

As indicated earlier, the direct integration of equations (2.1) and (2.2) is complex because the probability integration is multidimensional, as a number of random variables

X are involved in $f_x(\mathbf{x})$. Again the integrand $f_x(\mathbf{x})$ and the integration boundary $g(\mathbf{X})=0$ are normally nonlinear multidimensional functions, which invites a new problem. Therefore, the analytical solution to the probability integration problem in equations (2.1) and (2.2) is seldom available. The numerical solution is also impractical due to the high dimensionality of most engineering problems. Therefore the approximation methods, such as FORM and SORM have been used over the years to solve engineering problems.

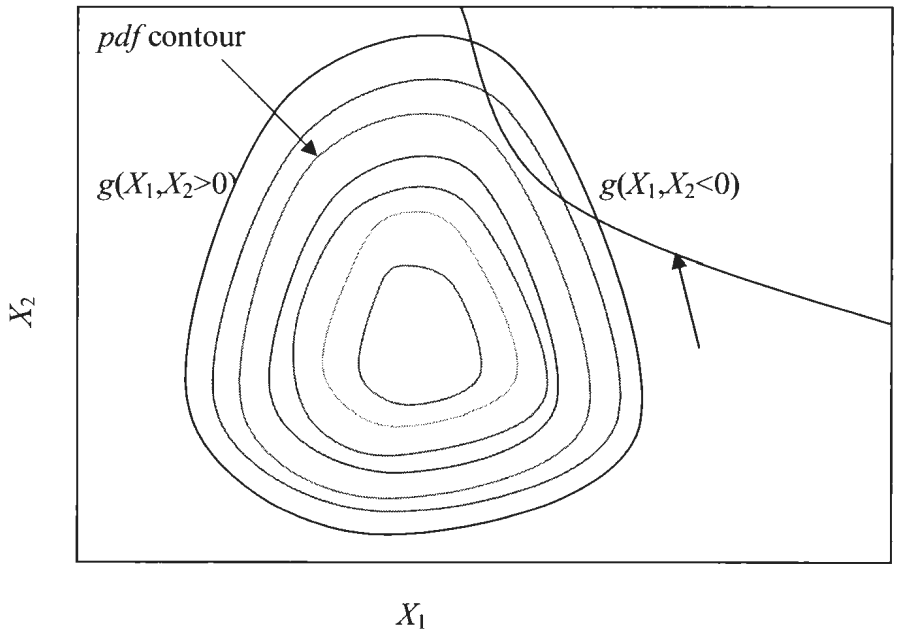

Figure 2.3: Probability Integration in X-Space

The approximation methods, FORM and SORM, follow two steps to make the probability integration easy. The first step simplifies the integrand, $f_x(\mathbf{x})$, so that its contours become more regular and symmetric. The second step approximates the integration boundary $g(\mathbf{X})= 0$. The way of approximation divides the probability

integration into two types: the First Order Reliability Method (FORM) and the Second Order Reliability Method (SORM). The two steps are described below.

2.2.1.2 Simplification of the Integrand

The random variables $\mathbf{X}= (X_1, X_2, ..., X_n)$ of the integrand $f_{\mathbf{x}}(\mathbf{x})$ are transformed from X-space to U-space where the transformed random variables are $\mathbf{U}= (U_1, U_2, ..., U_n)$. The transformation from **X** to **U** is based on the condition that the *cdf*s of the random variables remain the same before and after the transformation. This transformation given in equation (2.3) is called the Rosenblatt transformation [21] where $\Phi(\cdot)$ is the *cdf* of the standard normal distribution. The standard normal variable is given in equation (2.4)

$$F_{X_i}(x_i) = \Phi(u_i) \tag{2.3}$$

$$U_i = \Phi^{-1}\left[F_{X_i}(x_i)\right] \tag{2.4}$$

It may be noted that the general transformation from a non-normal variable to a standard normal variable may be nonlinear after the transformation.

The performance function is given in equation (2.5) and the probability integration is given in equation (2.6) where $\phi_{\mathbf{u}}(\mathbf{u})$ is the joint *pdf* of **U**.

$$Y = g(\mathbf{U}) \tag{2.5}$$

$$p_f = P\{g(\mathbf{U}) < 0\} = \int_{g(\mathbf{U})<0} \phi_{\mathbf{U}}(\mathbf{u}) d\mathbf{u} \tag{2.6}$$

The joint *pdf* is the product of the individual *pdf*s of standard normal distribution since all the random variables are assumed to be independent, and is given by

$$\phi_U(\mathbf{u}) = \prod_{i=1}^{n} \frac{1}{\sqrt{2\pi}} \exp\left(-\frac{1}{2}u_i^2\right) \tag{2.7}$$

The failure probability becomes

$$p_f = \int_{g(u_1,u_2,\ldots,u_n)<0} \cdots \int \prod_{i=1}^{n} \frac{1}{\sqrt{2\pi}} \exp\left(-\frac{1}{2}u_i^2\right) du_1 du_2 .. du_n \tag{2.8}$$

It may be noted that equation (2.1) in X-space and equation (2.8) in U-space calculate the same probability of failure. However, a change may be noticed in the contours of the integrand ϕ_u which become concentric circles as evident in Figures 2.4. It is obvious that the integrand ϕ_u is easier to integrate.

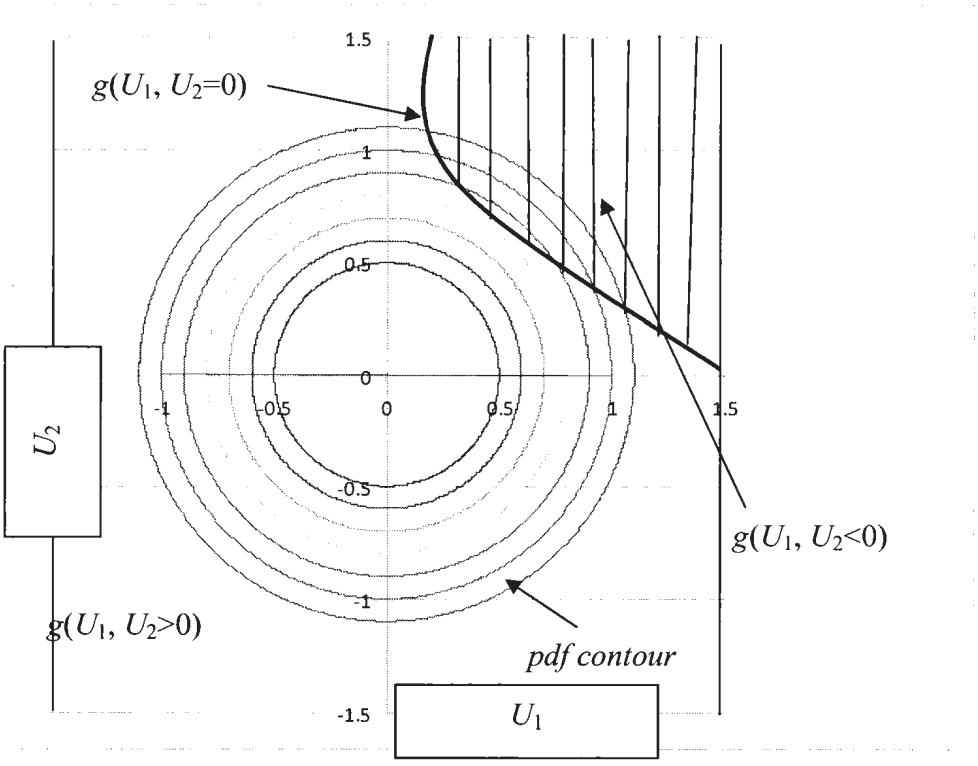

Figure 2.4: Probability Integration after normal transformation

2.2.1.3 Approximating the Integration Boundary

The integration boundary $g(\mathbf{U}) = 0$ is approximated to further make the probability integration easier to evaluate. The FORM method uses a linear approximation of the first order Taylor expansion as shown in equation 2.9

$$g(\mathbf{U}) \approx L(\mathbf{U}) = g(\mathbf{u}^*) + \nabla g(\mathbf{u}^*)(\mathbf{U} - \mathbf{u}^*)^T \tag{2.9}$$

where $L(\mathbf{U})$ is the linearized performance function, $\mathbf{u}^* = (u_1^*, u_2^*, ..., u_n^*)$ is the expansion point, $\nabla g(\mathbf{u}^*)$ is the gradient of $g(\mathbf{U})$ at $\mathbf{u}^*$, and T stands for a transpose. $\nabla g(\mathbf{u}^*)$ is given by

$$\nabla g(\mathbf{u}^*) = \left(\frac{\partial g(\mathbf{U})}{\partial U_1}, \frac{\partial g(\mathbf{U})}{\partial U_2}, ..., \frac{\partial g(\mathbf{U})}{\partial U_n} \right)\Bigg|_{\mathbf{u}^*} \tag{2.10}$$

It is preferable to expand the performance function $g(\mathbf{U})$ at the point that has the highest value of the integrand, namely, the highest probability density. The point that has the highest probability density of the performance $g(\mathbf{U}) = 0$ is termed the *Most Probable Point* (MPP) or the *Design Point*. The performance function is therefore approximated at the MPP. Maximizing the joint *pdf* $\phi_{\mathbf{u}}(\mathbf{u})$ at the limit state of $g(\mathbf{U}) = 0$ gives the location of the MPP. The mathematical model for locating the MPP is given by

$$\begin{cases} \max\limits_{\mathbf{u}} & \prod_{i=1}^{n} \frac{1}{\sqrt{2\pi}} \exp\left(-\frac{1}{2} u_i^2 \right) \\ \textit{subject to } g(\mathbf{u}) = 0 \end{cases} \tag{2.11}$$

since $\prod_{i=1}^{n}\frac{1}{\sqrt{2\pi}}\exp\left(-\frac{1}{2}u_i^2\right)=\frac{1}{\sqrt{2\pi}}\exp\left(-\frac{1}{2}\sum_{i=1}^{n}u_i^2\right)$ maximizing

$\prod_{i=1}^{n}\frac{1}{\sqrt{2\pi}}\exp\left(-\frac{1}{2}u_i^2\right)$ is equivalent to minimizing $\sum_{i=1}^{n}u_i^2$. Therefore the MPP search can be rewritten as

$$\|\mathrm{u}\| = \begin{cases}\min \\ \mathrm{u}\end{cases} \quad \|\mathrm{u}\| = \sqrt{u_1^2 + u_2^2 + ... + u_n^2} = \sum_{i=1}^{n} u_i^2 \qquad (2.12)$$

subject to g(u)=0

where $\|\mathrm{u}\|$ stands for the length or magnitude of a vector. As shown graphically in Figure 2.5, the MPP is the shortest distance point from the limit state $g(\mathbf{U}) = 0$ to the origin O in U-space. The minimum distance $\beta = \|\mathrm{u}\|$ is called the *reliability index*.

As at MPP $\mathbf{u}^*$, $g(\mathbf{U}) = 0$, equation 2.9 becomes

$$L(\mathbf{U}) = \sum_{i=1}^{n}\left.\frac{\partial g(\mathbf{U})}{\partial \mathbf{U}_i}\right|_{\mathbf{u}^*}\left(\mathbf{U}_i - \mathbf{u}_i^*\right) = a_0 + \sum_{i=1}^{n} a_i U_i \qquad (2.13)$$

where $a_0 = -\sum_{i=1}^{n}\left.\frac{\partial g(\mathbf{U})}{\partial U_i}\right|_{\mathbf{u}^*}\mathbf{u}_i^*$ and $a_i = \left.\frac{\partial g(\mathbf{U})}{\partial U_i}\right|_{\mathbf{u}^*}$. Equation 2.13 indicates that $L(\mathbf{U})$ is a linear function of standard normal variables. Therefore, $L(\mathbf{U})$ is also normally distributed. Its mean and standard deviation are given by

$$\mu_L = a_0 = -\sum_{i=1}^{n}\left.\frac{\partial g(\mathbf{U})}{\partial U_i}\right|_{\mathbf{u}^*}\mathbf{u}_i^* \qquad (2.14)$$

$$\sigma_L = \sqrt{\sum_{i=1}^{n} a_1^2} = \sqrt{\sum_{i=1}^{n}\left(\left.\frac{\partial g}{\partial U_i}\right|_{u_i^*}\right)^2} \qquad (2.15)$$

The probability of failure is thereby

$$p_f \approx P\{L(\mathbf{U}) < 0\} = \Phi\left(\frac{-\mu_L}{\sigma_L}\right) = \Phi\left(\frac{\sum_{i=1}^{n} \left.\frac{\partial g}{\partial U_i}\right|_{\mathbf{u}^*} u_i^*}{\sqrt{\sum_{i=1}^{n}\left(\left.\frac{\partial g}{\partial U_i}\right|_{\mathbf{u}^*}\right)^2}}\right) = \Phi\left(\sum_{i=1}^{n} \alpha_i u_i^*\right) \quad (2.16)$$

$$p_f \approx \Phi\left(\sum_{i=1}^{n} \alpha_i u_i^*\right) = \Phi\left(\mathbf{a}\mathbf{u}^{*T}\right) \quad (2.17)$$

where $\alpha_i = \dfrac{\left.\frac{\partial g}{\partial U_i}\right|_{\mathbf{u}^*}}{\sqrt{\sum_{i=1}^{n}\left(\left.\frac{\partial g}{\partial U_i}\right|_{\mathbf{u}^*}\right)^2}}$, $\mathbf{a} = (\alpha_1, \alpha_2, ..;.\alpha_n) = \dfrac{\nabla g(\mathbf{u}^*)}{\|\nabla g(\mathbf{u}^*)\|}$ and $\mathbf{a}\mathbf{u}^{*T}$ is the product of the unit vector **a** and the vector of the MPP **u*** .

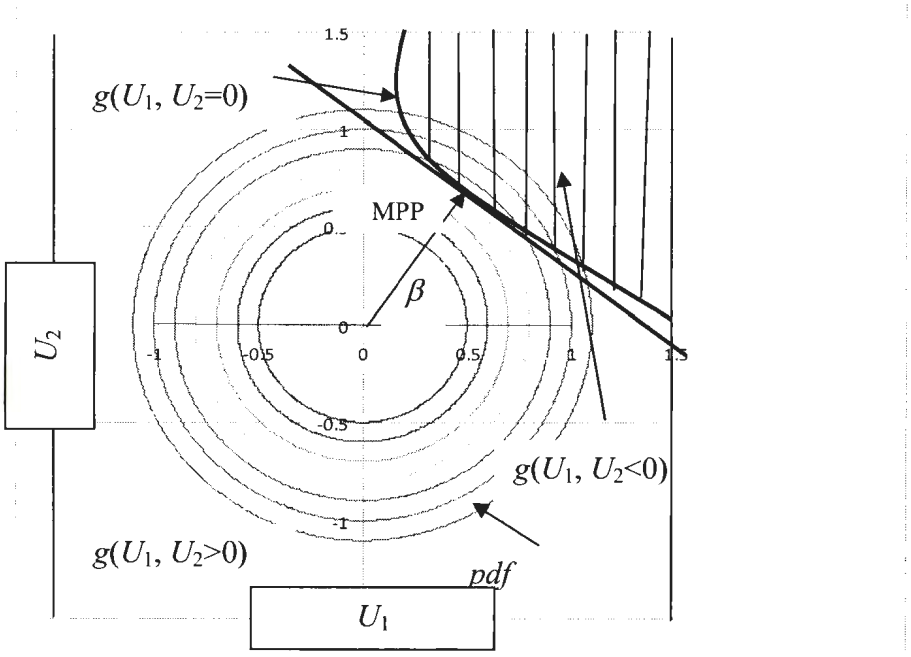

Figure 2.5: Reliability index in FORM

As the MPP **u*** is shortest distance point from the origin to the performance function curve $g(\mathbf{U}) = 0$, the MPP is the tangent point of the curve $g(\mathbf{U}) = 0$ and the circle with the radius of β as shown in Figure 2.6.

The direction of the gradient is also perpendicular to the curve at the MPP, and its direction can be represented by the unit vector **a**. Therefore

$$\mathbf{u}^* = -\beta\mathbf{a} \tag{2.18}$$

The probability of failure

$$p_f \approx P\{L(\mathbf{U}) < 0\} = \Phi(\mathbf{a}\mathbf{u}^{*T}) = \Phi(-\beta\mathbf{a}\mathbf{a}^T) = \Phi(-\beta) \tag{2.19}$$

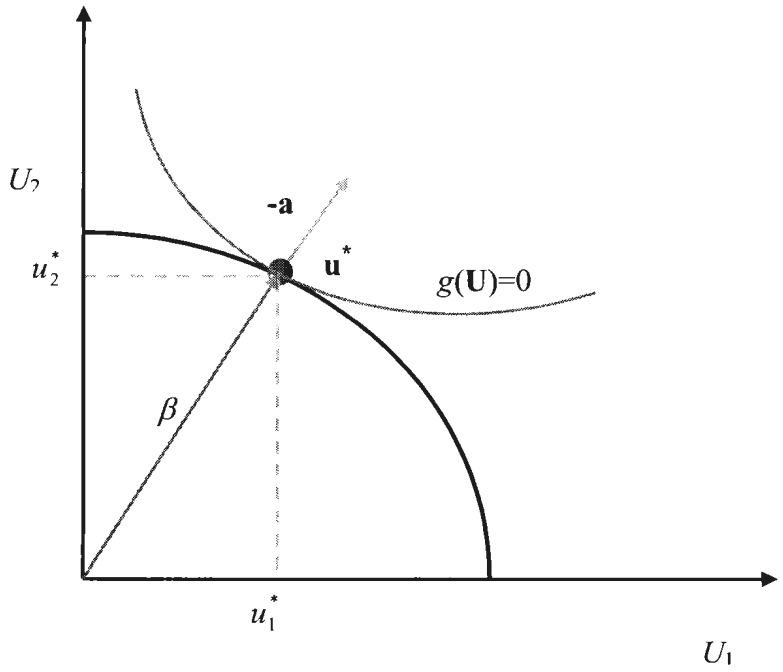

Figure 2.6: MPP located at tangent point

As its name implies, the Second Order Reliability Method (SORM) uses the second order Taylor expansion to approximate the performance function at the MPP **u***. The approximation is given by

$$g(\mathbf{U}) \approx q(\mathbf{U}) = g(\mathbf{u}^*) + \nabla(\mathbf{u}^*)(\mathbf{U}-\mathbf{u}^*)^T + \frac{1}{2}(\mathbf{U}-\mathbf{u}^*)\mathbf{H}(\mathbf{u}^*)(\mathbf{U}-\mathbf{u}^*)^T \quad (2.20)$$

where **H(u***) is the Hessian matrix at the MPP, namely,

$$\mathbf{H}(\mathbf{u}^*) = \begin{bmatrix} \frac{\partial^2 g}{\partial U_1^2} & \frac{\partial^2 g}{\partial U_1 U_2} & \cdots & \frac{\partial^2 g}{\partial U_1 U_n} \\ \frac{\partial^2 g}{\partial U_2 U_1} & \frac{\partial^2 g}{\partial U_2^2} & \cdots & \frac{\partial^2 g}{\partial U_2 U_n} \\ \cdots & \cdots & \cdots & \cdots \\ \frac{\partial^2 g}{\partial U_n U_1} & \frac{\partial^2 g}{\partial U_n U_2} & \cdots & \frac{\partial^2 g}{\partial U_n^2} \end{bmatrix} \quad (2.21)$$

The performance function is further simplified as

$$q(\mathbf{U}) = \mathbf{U_n} - \left(\beta + \frac{1}{2}\mathbf{U'^T D U'}\right) \quad (2.22)$$

where **D** is a $(n-1)\times(n-1)$ diagonal matrix whose elements are determined by the Hessian matrix **H(u***) , and $\mathbf{U}' = \{U_1, U_2, ...U_{n-1}\}$. When β is large enough, an asymptotic solution of the probability of failure can be then derived as

$$p_f \approx P\{g(\mathbf{X}) < 0\} = \Phi(-\beta)\prod_{i=1}^{n}(1+\beta\kappa_i)^{1/2} \quad (2.23)$$

where κ_i denotes the i-th main curvature of the performance function $g(\mathbf{U})$ at the MPP.

It may be noted that for statistically independent and normally distributed random variables the FORM method or Hasofer-Lind method [6] may be considered. For any

other situation it will not calculate the correct reliability index or probability of failure. Rackwitz et. al. [7], Chen et al. [22], and others corrected this shortcoming and included information on the distribution of random variables in the algorithm for both linear and nonlinear limit state equations. *Equivalent Normal Variables* [21] and *Two-Parameter Equivalent Normal Transformation* [6-7] are two methods utilized for non-normal variable to normal variable transformation.

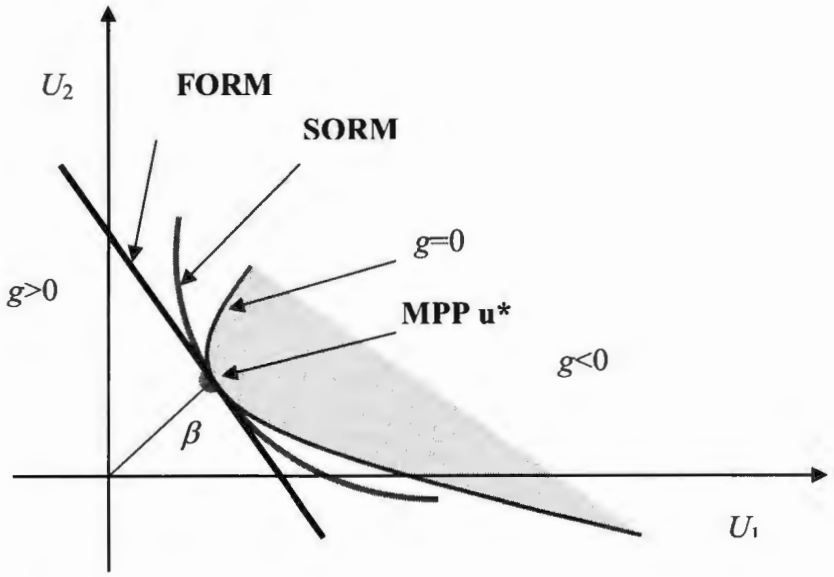

Figure 2.7: Relative accuracy of FORM and SORM

The SORM approach was first explored by Fiessler [23] using various quadratic approximations. A simple closed form solution for the probability computation using a second order approximation was given by Breitung [24] using the theory of asymptotic approximations. Hohenbichler et al. [25] have provided a theoretical explanation of FORM and SORM using the concept of asymptotic approximations.

Since the approximation of the limit state function in SORM, as in Figure 2.7, is better than FORM, SORM is believed to be more accurate than FORM. However, since SORM requires the second order derivatives, it is not as computationally efficient as FORM.

2.3 System Risk Evaluation

Using the reliability theory in the previous section, reliability may be estimated for a single performance criterion or limit state using FORM or SORM. In general many engineering systems have to satisfy more than one performance criterion. The concept used to consider multiple failure modes and/or multiple component failures is known as system risk evaluation. A complete risk analysis includes both component level and system level estimates.

Two basic approaches used for system risk evaluation are the cut set or failure mode approach (FMA), and the tie set or stable configuration approach (SCA). In the FMA all the possible ways a structure can fail are identified. Once the failure modes of a stable system are identified, system risk evaluation involves evaluating the probability of union and intersection of events considering the statistical correlation between them. However in many cases the statistical correlation may be difficult to estimate. Also it is difficult to estimate joint probabilities of more than two failure events. These difficulties result in an estimation of upper and lower bounds for the system risk evaluation. These bounds are usually estimated by assuming that all events are either perfectly correlated or statistically independent.

Alternatively an event tree which systematically identifies the possible sequence of events can also be used to identify the important failure sequences of the structure.

2.3.1 Fault Tree Analysis

Fault tree analysis (FTA) is a failure analysis in which an undesired state of a system is analyzed using Boolean logic to combine a series of lower-level events. The techniques have been extensively used in the aerospace and nuclear industries [26].

FTA is basically composed of logic diagrams that display the state of the system and is constructed using graphical design techniques. A subsystem of FTA is shown in Figure 2.8. In fault tree analysis, an undesired effect is taken as the top event of a tree of logic. There should be only one Top Event and all concerns must flow tree down from it.

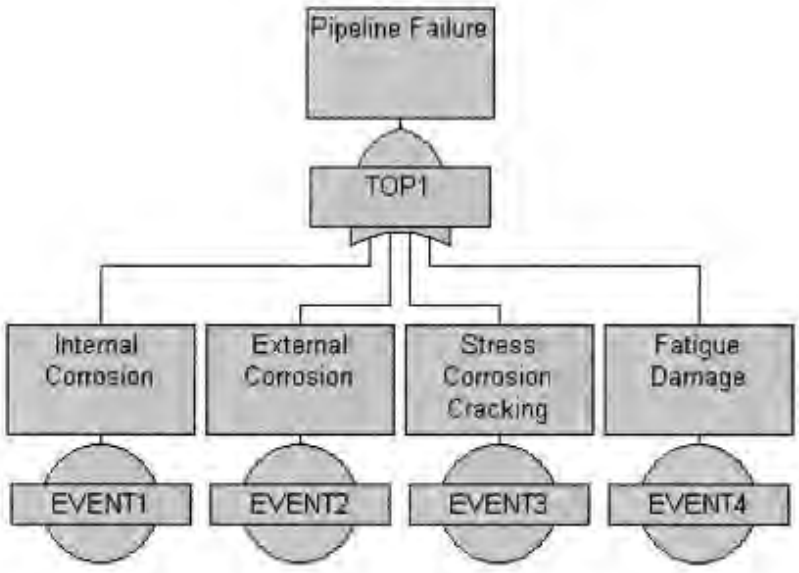

Figure 2.8: A fault tree diagram

The route through a tree between an event and an initiator in the tree is called a Cut Set. The shortest credible way through the tree from fault to initiating event is called a Minimal Cut Set.

2.3.2 Event Tree Analysis

Event tree analysis is based on binary logic, in which an event either has or has not happened or a component has or has not failed. A major limitation of the event tree is that components that are partially degraded cannot be considered as such [27]. However, it is valuable in analyzing the consequences arising from a failure or undesired event. A simple example of an event tree of a Sprinkler System is shown in Figure 2.9.

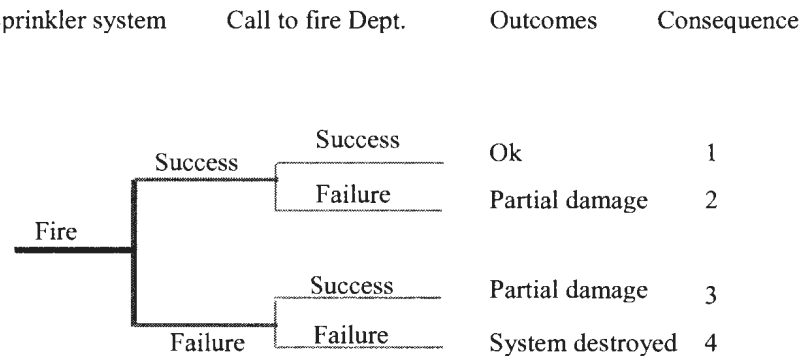

Figure 2.9: Event Tree for a Sprinkler system

This event tree was constructed to analyze the possible outcomes of a fire prevention system. The system has 2 components designed to handle this event: a sprinkler system and an automated call to the fire department. If the fire department is not

notified, the fire will be mostly contained by the sprinkler system. If the sprinkler system fails as well, the system will be destroyed. By analyzing all possible outcomes, a designer can determine the percentage of outcomes.

2.4 Defect Assessment

Based on the type of defect, there are different codes and standards for assessing a defect in pipelines. For instance, the most common methods for corrosion defects assessment are RSTRENG [28], Modified B31G [29] and DNV RP F101 [30] and the most popular codes for crack defect assessment are API 579 [31] and BS7910 [32]. Besides these codes and methods, there are numerical programs, such as CorLAS, which have been used successfully for assessing cracks in pipelines [33]. A list of codes and standards or individual models may be considered for defect or crack assessment.

2.4.1 Defect Assessment Codes or Models

The following codes/standard may be considered for defect assessment

- RSTRENG [28]
- Modified B31G [29]
- DNV RP F101 [30]
- ASME B31G [34]
- CSA Z 662-07 [35]
- Netto Model [36]

All of the above codes/standards or models are based on the NG-18 equation for failure of part-wall flaw, but they differ in approximation of the Folias factor, flow stress and the defect profile in the burst formula [29, 37]. The Folias factor (M) is a term that describes the bulging effect of a shell surface. The conservatism of the original B31G criterion leads to the development of modified B31G. ASME B31G assumes that the corroded area is a parabolic shape with 2/3 dL, but modified B31G assumes an arbitrary area with 0.85 dL. Again modified B31G assumes that the corrosion pits are blunt defects. It may be noted that sharp surface flaws have a significantly lower failure pressure than blunt surface defects [38]. The difference between Modified B31G and RSTRENG is the projected area; modified B31G calculates remaining strength based on the parabolic area (0.85 dL) of the corroded area, whereas RSTRENG uses an effective area method.

The burst formulas basically consider the linear elastic fracture mechanics (LEFM) or elastic-plastic fracture mechanics (EPFM) for defect assessment. LEFM is used when no significant yielding occurs prior to fracture. Depending on the material properties, loading conditions and defect shape and size, crack defects may fail either by fracture or plastic collapse. In general, the LEFM method can be used when the material toughness is low (brittle) and the stress intensity at the crack-tip is high. EPFM is considered when there is a significant plastic zone at the crack tip.

2.4.2 Crack Assessment Code

The following codes/standards may be considered for crack assessment:

- API 579 [31]
- BS7910 [32]

Cracks in high pressure pipelines may result from the interaction of susceptible metallic material, tensile stress or an aggressive electrolyte. The crack characteristics can vary greatly depending on the cause of the crack, the material, and the environment. Cracks can initiate on the external pipeline surface and grow in both the depth and surface directions. There are several common methods for assessing crack defects in pipelines.

The failure assessment diagram (FAD) is widely used for assessing crack-like flaws in pipelines. The FAD approach can be used for a wide range of material behaviors, from brittle fracture under LEFM conditions to ductile fully plastic collapse in three different levels: Level I, Level II and Level III FAD. The level II FAD provides a better estimate of the structural integrity of a component than a level I FAD assessment because level I FAD considers elastic-perfectly plastic stress-strain curve with no strain hardening. Level II and Level III allow more capacity by using the actual shape of the material stress-strain curve [32].

No effort is made to discuss the codes and standards since the details are available in respective references. Again no effort is made to discuss LEFM or EPFM as they are discussed in standard fracture mechanics book. The details of FAD is not discussed since this is available in every code for crack assessment. The ideas of fracture mechanics and FAD may be obtained from the author's 3rd and 4th work respectively SCC (6th Chapter) and the fatigue analysis of the weld crack defect (7tth Chapter).

2.5 Pipeline Failure Equations

The work at Battelle led to the development of strength (flow stress, as in Figure 2.10) dependent and the toughness dependent, through-wall and part-wall NG-18 equations. Flow stress is a concept introduced by Battelle to help model the complex plastic flow and work hardening associated with structural collapse.

Through wall defect [39]

$$\frac{K_c^2 \pi}{8c\bar{\sigma}^2} = \frac{C_v \frac{12}{A} E\pi}{8c\bar{\sigma}^2} = \ln \sec\left(\frac{\pi M \sigma_\theta}{2\bar{\sigma}}\right) \quad \text{toughness dependent} \tag{2.24}$$

$$M = \sqrt{1 + 0.4\left(\frac{2c}{\sqrt{Rt}}\right)^2} = \sqrt{1 + 0.80\left(\frac{2c}{\sqrt{Dt}}\right)^2} \tag{2.25}$$

$$\sigma_\theta = M^{-1}\bar{\sigma} \quad \text{strength dependent} \tag{2.26}$$

Part wall defect [39]

$$\frac{K_c^2 \pi}{8c\bar{\sigma}^2} = \frac{C_v \frac{12}{A} E\pi}{8c\bar{\sigma}^2} = \ln \sec\left(\frac{\pi M_P \sigma_\theta}{2\bar{\sigma}}\right) \quad \text{toughness dependent} \tag{2.27}$$

$$M_P = \left[\frac{1 - \frac{d}{t}\left(\frac{1}{M}\right)}{1 - \frac{d}{t}}\right] \tag{2.28}$$

$$\sigma_\theta = \bar{\sigma}\left[\frac{1 - \frac{d}{t}\left(\frac{1}{M}\right)}{1 - \frac{d}{t}}\right] \quad \text{strength dependent} \tag{2.29}$$

where M Folias factor

E	elastic modulus
D	outside diameter of pipe (R=D/2=radius)
R	radius of pipe
t	pipe wall thickness
d	part wall defect depth
σ_θ	hoop (circumferential) stress at failure (or *sf*)
$\bar{\sigma}$	flow stress (function of SMTS and SMYS))
2c	defect axial length
Cv	upper shelf Charpy V-notch impact energy
A	*a*rea of Charpy specimen fracture surface

It may be noted that the models accommodate a very complex failure process of a defect in a pipeline which involves plastic flow, bulging, crack initiation and ductile tearing. These models are safe due to inherent conservative assumptions with validation for thin walled plane stress, lower grade, low yield to tensile ratio line pipe. Again the strength dependent formulas are not applicable to low toughness material [39].

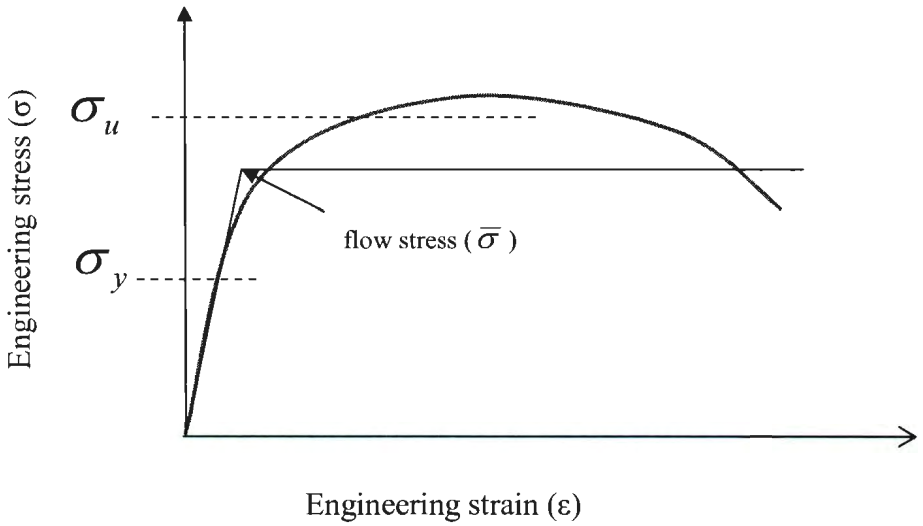

Figure 2.10: Flow stress modeling of stress-strain behavior in pipeline

If equation (2.29) is plotted for part wall defects the following curves may be available for the ductile linepipe as given in Figure 2.11. These curves are considered 'universal' assessment curves where a pipeline with a defect depth of (1-(d/t)) and length of (2c/(Rt)0.5) will fail if the applied hoop stress is more than the calculated stress. Figure 2.12 is a simple summary of equations (2.25) and (2.26), showing the leak-rupture boundary for through wall defect.

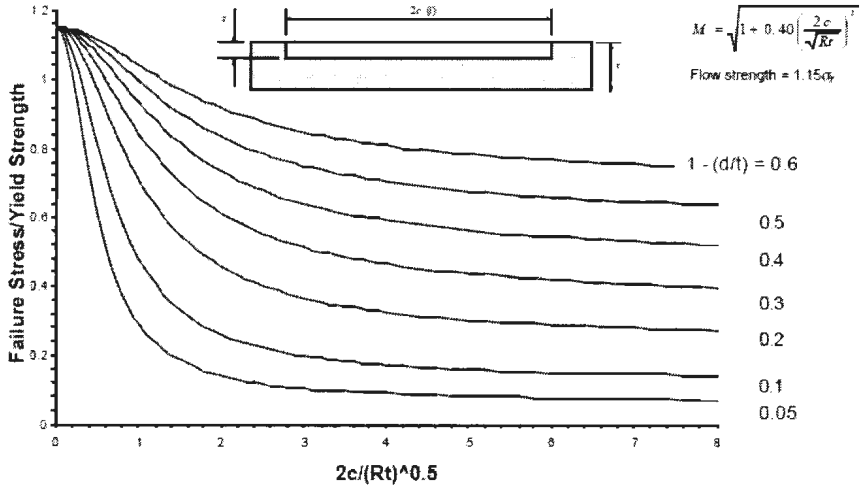

Figure 2.11: Failure Stress of Part Wall Defects in Ductile Pipeline[39]

2.6 Conclusion

There is not much work done on risk-based design though it represents a comprehensive scenario of cost issues of a project which is not truly reflected in reliability-based design [40]. There has been little work done on risk-based design. Most of the work [41-46] has considered risk assessment, risk-based inspection, and risk-based

design for hydraulic engineering. As the area is still in its infancy stage there is much scope to work on ris-based design. The present study will mainly concentrate on failure probability assessment of pipeline steel under different degradation mechanism.

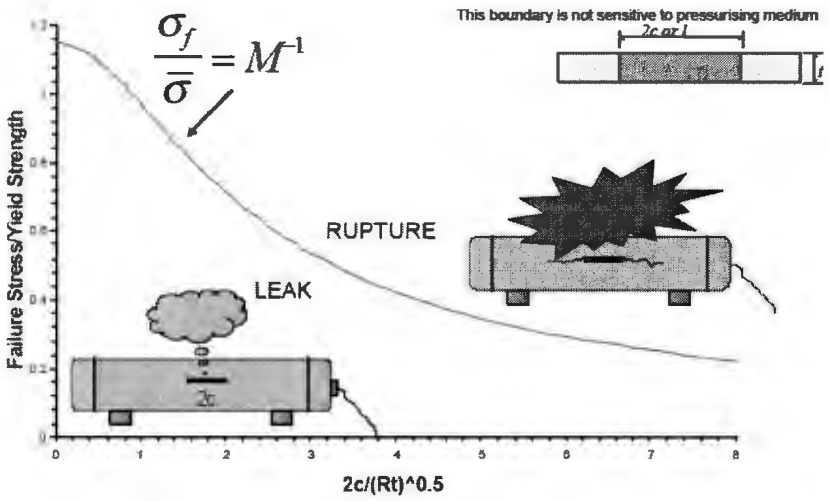

Figure 2.12: Leak/Rupture behavior of Through- wall Defects in Ductile Pipeline [39]

2.7 References

[1] Pugsley, A.G. (1951). *Concepts of Safety in Structural Engineering Proceedings.* Institute of Civil Engineers.

[2] Freudenthal, A.M., Garrelts, J.M., & Shinozuka, M. (1966). The Analysis of Structural Safety. *ASCE Proceedings.*

[3] Ravindra, M.K. & Galambos, T.V. (1978). Loads and Resistance Factor Design for Steel. *ASCE, Journal of Structural Engineering*, Vol. 104, No. ST9.

[4] CSA-S16.1. (1994). *Limit States Design of Steel Structures*. Canadian Standards Association, Rexdale, Ontario.

[5] CSA-A23.3. (1994). *Design of Concrete Structures for Buildings*. Canadian Standards Association, Rexdale, Ontario.

[6] Hasofer A. M., & Lind N. C. (1974). Exact and Invariant Second Moment Code Format. *Journal of the Engineering Mechanics Division*, ASCE Vol. 100, No EM1, pp. 111-121

[7] Rackwitz R., & Fiessler B. (1978). Structural Reliability Under Combined Random Load Sequenc. *Computer and Structure,* Vol. 9, No., 5, pp. 484-494.

[8] DnV. (1989). *Rules for Classification of Fixed Offshore Installations*. Det norske Veritas Classification A/S.

[9] CSA-S6. (1988). *Design of Highway Bridges*. Canadian Standards Association, Rexdale, Ontario.

[10] Nessim, M. A. & Hong, H. P. (1993). Load Factors Used in the Design of CANDU Concrete Containment Structures. *Submitted to Atomic Energy Control Board*, C-FER Report 93005.

[11] Henderson, CA. & Nessim, M.A. (1990). Probabilistic Analysis of Arctic Gas Pipelines Subject to Thaw Settlement. *Submitted to Esso Resources Canada Limited*, C-FER Report 89-24

[12] Sotberg, T. (1990). *Application of Reliability Methods for Safety Assessment of Submarine Pipelines*. Norwegian Institute of Technology, Trondheim, Norway.

[13] Gresnigt, A. M. (1986). *Plastic Design of Buried Steel Pipelines in Settlement Areas*. Heron.

[14] Row, D.G., Hollings, J.P., Sause, R. & Der Kiureghian, A. (1987). Design Criteria for Offshore Arctic Pipelines. *ASME Pipeline Engineering Symposium*, Dallas.

[15] Zimmerman, T.J.E., Price, P.St.J., Colquhoun, I.R. & Smith, R.J. (1992). Development of a Limit States Guideline for the Pipeline Industry. *Proceedings of the 11th International Conference on Offshore Mechanics and Arctic Engineering*.

[16] CSA 2662. (1996). *Oil and Gas Pipeline Systems*. Canadian Standards Association, Rexdale, Ontario.

[17] ASME B31.8 (1995). *Gas Transmission and Distribution Piping Systems*. American Society of Mechanical Engineers (ASME).

[18] ASME B31G (1991). *Manual for determining the Remaining Strength of Corroded Pipelines*. A Supplement to ASME B31 Code for Pressure Piping, American Society of Mechanical Engineers (ASME)

[19] Dawson, S.J. & Clyne, A. J. (1997). *Probabilistic Approach to Pipeline Integrity*. UK: The Aberdeen Exhibition and Conference Centre.

[20] Safian M. A., (2006). *Integrity Assessment Of Corroded Pipeline Using In-Line Inspection Data*. Universiti Teknologi Malaysia, Malaysia.

[20a] Xiaoping Du, (2005). First Order and Second Reliability Methods (pdf). Retrieved from http://web.mst.edu/~ccli/me360/ch7.pdf

[20b] Du X., Chen W., & Wang Y., (2010). Most Probable Point-Based Methods. *Extreme Statistics in Nanoscale Memory Design*, Springer

[21] Rosenblatt, M., (1952). Remarks on a Multivariate Transformation. *Annals of Mathematical Statistic*, Vol. 23, 1952, pp. 470-472.

[22] Chen, X., & Lind N. C. (1983). Fast Probability Integration by Three-Parameter Normal Tail Approximation. *Structural Safety,* Vol. 1, pp. 269-276.

[23] Fiessler B., Neumann H. J., & Rackwitz R. (1979). Quadratic Limit State in Structural Reliability. *Journal of the Engineering Mechanics*, ASCE Vol. 1095, No 4, pp. 661-676

[24] Breitung K. (1984). Asymptotic Approximations for Multinomial Integral. *Journal of the Engineering Mechanics*, ASCE Vol. 110, No 3, pp. 357-366

[25] Hohenbichler M., Gollwotzer S., Kruse W., & Rackwitz R. (1987). New Light on First and Second Order Reliability Method. *Structural Safety*, Vol. 4, pp. 267-284

[26] Robert H. R., Vesely W. E., Hasst D. F., & Goldberg F. F. (1981). *Fault Tree Handbook.* US Nuclear Regulatory Commission, NURE G-0492

[27] Levine S., & Vesely W. E. (1976). Important Event Tree and Fault Tree Considerations in the Reactor Safety Study. *IEE Transaction on Reliability*, R-25, pp132-139.

[28] J. F. Kiefner and P. H. Vieth, (1989). *A modified criterion for evaluating the remaining strength of corroded pipe.* Final report on PR 3-805 to Pipeline Corrosion Supervisory Committee of the Pipeline Research Committee of the American Gas Association, Battelle, Ohio.

[29] Escoe A.K. (2006). *Piping and Pipeline Assessment Guide*, Elsevier.

[30] DNV RP-F101 (2004). *Corroded Pipelines*. Recommended Practice.

[31] API -579 (2000). *Recommended Practice for Fitness for Service.*

[32] BS 7910 (2000). *Guide on Methods for Assessing the Acceptability of Flaws in Metallic Structure*. British Standards Institute,

[33] Cronin D.S., & Plumtree, A. (2007). *Assessment of Crack in Corrosion Defects in natural Gas Transmission Pipeline.* Confidential report to TCPL.

[34] ASME B31G, (1995). *Manual for determining the remaining strength of corroded pipelines*. A supplement to ANSI/ASME B31 code for pressure piping.

[35] CSA Z662-07 (2007). *Oil and Gas Pipeline Systems*. Canadian Standards Association.

[36] Netto T. A., Ferraz U. S., & Estefan S. F. (2005). The Effect of Corrosion Defect on The Burst Pressure of The Pipeline. *Journal of Constructional Steel Research*, Vol 61 pp 1185-1204

[37] Hasan, M., Khan, F., & Kenny, S. (2011). Identification of the Cause of Variability of Probability of Failure for Burst Models Recommended by Codes/Standards. *Journal of Pressure Vessel and Technology*, vol. 133, n. 041101.

[38] Hosseini S. A. (2010). *Assessment of Crack in Corrosion Defects in Natural Gas Transmission Pipelines*. University of Waterloo, Ontario, Canada.

[39] Hopkins P. (2002). The Structural Integrity Of Oil And Gas Transmission Pipelines. *Comprehensive Structural Integrity* Volume 1, Elsevier, UK.

[40] Chen Q. (1994). *Risk Based Calibration of Reliability Levels for Limit State Design of Pipelines*. National Energy Board

[41] Pula R., Khan F. I., Veitch B., & Amoytte P. R. (2005). Revised Fire Consequence Models for Offshore Quantitative Risk Assessment, *Journal of Loss Prevention in the Process Industries*, v 18, n 4-6, p 443-454

[42] Turner I. Y., Barrientos F. A., & Mehr, A. F. (2005). Towards risk based design (RBD) of space exploration missions: A review of RBD practice and research trends at NASA. *Proceedings of the ASME International Design Engineering Technical Conferences and Computers and Information in Engineering Conference* - DETC2005, v 4, p 687-695

[43] Dinovitzer A., Comfort G., Lazor R., & Hinnah, D. (2004). Offshore Arctic Pipeline Oil Spill Risk Assessment, *Proceedings of the International Conference on Offshore Mechanics and Arctic Engineering*, v 3, p 113-121

[44] Bellendir E.N., Glagovsky V. B., & Finagenov O. M. (2006). Conceptual Risk Assessment of Offshore Structures. *Proceedings of the International Offshore and Polar Engineering Conference*, p 411-417

[45] Khan F. I., Sadiq R., & Haddara M. M. (2004). Risk-Based Inspection And Maintenance (RBIM) Multi-Attribute Decision-Making with Aggregative Risk Analysis. *Process Safety and Environmental Protection*, v 82, n 6 B, p 398-411

[46] Faber M. H., Straub D., Goyet J. (2003). Unified Approach to Risk-Based Inspection Planning for Offshore Production Facilities. *Journal of Offshore Mechanics and Arctic Engineering*, v 125, n 2, p 126-131

Chapter 3

Risk-based Design

3.1 General

The strength of a pipeline deteriorates due to corrosion damage, and becomes weaker with increasing age. Hence, the remaining strength of the pipeline needs to be estimated by adopting suitable methods. Three levels of structural failure probability [1,2] may be considered to assess remaining strength and associated risk.

Level 1 - A semi-probabilistic approach where the characteristic values of loads and resistance are defined (referred to 95% fractile value) and combined with partial safety factors (load or resistance factors).

Level 2 - A probabilistic design approach with some approximation. The loads and resistance are represented by respective distributions (defined in terms of relative parameters such as type, mean and standard deviation) and failure probability is assessed using First Order Reliability Method (FORM) or Second Order Reliability Method (SORM).

Level 3 - A probabilistic approach where each parameter of load and resistance is defined in the limit state with respective distribution and failure probability is assessed using the Monte Carlo method. The coding is developed in the MATLAB platform for each individual failure analysis.

The detail of Level 2 is discussed in Chapter 2. Since Level 1 is a basic approach, the risk-based design methodology is discussed based on the level 1 approach.

3.2 Load And Resistance Categories

Before starting risk based design it is important to categorize loads and resistances related to a pipeline system. The loads for pipeline design may be classified into the following categories:

- Permanent loads, G
- Operational loads, Q
- Environmental loads, E
- Accidental loads, A

Permanent loads, G: these are loads that remain constant for long periods of time. The material properties and geometry described in the design may be considered in the determination of the permanent load. The following permanent loads may be considered in the limit state [1]:

(a) pipeline self-weight;
(b) the weight of pipe coatings;
(c) the permanent overburden loads;
(d) external hydrostatic pressure; and
(e) pre-stressing (cold-sprung induced forces).

Operational loads, Q: these are loads associated with operational activities in the design phase. Operational loads may be determined with due consideration to relevant design

documentation, operational requirements, and the seasons. These are generally variable with respect to time and include [1]:

(a) internal pressure,
(b) the weight of contained fluids,
(c) thermal forces due to construction-operation temperature differential,
(d) the weight of temporary equipment,
(e) the variable portion of overburden loads.

Environmental loads, E: these are caused by environmental processes. They are generally variable with respect to time and include [1]:

(a) variations in the ambient temperature
(b) ground movements (differential settlement or heave, slope failure etc.)
(c) wind
(d) waves, tide and currents
(e) earthquakes and earthquake related effects
(f) snow and ice accumulation
(g) marine growth
(h) icebergs and sea ice.

The determination of the environmental load requires careful selection. The details are available in the codes; however, a comprehensive understanding is also available in the reference mentioned earlier. Consult [3] for geotechnical load, [4,5a,5b] for wind load, [4,6,7] for wave and current loads, [6] for ice load, and [3] for seismic load.

Accidental loads, A: these are based on accidental events. They include loads caused by outside forces during construction and operation. They include:

(a) outside force during construction and operation,

(b) fire and explosion, and

(c) loss of pressure control.

In addition to these four load categories, loads may be divided into primary loads and secondary loads.

Primary Loads: These loads are independent of structural deformations and induce the internal force necessary to satisfy the law of static equilibrium. The internal forces act as long as the loads are applied and do not diminish when yielding occurs. Some examples of primary loads are: internal pressure, external pressure, self weight of the pipe and its contents, soil overburden etc.

Secondary Loads: These loads are induced by structural deformations (or the prevention thereof) and satisfy the laws of compatibility of strains and deformations. The internal forces induced by secondary loads diminish when yielding occurs. Examples of secondary loads include differential temperature loads in restrained pipe sections and bending caused by ground movements.

3.3 Risk-Based Design Methodology

The risk based design methodology of the present research work is framed in the flow chart shown in Figure 3.1. The flow chart in Figure 3.1 may be divided into four segments.

Part I: Define Load and Resistance

Part II: Risk Estimation

Part III: Component Risk Evaluation

Part IV: Detail design

3.3.1 Part I: Define Load And Resistance

The load and resistance may be defined considering the level 1 design approach commonly known as limit states design (LSD) or load and resistance factored design (LRFD) as given in Figure 3.2. In the limit states design the factored load and resistance are obtained by multiplying characteristic load and resistance values with safety factors α and ϕ respectively. The basic design equation is given by:

$$\phi R \geq \sum_{i=1}^{n} \alpha_i L_i \qquad (3.1)$$

where ϕR represents the factored resistance, and $\alpha_i L_i$ represents the factored load effects. It may be noted that many loads may act simultaneously on the structure. The characteristic values of load and resistance are selected on the basis of probabilistic criteria. The load factor, α , is generally > 1.0 and the resistance factor, ϕ, is generally < 1.0. Many limit states design codes include *class factor* γ to account for the severity of the consequences of the failure. The class factor introduces the criticality to reduce the chance of damage to human life or the environment. The basic design equation becomes:

$$\phi R \geq \gamma \sum_{i=1}^{n} \alpha_i L_i \qquad (3.2)$$

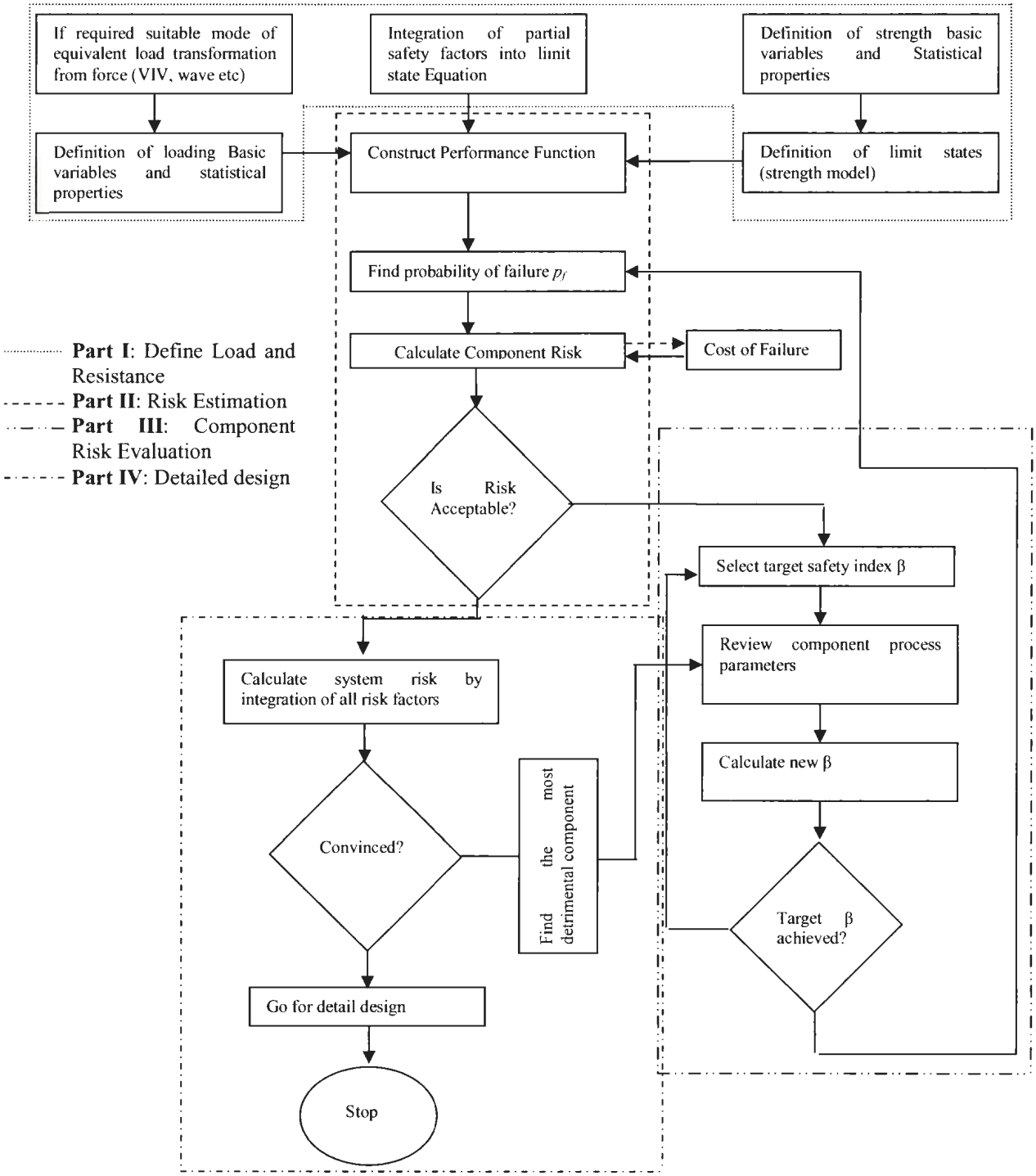

Figure 3.1: Flow chart for risk based design methodology.

Higher safety class factors are considered for densely populated areas than for low density areas. Again the pipelines that transport toxic or explosive gases have a higher safety class factor than those of low vapor pressure fluids.

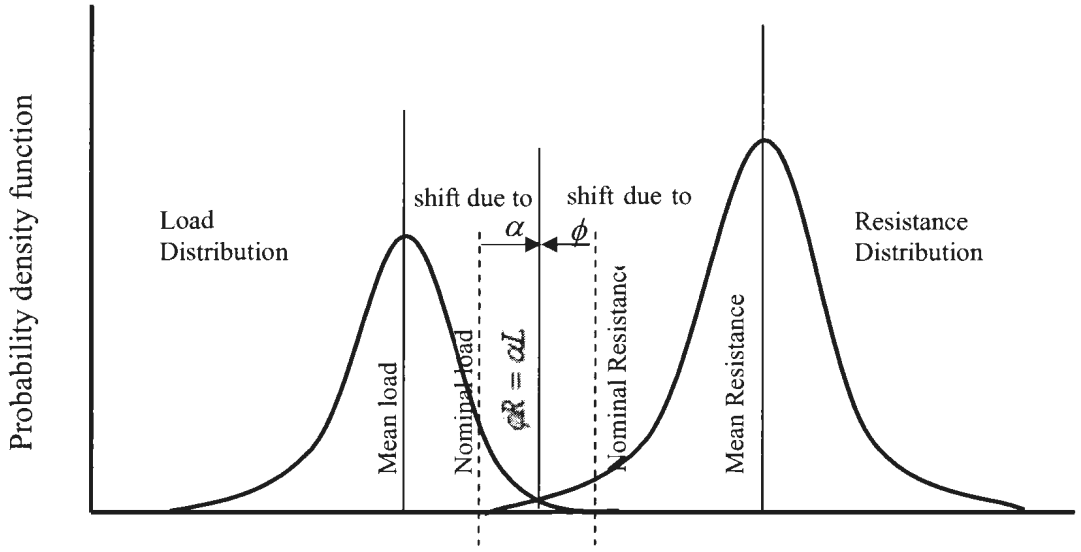

Figure 3.2: Load and Resistance factor and frequency distribution [1]

Equation (3.2) may be further expanded to show the individual component of load:

$$\phi R \geq \gamma(\alpha_G G + \alpha_Q Q + \alpha_E E + \alpha_A A) \qquad (3.3)$$

where ϕ = resistance (strength) factor

R= characteristic resistance or strength

γ = safety class factor

α_G, α_Q, α_E, α_A = load factors for G, Q, E and A load effects, where G, Q, E, and A = permanent, operational, environmental and load effects respectively.

Figure 3.3 depicts the limit state design methodology used in the Canadian Code [2]. The safety class factor γ is given in Table 3.1 and Table 3.2 and partial load factor α_G, α_Q, α_E, α_A in Table 3.3. The resistance factor ϕ is given in Table 3.4. The safety class factor can vary along the length of the pipeline. Figure 3.4 is a possible relationship between the safety class factor, human exposure and target values of annual reliability [2].

Table 3.1: Safety Class [1]

Recommended LSD designation		Area Type		
Safety Class	Number of Dwelling units (1.6 km ×400 m area)		Location class	Number of Dwelling units (1.6 km ×400 m area)
1	0 to 10	Rural, remote	1	0 to 10
2	10 to 100	Suburban fringes, industrial	2	10 to 45
3	100 to 1000	Suburban, residential	3	46
4	>1000	Urban, heavy traffic	4	multistory

Table 3.2: Safety class factors for ultimate limit states [2]

Class location	Gas sour service	Gas (non-sour)	HVP and CO_2	LVP
1	1.1	1.0	1.0	1.0
2	1.3	1.1	1.2	1.0
3	1.6	1.4	1.2	1.0
4	2.0	1.8	1.2	1.0

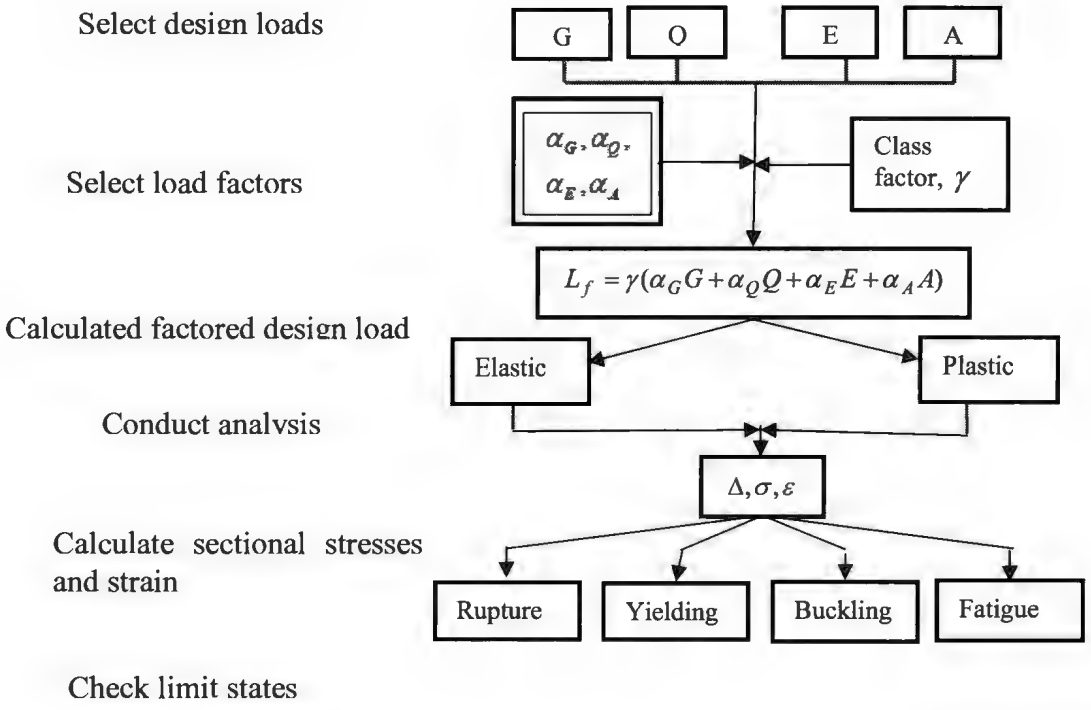

Figure 3.3: LSD method [2]

Table 3.3: Load factor values [2]

	Load Factors				
	α_G	α_Q		α_E	α_A
Load Combinations		Pressure	Other		
ULS 1: Max Operating	1.25	1.13	1.25	1.07	0
ULS:2 Max environmental	1.05	1.05	1.05	1.35	0
ULS 3: Fatigue	1.0	1.0	1.0	0	1.0
ULS 4: Fatigue	1.0	1.0	1.0	1.0	0
SLS	1.0	1.0	1.0	1.0	0

Table 3.4: Resistance factor [1]

Resistance parameter	Resistance factor, ϕ
Yield strength, ϕ_y	0.9
Stability, ϕ_c	0.7
Tensile strain, ϕ_{st}	0.7
Compressive strain, ϕ_{sc}	0.8

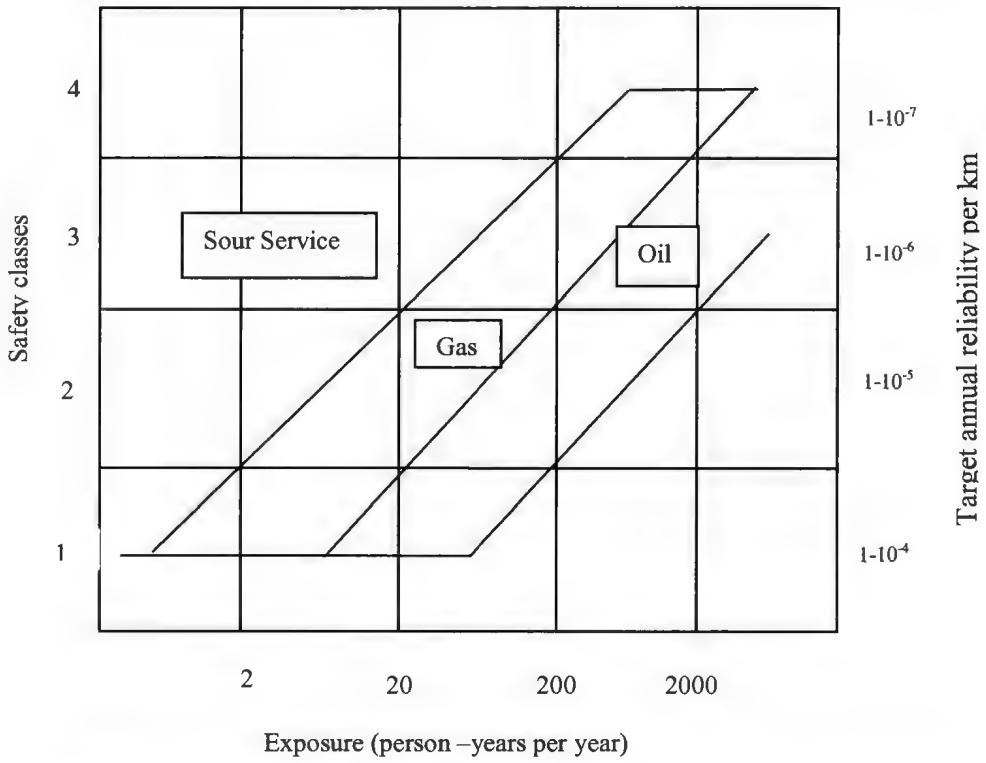

Figure 3.4: Safety class factor related to target annual reliability [2]

3.3.2 Part II: Risk Estimation

Assessment of Structural Failure Probability (P_f): The distribution of stresses, strains, or any other kind of displacements in the pipeline should be determined from

principles of statics, dynamics, or kinematics. The selection of a model (elastic or plastic analysis) should be based on specified material properties and material behaviors. In many design situations the primary load is the internal pressure and the other loads are considered secondary load. The elastic analysis therefore, may be conservative, as it does not recognize the ability of the pipe to plastically deform and still maintain pressure integrity. A plastic design approach does recognize such behaviors, and can therefore be used to get an advantage. The analysis also should consider the restraint boundary conditions if available in an axial or lateral direction.

Consequence Analysis (C_f): the consequence analysis is concerned to see the severity of adverse effects of accident on people, property, the environment, or combination of thereof. Consequence analyses predict the magnitude of the effects resulting from release of toxic or flammable fluids and disruption of pipeline throughput.

Risk Estimation: risk estimation involves combining the results of frequency and consequence analysis to produce a measure of risk. The risk associated with a pipeline failure can be expressed as:

$$Risk = P_f \times C_f$$

where R is the annual risk, P_f is the annual failure probability considering all causes, and C_f is a measure of the consequences of failure. A risk matrix may be constructed as given in based on the calculated probability of failure and consequence.

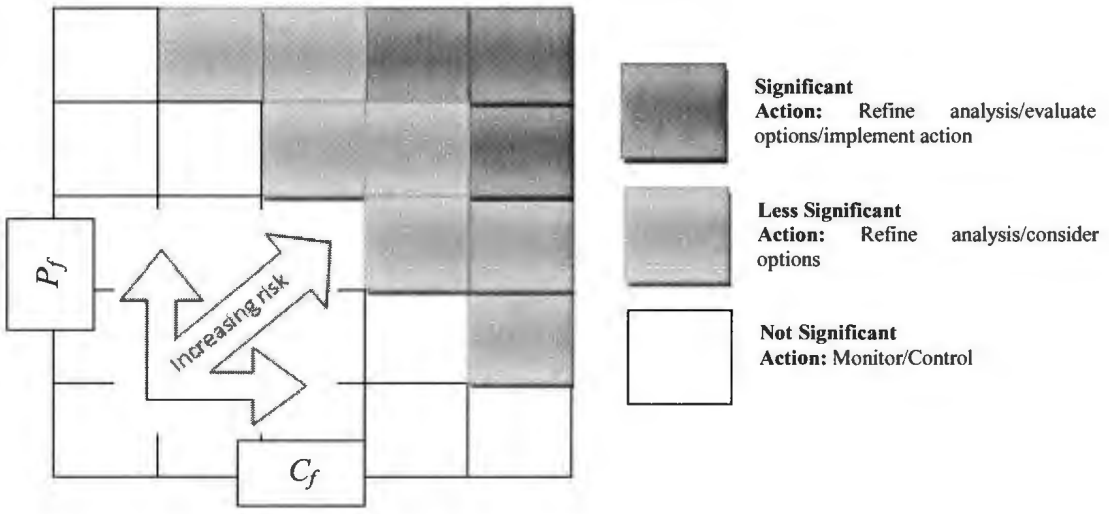

Figure 3.5: Sample Risk Matrix

3.3.3 Part III: Component Risk Evaluation

Risk analysis provides the most consistent and rational basis for selecting target reliability levels, based on criteria such as economic optimization, safety, and environmental protection. On the basis of probability and consequence analyses, a target reliability can be selected either to meet a predetermined acceptable risk level or to optimize the total cost considering the cost of failure. The details of economic optimization, life safety, and environmental protection may be consulted from Zimmerman et. al. [1] and references [8,9]. Zimmerman et. al. [1] recommend the following steps for risk evaluation

Consequence optimization. This includes the initial cost associated with a given level of reliability and the expected cost of possible failures. An optimum value of the failure probability is determined by minimizing the total expected loss.

Fixed cost versus benefit ratio. This is a cost benefit ratio approach where the incremental cost and incremental reduction of failure probability are considered. Thus the reliability level is selected based on an acceptable cost-benefit ratio.

Fixed risk level. This approach is based on acceptable level of risk which can be determined by following the acceptability guidelines, or by calculating the societal risks that are acceptable. For example, by examining the risk related to the failure of other structures, the acceptable level of life risk associated with pipeline failures can be reasonably established.

The best choice among these methods depends on the criteria used to measure consequences. For instance, consequence optimization can be used when the analysis is carried out in economic terms. On the other hand, a fixed risk level may be more suitable for the analysis of safety. If the estimated $Risk = P_f \times C_f$ is not convincing, the process parameters (D, t, and σ for pipeline) may be revised to meet the target safety level.

3.3.4 Part IV: Detailed Design

Up to this point the methodology calculates risk for a single mode of failure. Like- wise the risk for all modes of failure will be determined to calculate combined risk. Once the risks for all failure modes are evaluated, FTA will be considered to calculate system risk. Thus, unified risk will be minimized for individual components by achieving the target safety level of the system.

If the designer is not satisfied with the system risk overall, the next option is to review the process component parameters. Find the most detrimental risk component

responsible for system risk. Change the design parameters. If the designer is convinced with the revised overall risk, the next task is to go for detailed design.

It might be noted that the risk-based design methodology is applicable for both onshore and offshore pipeline design with careful consideration of local environmental condition, pipeline steel material, loading condition etc. For example, in SCC analysis, the local pH at the soil determines whether the pipeline is subjected to transgranular stress corrosion cracking (SCC) or intergranular SCC. High strength low alloy (HSLA) steel might be more susceptible to SCC compared to carbon steel.

3.4 Algorithm of Risk-Based Design

The algorithm is based on the framework developed in Figure. 3.1

Step1: generate a random variable considering distribution and characteristics values with the required confidence level for both load and resistance.

Step2: construct the limit state such as $Z = g(R,S) = R - S$ for load and resistance and calculate the probability of failure using the equations $\beta = \frac{\mu_Z}{\sigma_Z}$ and $p_f = 1 - \Phi(\beta)$. The mean and standard deviation will be calculated using FOSM, AFOSM or the SORM method whichever is applicable

Step3: Apply Monte Carlo simulation to calculate probability of failure which is calculated with a probabilistic approach.

Step4: Calculate risk using the equation, $Risk = P_f \times C_f$

Step5: If risk is high, review design parameters of the component and recalculate the risk.

Step6: Up to this step, this is a component design for a specific mode of failure. Now, likewise calculate all other modes of failure.

Step7: Integrate the failure modes using FTA with the necessary correlation between the failure modes. If there is no correlation, assume independent failure modes. Find a single probability of failure for a process system.

Step8: If risk is not acceptable find the most detrimental failure modes and adjust the design parameters of the respective component. Continue the iterative procedure until the target safety level is reached. The specified design parameters at this stage where the target safety level is meet, will be used for final design and construction.

3.5 References

[1] Zimmerman T. J. E, Chen Q., & Pandey M. D. (1997). *Limit State and Reliability Based Pipeline Design.* PR-244-9517. A PRCI Publication.

[2] Mohitpour M., Golshan H., & Murray A. (2003). *Pipeline Design & Construction.* pp 345-348 ASME press USA.

[3] *Guidelines for the Seismic Design of Oil and Gas Pipeline Systems* (1984). American Society of Civil Engineers (ASCE)..

[4] RP 2A-LRFD, (1993). *Recommended Practice for Planning, Designing and Constructing Fixed Offshore Platforms - Load and Resistance Factor Design.* American Petroleum Institute (API).

[5a] NBC (1995a). *National Building Code of Canada.* National Research Council of Canada.

[5b] NBC (1995b). *Supplement to the National Building Code of Canada.* National Research Council of Canada.

[6] CSA-S471, (1992). *General Requirements, Design Criteria, the Environment, and Loads.* Forming Part of the Code for the Design, Construction, and Installation of Fixed Offshore Structures. *Canadian Standards Association*, Rexdale, Ontario.

[7] DnV. (1981). *Rules for Submarine Pipeline Systems.* Det Norske Veritas Classification A/S. Reprint 1993.

[8] CSA-S408 (1981). *Guidelines for the Development of Limit States Design.* Canadian Standards Association. December.

[9] CIRIA Report 63 (1977). *Rationalization of Safety and Serviceability Factors in Structural Codes.* London.

Chapter 4

Probability Assessment of Burst Limit State Due to Internal Corrosion*

Preface

This chapter provides an extensive review of recommended burst models of codes/standards. The internal corrosion defect is characterized and failure probability is assessed. A version of this manuscript has been published in international *Journal of Pressure Vessels and Piping.*

The co-authors, Dr Khan and Dr. Kenny supervised the principal author, Hasan, to develop the research on the entitled topic. The principal author identified theories and techniques available on this topic. The principal author conducted failure analysis and analyzed relative conservatism of the recommended models. The co-authors reviewed the manuscript and provided necessary suggestions and comments to improve the quality of the manuscript.

*this paper has been published in International Journal of Pressure Vessels and Piping; the reference is provided below.

Hasan, M., Khan, F., Kenny, S., (2012). *Probability Assessment of Burst Limit State Due to Internal Corrosion*, International Journal of Pressure Vessels and Piping 89 (2012) pp 48-58

Abstract:

The failure probability of an oil and gas pipeline, with longitudinally oriented internal corrosion defects, due to burst from internal operating pressure, can be estimated through characterization of defect geometry, internal corrosion growth rate, and remaining mechanical hoop strength capacity. A number of candidate models to estimate the corrosion defect depth growth rate were evaluated. Defining a corrosion defect length, the corrosion feature geometry was integrated within burst pressure models, which have been adopted by oil and gas industry standards, codes and recommended practices. On this basis the burst pressure failure probability of a pipeline with internal corrosion defects can be estimated. A comparative analysis of pipe burst limit states and failure estimates was conducted, using Monte Carlo simulation and First Order Second Moment (FOSM) methods. Results from the comparative analysis closely matched and demonstrated consistent trends. Based on the probabilistic assessment, the relative conservatism between burst pressure models was analyzed and recommendations provided to assist designers in model selection.

Key words: Internal corrosion, First Order Second Moment, Monte Carlo, Probability of failure, limit state function etc.

Nomenclature

σ_u	specified minimum tensile strength of pipe material, SMTS
σ_y	specified minimum yield strength of pipe material, SMYS
σ_{hip}	hoop stress of intact pipe
σ_{xip}	axial stress of intact pipe
σ_{hdp}	hoop stress of defected pipe
σ_f	flow stress
D	outside diameter of pipeline
t	thickness of pipeline
l	length of internal corrosion defect
l_c	characteristic length of internal corrosion defect
d	depth of internal corrosion defect
d_c	critical defect depth of internal corrosion defect considered for Kale et al [11]
c	width of internal corrosion defect
F	design factor
P	internal pressure
P_{yip}	yield pressure of defect free intact pipe
P_{bdp}	burst pressure of defected pipe
P_{op}	operating pressure
A_c	actual longitudinal corroded area
A_o	original area
M	Folias factor/stress concentration factor
da/dt	internal corrosion rate mm/yr

4.1 Background

The production and transportation of hydrocarbon from offshore facilities involves a complex process system. The components in such a process system are exposed to extreme operating and environmental conditions. Therefore, proper identification of risk sources, quantification of their magnitude, and incorporation of risk in the designing of the process component are necessary to improve operations and maintenance practices, and to mitigate the frequency of catastrophic system failures.

A research program is currently developing a risk-based design framework for a process system. Part of the work scope is to collate available engineering models defining time dependent failure mechanisms (e.g. internal corrosion, external corrosion, stress corrosion cracking, fatigue) and to conduct a deterministic and probabilistic failure assessment of pipeline. The conceptual risk-based design framework is summarized in Figure 4.1. In Figure 4.1 risk, rather than reliability, is optimized in a process system. The risk estimate for different failure scenarios will be integrated using fault tree analysis to obtain the overall risk of the process system. The unified risk will be minimized to design individual components and thus achieve the system target safety level.

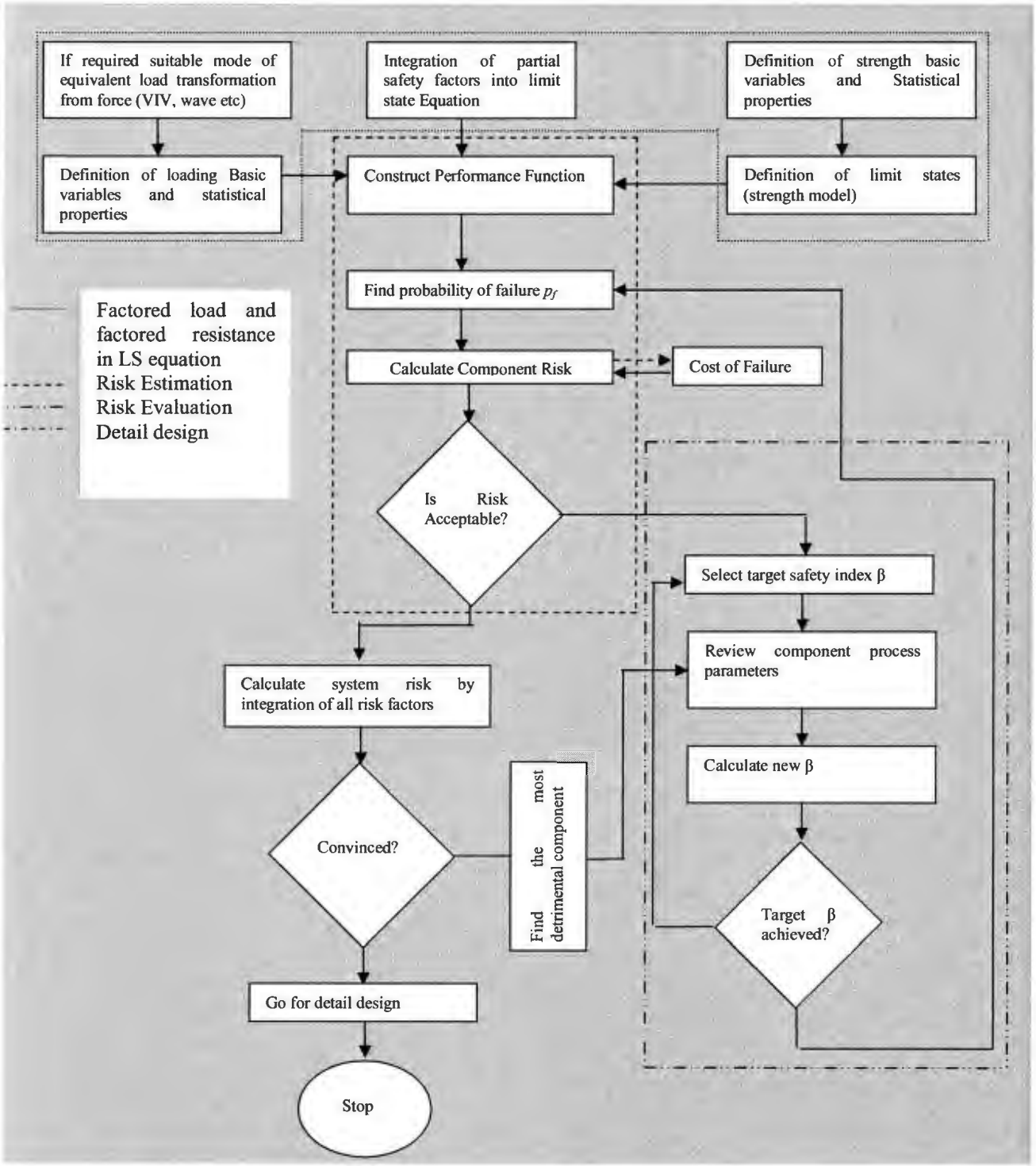

Figure 4.1: Risk based design methodology

Pipe wall thinning due to internal corrosion mechanisms and loss of pressure containment function due to burst (i.e. leak or rupture) are significant operational hazards for pipelines. This study is focused on estimating the probability of pipe failure due to burst associated with internal corrosion mechanisms. There exist a number of engineering models characterizing defect geometry, defect evolution and growth rate, significance of defects on local stress concentrations, and strength reduction for pressure containment. For model selection, the question remains with respect to data and model uncertainty, and utility with respect to practical application. For example, Law and Bowie [1] examined a number of engineering models predicting pipe burst limits for defect-free pipe with high yield-to-tensile strength ratio material. The study found significant scatter in comparison with experimental data and identified several candidate models for predicting failure pressure but no reliable methods for predicting failure strain. One of the key factors was variation in the reference stress calculations assumed in each model. Uncertainty in existing models, which may be conservative or exhibit significant scatter, in addressing failure pressure and pipe burst for higher grade materials has also been identified [2]. The analysis presented in this paper illustrates that there exists a variability in the burst pressure prediction for a pipeline having the same defect geometry and material properties. Since accurate prediction of remaining strength is crucial in the engineering integrity assessment of pipelines, there should exist consistency among the models [3] in predicting the remaining strength.

This study investigates the suitability of available internal corrosion models and pipe burst models, as adopted by codes, standards or recommended industry practice, to answer these questions and address these issues within a risk based framework. This paper focuses on internal corrosion defect models for low grade (X65) ductile pipe material and examines the failure probabilities due to the pipe burst mechanism. Similar studies have been conducted examining other materials (i.e. AISI 1020 mild steel) while focusing on a single code of practice [4].

4.2 Internal Corrosion

Subsea pipelines provide an efficient, safe and reliable mode of transportation of hydrocarbons. The transmitting product may carry corrosive elements such as water, carbon dioxide, hydrogen sulfide and sulphate reducing bacteria. The growth of corrosion defects in a pipeline is time dependent and hence may become a potential threat to pipeline integrity as the pipeline ages. The knowledge of the remaining pipeline strength for hoop pressure containment is required to assess the safe mode of operation of the transmitting fluid. Several engineering models have been developed to calculate the remaining pipeline hoop strength. These models have been developed through physical testing or numerical simulation [5,6].

Internal corrosion initiates defects which may be distributed in the radial, circumferential and axial directions. In general the internal corrosion defect is defined by length (l) and depth (d) as these represents the worst case scenario with respect to the applied hoop stress. The circumferential extent of the defect geometry has been typically

ignored. The defect profile is generally idealized rectangular or parabolic geometric shapes [7-10].

4.2.1 Pressure Calculation of Defect Free Pipe

Consider a defect free circular pipe as specified by Figure 4.2. Depending on the *D/t* ratio, the pipe may be generally classified as either thin walled (D/t ≥ 20) or thick walled pipe. Considering the effect of internal pressure *P* (ignoring the external pressure effect), the Barlow's equation calculates tangential or hoop stress σ_{hip} as:

$$\sigma_{hip} = \frac{PD}{2t} \tag{4.1}$$

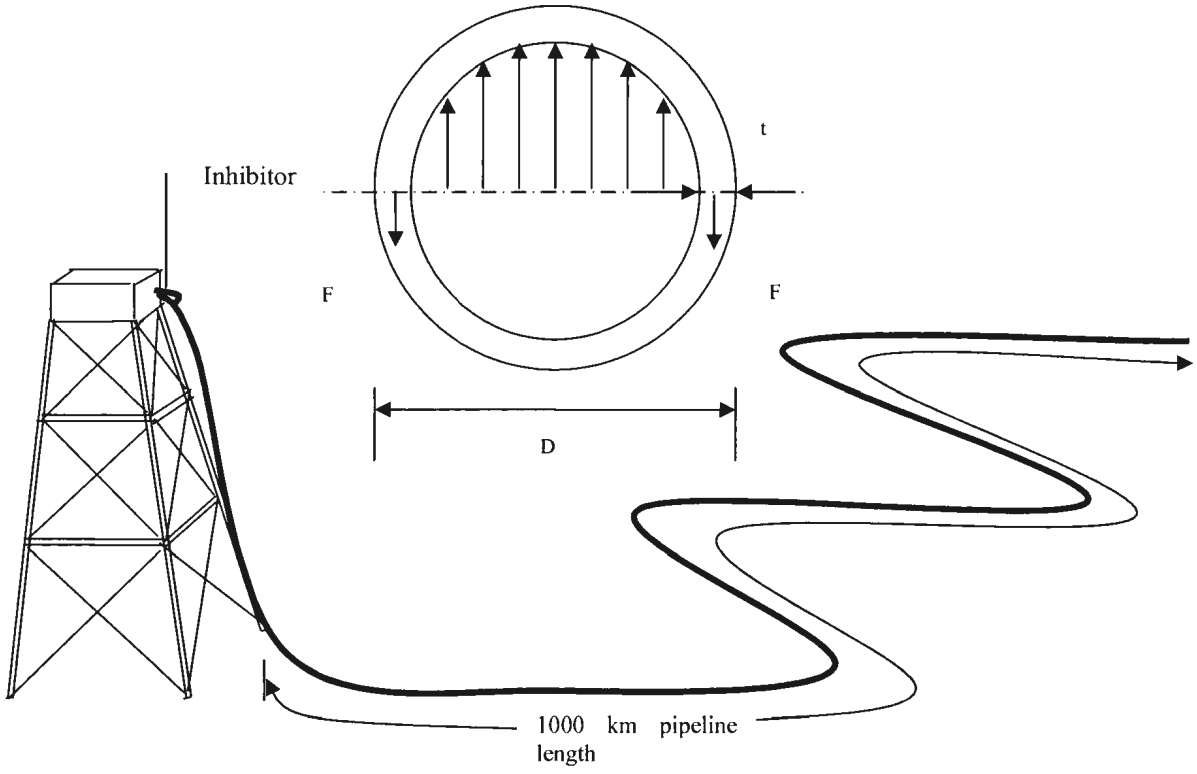

Figure 4.2: Force equilibrium in a pressurized thin pipe

If σ_{hip} is replaced by yield strength σ_y and a factor F is introduced, then the yield pressure for a defect free intact pipe (P_{yip}) is

$$P_{yip} = \frac{2\sigma_y t}{D} F \tag{4.2}$$

This is the burst pressure equation for an intact pipe (defect free) that is considered by most of the codes, standards [7-9] and models [10-11] with some minor adjustment. The value of F is adjusted to the design condition. For example, ASME B31G [9] assumes the value of F is 1.1, whereas DNV RP-F101 [8] assigns different values to F in relation to the safety class or design condition. It also considers ultimate strength instead of yield strength for intact pipe burst approximation, or in other words, flow stress approximation, of intact pipe.

4.2.2 Pressure Calculation for Defected Pipe

The strength of a pipeline deteriorates due to corrosion damage, and generally a pipeline becomes weaker with increasing age. Hence, the remaining strength of the pipeline needs to be estimated by adopting a suitable method.

Kiefner et al. and Shannon [12-13] have developed the following semi empirical model to calculate the remaining strength. This is the basic approach considered by most international codes and standards. For a longitudinally oriented corrosion defect, the remaining hoop stress at failure (σ_{hdp})can be estimated by

$$\sigma_{hdp} = \sigma_f \left[\frac{1 - \frac{A_c}{A_o}}{1 - \frac{A_c}{A_o M}} \right] \tag{4.3}$$

The bracketed term can be considered a strength reduction factor that accounts for the reduction in the pipe steel area available to resist internal pressure and the stress concentration or Folias factor (M). The corroded area can be approximated by parabola

$$\frac{A_c}{A_o} = \frac{(2/3)lD}{lt} = \frac{2d}{3t} \tag{4.4}$$

and the Folias factor defined as

$$M = \sqrt{\left[1 + \frac{0.8l^2}{Dt} \right]} \tag{4.5}$$

The burst pressure of a defected pipe is therefore

$$P_{bdp} = \sigma_{hdp} \frac{2t}{D} = \sigma_f \left[\frac{1 - \frac{A_c}{A_o}}{1 - \frac{A_c}{A_o M}} \right] \frac{2t}{D} \tag{4.6}$$

The flow stress (σ_f) is usually expressed in specified minimum yield stress times the design factor F; such as 1.1 times SMYS. Fabrication processes, material ageing and corrosion fatigue mechanisms can influence the flow stress.

In this paper, an approach has been developed that calculates the burst pressure for internal corrosion considering the rectangular and parabolic shaped defect ($l \times d$) and the corresponding failure probability of the pipeline, using available codes and standards

[7-9] and models [10-11, 14]. Among the engineering models considered in the present study, the RAM PIPE [11] models and Kale et al. [14] models account for the defect depth (d) only.

4.2.3 Corrosion Rate Equation

Corrosion in the pipeline occurs with the initiation of individual pits or colonies of pits, or in general wall thickness reduction. Figure 4.3 shows a single, longitudinally oriented, rectangular shaped internal corrosion defect. This type of defect occurs at a discrete location and is discontinuous throughout the pipeline length.

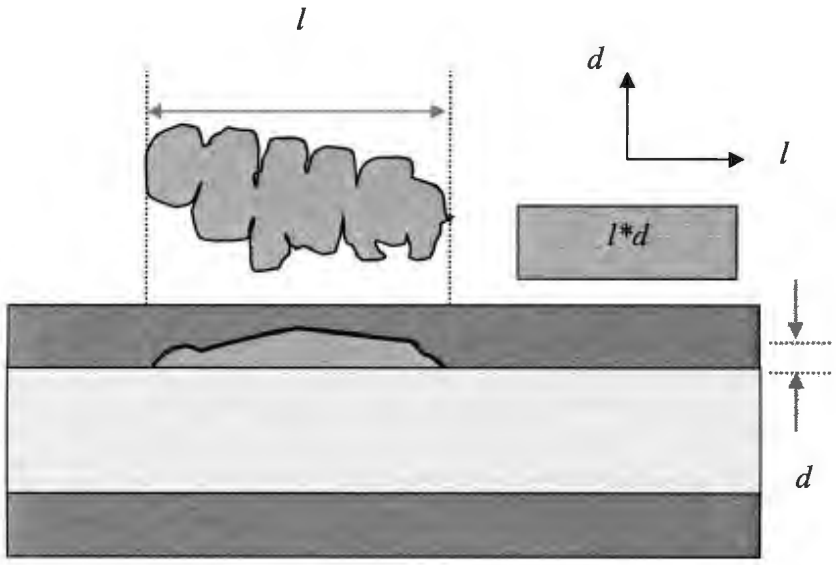

Figure 4.3: A simplified internally corroded surface flaw in a pipeline

4.2.3.1 Depth of Defect (*d*)

Different mathematical models for CO_2 corrosion are used by engineers in the oil and gas industry [15]. The NORSOK-model [16] was considered by Gartland et al. [17] for internal corrosion rate estimation. Three candidate corrosion rate models were considered by Kale et al. [14] including the de Waard-Millams Equation [18], de Waard-Lotz Equation [19] and SwRI [14] equation The first two equations were found to provide comparatively higher corrosion rates with lower correlation with data. Therefore, the third equation, developed by SwRI, is considered for rate estimation.

$$\frac{da}{dt} = k \times C_I \times 0.0254 \times \begin{pmatrix} 8.7 + 9.86\times10^{-3}(O_2) - 1.48\times10^{-7}(O_2)^2 - 1.31(pH) + 4.93\times10^{-2}(pCO_2)(pH_2S) \\ -4.82\times10^{-5}(pCO_2)(O_2) - 2.37\times10^{-3}(pH_2S)(O_2) - 1.11\times10^{-3}(O_2)(pH) \end{pmatrix} \quad \text{mm/year} \qquad (4.7)$$

$$C_I = 1 - e^{\left(-A\frac{L}{L_o}\right)} \qquad (4.8)$$

In Equation (4.7), pCO_2 is the partial pressure of carbon dioxide in the mixture, pH_2S is the partial pressure of hydrogen sulfide in the mixture, O_2 is the concentration of oxygen in parts per million, k is the modeling error, and C_I is the inhibitor correction factor given by Equation (8). Since the inhibitor's effect diminishes with the pipeline length (L), the inhibitor correction factor (C_I) uses an exponential model along the pipeline length. In Equation (4.8), A is the model parameter, L is the pipeline length and L_o is the characteristic length (hence L_o= 1000 km) to describe the effect of the inhibitor. The depth of defect (d) to wall thickness (t) ratio, $\frac{d}{t}$, and Std of $\frac{d}{t}$ are presented in

Figure 4.4, which describes the corrosion profile for the 1000 km pipeline length with the assumption of no velocity change, and no elevation change or other factors where preferential corrosion may occur in the pipeline route. The inhibitor effect is considered at the inlet and no other inhibitor injector was considered throughout the remaining pipeline length. Table 4.1 presents random variables with probabilistic data responsible for internal corrosion in a demonstrative pipeline scenario. The depth of defect (d) was calculated considering corrosion rate, da/dt, times T, a 20 years design life in this study.

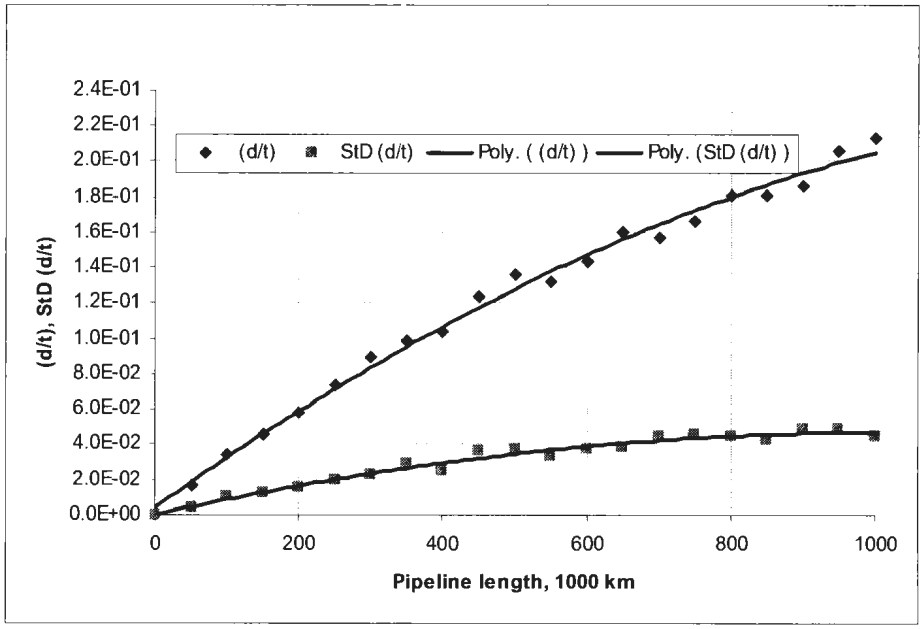

Figure 4.4: Increasing defect depth profile (injector's effect) over 1000 km pipeline length

Table 4.1: Probabilistic data for the random variable- depth of defect (d)

(wet gas pipeline corrosion growth parameters) (partly [14])

Variables	$\%Co_2$ (mole)	O_2 (ppm)	pH	$\%H_2S$ (mole)	K, corrosion model error	A, Inhibitor factor
Type	Lognormal	Lognormal	Lognormal	Lognormal	Lognormal	Lognormal
μ	4	4800	5.5	0.05	1.0	1.0
CoV	0.25	0.30	0.18	0.08	0.5	0.5

4.2.3.2 Length of Defect

The defect depth (d) for internal corrosion was estimated considering model parameters i.e, $\%pCO_2$, $\%pH_2S$ etc. However, this kind of model, which considers model parameters i.e, $\%pCO_2$, $\%pH_2S$ etc. is not available for defect length (l) estimation. In fact corrosion measurements revealed that there is no correlation between the depth of defect (d) and length of defect (l); instead it's observed that for a given depth of defect (d) there is a range of associated length of defect (l) [20]. For example, for a depth of 20% wall thickness, the length varied (l) from 8 to 608 mm. However, Zimmerman et al [21] suggested corrosion defect length (l) can be assumed by Weibull distribution with a CoV of 0.50. The CoV 0.50 means the shape parameter (β') of Weibull is 2.1. The scale parameter (θ) was calculated considering Equation (4.9). The calculation considered cumulative distribution F(l)=0.90 and characteristic length (l_c) as 80% of the diameter of the pipeline. The mean defect length thus evaluated is 340 mm, which represents the defect length after the design life, T=20 years. Table 4.2 shows the probabilistic data for the defect length (l)

$$P(l \geq l_c) = 1 - F(l) = e^{-\left(\frac{l}{\theta}\right)^{\beta}} = \int_{l_c}^{\alpha} f(l)dl \qquad (4.9)$$

Table 4.2: Probabilistic data for the random variable- length of defect (l)

Variables	l-defect length (mm)
Type	Weibull
μ	340
CoV	0.50

4.3 Burst Models and Standards

The pipeline burst pressure is considered as the remaining strength or the resistance in the limit state analysis. The burst pressure calculations are discussed in the following subsections. It may be noted that the burst pressure models and standards are based on closed end conditions and the hoop stress that governs the bursting process. The axial, radial or combined loads such as thermal or bending load are not considered in this study. The notations (burst pressure of defected pipe, yield pressure of defect free intact pipe etc.) are kept the same in this paper as originally developed and presented in the corresponding references. The notations for defect length are specified by l in some codes and standards [7, 10], whereas others [8, 9] specify this parameter by L.

4.3.1 CSA Z662-07 [7]

For large leaks and ruptures, the limit state function g_2 for plastic collapse at a surface corrosion defect with a total axial length (l) in mm, and average defect depth d_a (in mm) is given by CSA Z662-07 [7] standard

$$g_2 = r_a - p \tag{4.10}$$

where r_a = the estimated pressure resistance including model error, in MPa

$$= e_1 r_c + (1 - e_1) r_o - e_2 \sigma_u \text{ for SMYS} > 241 \text{ MPa} \tag{4.11}$$

$$= e_3 r_c + (1 - e_3) r_o - e_4 \sigma_y \text{ for SMYS} \leq 241 \text{ MPa}$$

r_c = the calculated pressure resistance, MPa

$$= r_o \left(\frac{1 - \frac{d_a}{t}}{1 - \frac{d_a}{m \times t}} \right) \tag{4.12}$$

r_o = the pressure resistance for perfect pipe, MPa

$$= 1.8 \frac{t \sigma_u}{D} \text{ for SMYS} > 241 \text{ MPa} \tag{4.13}$$

$$= 2.3 \frac{t \sigma_y}{D} \text{ for SMYS} \leq 241 \text{ MPa}$$

SMYS=Specified Minimum Yield Strength and $d_a = d$, the depth of defect

m = the Folias factor

$$= \sqrt{1 + 0.6275 \frac{l^2}{D \times t} - 0.003375 \frac{l^4}{D^2 \times t^2}} \text{ for } l^2/Dt <= 50 \tag{4.14}$$

$$= 0.032 \frac{l^2}{D \times t} + 3.3 \text{ for } l^2/Dt > 50$$

e_1 = a deterministic multiplicative model error term that equals 1.04

e_2 = an additive model error term, defined by a normally distributed random variable with a mean of –0.00056 and a standard deviation of 0.001469

e_3 = a deterministic multiplicative model error term that equals 1.17

e_4 = an additive model error term, defined by a normally distributed random variable with a mean of –0.007655 and standard deviation of 0.006506

4.3.2 DNV RP-F101 [8]

In DNV-RP-F101 [8], the maximum operating pressure for a pipeline with a corrosion defect is given by

$$P_{corr} = \gamma_m \frac{2tSMTS\left(1-\gamma_d (d/t)^*\right)}{(D-t)\left(1-\frac{\gamma_d (d/t)^*}{Q}\right)} \tag{4.15}$$

where $(d/t)^* = (d/t)_{meas} + \varepsilon_d .StD[d/t]$ (4.16)

$$Q = \sqrt{1+0.31\left(\frac{L}{\sqrt{Dt}}\right)^2} \tag{4.17}$$

In this study, $\gamma_m = 0.77$ (as per Table 3.2 of DNV-RP-F101 [8], for normal safety class and absolute value), $\gamma_d = (1+4.6a-13.9a^2)$ where a is the standard deviation, StD(d/t), L is the length of the defect and ε_d is considered according to the guideline of Table 3.7 of DNV-RP-F101 [5], and SMTS is the Specified Minimum Tensile Strength.

It may be noted that DNV-RP-F101 [8] developed two equations for burst estimation: one for allowable maximum operating pressure and the other for capacity estimation considering the rectangular defect. The capacity equations were not demonstrated here, but were considered in the analysis. It may be noted that allowable maximum operating pressure is referred as DNV-RP-F101 MOP [8] and capacity pressure is referred to DNV-RP-F101 CP [8]. In reality DNV-RP-F101 MOP **[8]** is more conservative than DNV-RP-F101 CP [8].

4.3.3 ASME B31G [9]

Among the existing criteria for evaluating the residual strength of corroded pipeline, the ASME B31G [9] code is still the most widely used criterion. Kiefner et al. [22, 23] recognized that the ASME B31G [9] code could be too conservative for some kinds of defects. They modified the code to develop what is known as the 0.85 *dL* method. Like the original, the defect length and the defect depth are the only parameters required to define the defect.

The burst pressure defined by ASME B31G [9] is

$$P_b^{B31G} = \frac{2t}{D}\left(1.1\sigma_y\right)\left[\frac{1-(2/3)(d/t)}{1-(2/3)(d/t)M^{-1}}\right] \tag{4.18}$$

where $M = \sqrt{1+0.8\left(\frac{L}{D}\right)^2\left(\frac{D}{t}\right)}$ (4.19)

4.3.4 Netto et al. [10] Model

Netto et al. [10] developed a burst pressure equation for external corrosion considering the depth of defect, length of defect, width of corrosion, pipeline wall thickness and pipeline diameter. The effect of external corrosion defects was investigated through a series of small-scale experiments using non-linear numerical models based on the finite element method. The experimental and numerical results were then used to calibrate their equation. The burst pressure for defected pipe Equation (4.20) was developed with limiting conditions of corrosion defect depth to wall thickness ratio ($0.1 \leq d/t \leq 0.8$).

$$\frac{P_b}{P_{bi}} = 1 - 0.9435\left(\frac{d}{t}\right)^{1.6}\left(\frac{l}{D}\right)^{0.4} \tag{4.20}$$

where $P_{bi} = \frac{1.1\sigma_y 2t}{D}$ (4.21)

4.3.5 RAM PIPE REQUAL [11]

The Pipeline Requalification Guidelines Project [11] developed an equation for burst pressure as

$$P_b = 2.2(t-d)\frac{SMTS}{(D-t)\times SCF} \tag{4.22}$$

$$SCF = 1 + 2\sqrt{\frac{d}{R}} \tag{4.23}$$

where SMTS is the Specified Minimum Tensile Strength and SCF is the Stress Concentration Factor. The burst Equation (4.22) does not consider the corrosion defect length. This may be a significant issue where aspect ratio plays an important role in biaxial stress states.

4.3.6 Kale et al. [14] Model

The Kale et al. [14] model describes a methodology for predicting the location of internal corrosion damage in gas pipelines considering uncertainties in flow characteristics, pre-existing conditions, corrosion resistance, elevation data, and test measurements. The prediction is then updated using Bayesian techniques based on inspection data. The approach computes the probability of critical corrosion damage as a function of location along the pipeline length. This procedure helps to focus the location of the most probable excavation spot with higher probability of corrosion damage along the pipeline length. The Kale et al. [14] model used three candidate corrosion models. A weight factor for probability calculation, starting with $W_1=W_2=W_3=0.3333$ is used, and later the model is adjusted with Bayesian updating techniques using the inspection data. However, in this study, only the SwRI equation will be considered to study the Kale et al. [14] model. The core concept of the model is whether the defect depth (d) exceeds the critical defect depth (d_c). The critical defect depth (d_c) was considered as 80% of wall thickness (t) in their model. This is not a burst model but rather a model defining the probability of defect depth exceeding the critical defect depth.

4.4 Failure Model

The RAM PIPE [11] and Kale et al. [14] models do not account for the corrosion defect length (l) but they consider defect depth (d). Other models evaluated in this study considered both the defect depth (d) and defect length (l). The main assumptions for the analysis conducted in this study are:

1. Burst pressure equations for external corrosion defects developed by codes and standards [10, 11, 12] and individual models [10, 11] are considered to be valid for the effects of internal corrosion defects.
2. The rate of corrosion only affects the corrosion defect depth (d). The defect length (l) is not directly correlated with defect depth (d). Uniform corrosion was considered for defect depth (d) evaluation.
3. The length of defect (l) is assumed to be the same as Weibull distribution with a CoV of 0.50 over the pipeline length. The inhibitor effect on defect length (l) as compared to defect depth (d) is considered negligible.
4. The corrosion defect ($l \times d$) is assumed to have the length (l) oriented on the longitudinal axis (axial direction) and depth (d) through the wall thickness (radial direction). The circumferentially oriented corrosion defect width (c) is not considered in this study.
5. In this study, the minimum value of reliability index, β is assumed to be zero, β=0. The minimum value could be negative, but is not logically correct.

6. The probability of failure of an internally corroded pipe was calculated using the burst pressure and operating pressure in the limit state equation considering Equations (4.24) and (4.25). Data was generated by the SwRI corrosion model equation, Equation (4.7), for defect depth (*d*) and Equation (4.9), for defect length (*l*). .

The limit state function for internally corroded pipelines can be written as follows:

$$g(X) = P_{bdp} - P_{op} \tag{4.24}$$

where P_{bdp} is the burst pressure of the defected pipe, and P_{op} is the operating pressure. The burst pressure of defected pipe, P_{bdp}, is considered as the resistance, and the operating pressure, P_{op}, is considered as the load in the limit state function defined by Equation (4.24). The burst pressure of the defected pipe, P_{bdp}, can be calculated from the respective models as discussed in Section 4.3. It may be noted that Equation (10) of CSA Z662-07 [7] standard is similar to Equation (4.24), which is the generalized limit state function considered for all codes and standards and models (except for the Kale et al. [14] model) where g_2 is $g(X)$, r_a is P_{bdp} and P is P_{op} in Equation (4.24).

The reliability index β may be obtained from load and resistance variables. Hence, in this case

$$\beta = \frac{\mu_{P_{bdp}} - \mu_{P_{op}}}{\sqrt{\sigma^2_{P_{bdp}} + \sigma^2_{P_{op}}}} \tag{4.25}$$

Using this equation reliability index, β may be calculated for any code and standard except the Kale et al. [14] model.

The Kale et al. [14] model does not explicitly define pipe burst limit state function as stated in Equation (4.24). For this study the limit state function can be defined as:

$$g(X) = d_c - d \tag{4.26}$$

where d_c= 80% of wall thickness (t), and (d) is the defect depth. Using the limit state equation, Equation (4.26), one can now determine reliability index, β, for the Kale et al. [14] model considering Equation (4.27). Thus

$$\beta = \frac{\mu_{d_c} - \mu_d}{\sqrt{\sigma_{d_c}^2 + \sigma_d^2}} \tag{4.27}$$

In this study, it was assumed that the defect depth (d) exceeding critical depth (d_c) is eventually a failure state. Once the reliability index, β, is calculated for any selected model, the failure probability (P_f) can be calculated using Equation (4.28)

$$P_f = \varphi(-\beta) = 1 - \varphi(\beta) \tag{4.28}$$

One can calculate the risk (R) if the consequence (C) is known for a specific material and specific location considering Equation (4.29).

$$R = P_f \times C \tag{4.29}$$

A flow chart of calculation procedure is shown in Figure 4.5.

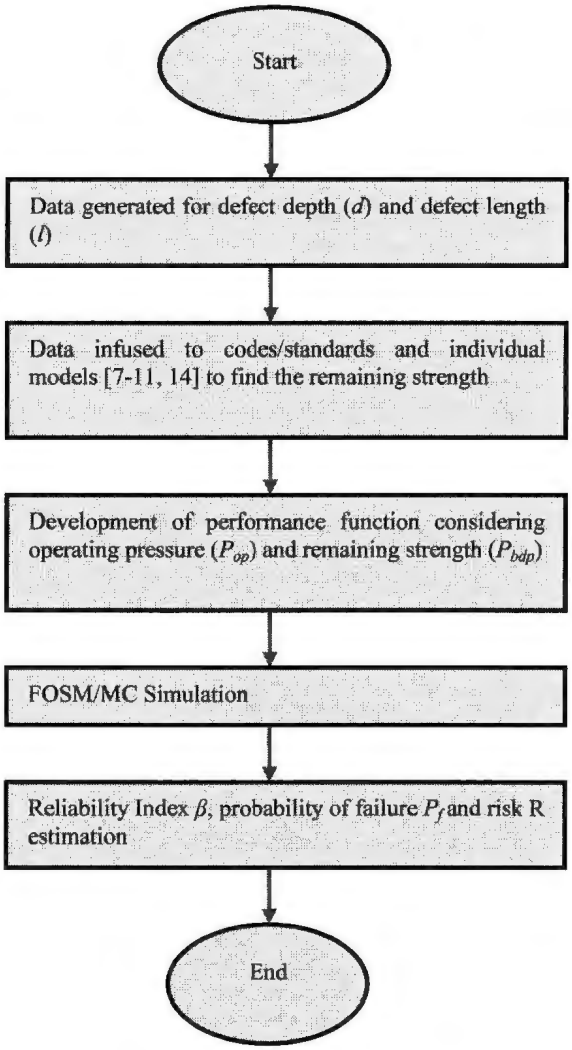

Figure 4.5: The flow chart depicts the calculation procedure followed in this study

4.5 Failure Analysis

The failure analysis was carried out using the generalized limit state equation, Equation (4.24), for the candidate models selected [7-11] except the Kale et al. [14]

model. For the failure analysis of the Kale et al. [14] model the limit state equation, Equation (4.26) was used. It may be noted that Equation (4.24) is a burst limit state, which considers burst pressure (P_{bdp}) and operating pressure (P_{op}), whereas Equation (4.26) is a defect depth limit state which considers defect depth (d) and critical defect depth (d_c). The calculation proceeds with follow up equations, Equations (4.25) and (4.27) to further calculate the reliability index, β. Equations (4.28) and (4.29) can be used to calculate probability of failure (P_f) and to estimate the risk (R) at a specific location and for a specific material if consequence (C) is known.

For example, the Netto et al. [10] model can be considered to calculate the probability of failure. The burst pressure is now represented by Equation (4.30), which considers the basic variables presented in Table 4.1 (for defect depth (d)), Table 4.2 (for defect length (l)) and Table 4.3 (for diameter (D), thickness (t) and SMYS (σ_y) or SMTS (σ_u)). This burst pressure is used by the limit state equation, Equation (4.24). The new burst limit state Equation (4.31) was derived for the Netto et al. [10] model from Equation (4.24).

$$P_{bdp} = P_b = \left(\frac{1.1\sigma_y 2t}{D}\right)[1 - 0.9435(d/t)^{1.6}(l/D)^{0.4}] \qquad (4.30)$$

Table 4.3: Probabilistic models of the basic variables for material- API 5L X 65

Variables	σ_u/ MPa	σ_y/MPa	D/mm	t/mm	P_{op}/MPa
Type	Lognormal	Lognormal	Normal	Normal	Gumbel
μ	531	448	713	20.24	17.12
CoV	0.05	0.07	0.001	0.001	0.08

The limit state function for the Netto et al. [7] model is

$$g(X) = \left(\frac{1.1\sigma_y 2t}{D}\right)[1 - 0.9435(d/t)^{1.6}(l/D)^{0.4}] - P_{op} \qquad (4.31)$$

In Equation (4.31), all the parameters are available in Tables 4.2 and 4.3 except the defect depth (d). The defect depth (d) is calculated considering probabilistic data provided in Table 4.1 and considering the SwRI equation, Equation (4.7). The procedure specified above is the same for all candidate models examined [7-11] except the Kale et al. [14] model. The probability of failure (P_f) can be calculated considering Equation (4.25) and (4.28) by the FOSM method. The failure function g(), Equation (4.24), may be considered for the direct evaluation of the probability of failure (P_f) by the Monte Carlo method.

The Kale et al [14] model considers Equation (4.26) for the limit state analysis. In their analysis, Kale et al. [14] have assumed the critical depth, (d_c), is 80% of wall thickness for oil and gas pipelines. Equation (4.27) was used to calculate the probability of failure for internal corrosion for the Kale et al [14] model.

In Table 4.3, the mean value of operating pressure (P_{op}) was calculated from the characteristic operating pressure (p_{cop}), which again was calculated from yield pressure (P_{yip}) of defect free intact pipe. The characteristic operating pressure (p_{cop}) was considered as 72% of the yield pressure (P_{yip}). The characteristic values for load (P_{op}) were calculated considering the EURO Code EN 1990 [24] recommendation that the

characteristic values should correspond to a 95% upper and 5% lower value respectively for load and resistance variables.

Therefore, $p_{cop} = P_{yip} \times 0.72 = \frac{2 \times 448 \times 20.24}{713} \times 1.1 \times 0.72 = 20.14$ MPa

The characteristic value of operating pressure (P_{cop}) was considered to calculate the Gumbel mean and standard deviation. It may be noted that operating pressure can be characterized by Gumbel distribution as per the CSA Z662-07 [7] recommendation. Equations (4.32) to (4.35) were considered to calculate Gumbel parameters.

$$F_{P_{op}}\left(p_{cop}\right) = \exp\left[-e^{-\alpha_{op}\left(p_{cop}-u_{op}\right)}\right] \tag{4.32}$$

$$P\left(P_{op} \geq p_{cop}\right) = 1 - F_{P_{op}}\left(p_{cop}\right) \tag{4.33}$$

$$\alpha_{op} = \frac{1}{\sqrt{6}}\left(\frac{\pi}{\sigma_{P_{op}}}\right) \tag{4.34}$$

$$u_{op} = \mu_{P_{op}} - \frac{0.5772}{\alpha_{op}} \tag{4.35}$$

where $\mu_{P_{op}}$ is the Gumble mean, $\sigma_{P_{op}}$ is the Gumble standard deviation and P_{op} is the operating pressure, considered as an extreme random variable. The parameters u_{op} and α_{op} are related to the Gumbel mean and standard deviation.

CO_2 partial pressure is calculated from the mole fraction ($\%CO_2$) presented in Table 4.1 and operating pressure (P_{op}) presented in Table 4.3:

$$pCO_2 = P_{op} \times \%CO_2 \times 10^{-5}\, bar$$

where P_{op} is in MPa. The partial pressure of H_2S is also calculated in the same manner.

4.6 Results and Discussion

The probabilities of failure of different candidate models were calculated and assessed. A pipeline length of 1000 km was considered in the analysis with a single inhibitor injector at the inlet. The material considered API 5L X65 for design. The analysis used First Order Second Moment (FOSM) and Monte Carlo (MC) simulation methods. The results are presented in Figure 4.6 for the FOSM method.

The simulated results by FOSM and Monte Carlo have been compared and it was found that they closely match with one another at the tail end of the pipeline length. The results are presented in Table 4.4.

Examination of the failure probability (P_f) calculated by using different candidate models, as illustrated in Figure 4.6 and summarized Table 4.4, indicates a gap or discrepancy. RAM PIPE [11] and DNV RP-F101 MOP [8] calculate greater failure probability than other models including CSA Z662-07 [7], ASME B31G [9], Netto et al. [10] and Kale et al. [14]. It may be noted that in Figure 4.6, DNV RP-F101 MOP [8] refers to the failure probability for the allowable maximum operating pressure equation, whereas DNV RP-F101 CP [8] refers to the failure probability for the capacity pressure equation. There is a significant difference in the estimation of probability of failure: DNV RP-F101 CP [8] calculates in the range of 10^{-6}, whereas DNV RP-F101 MOP [8] calculates in the range of 10^{-2}. It may be noted that the DNV RP-F101 MOP [8] equation is not a capacity equation like the DNV RP-F101 CP [8] equation; rather it is the maximum allowable operating pressure equation.

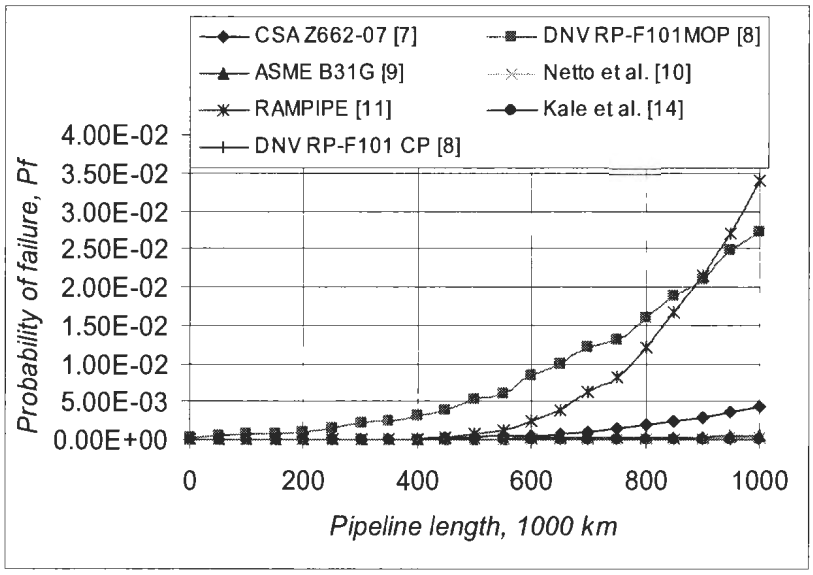

a)

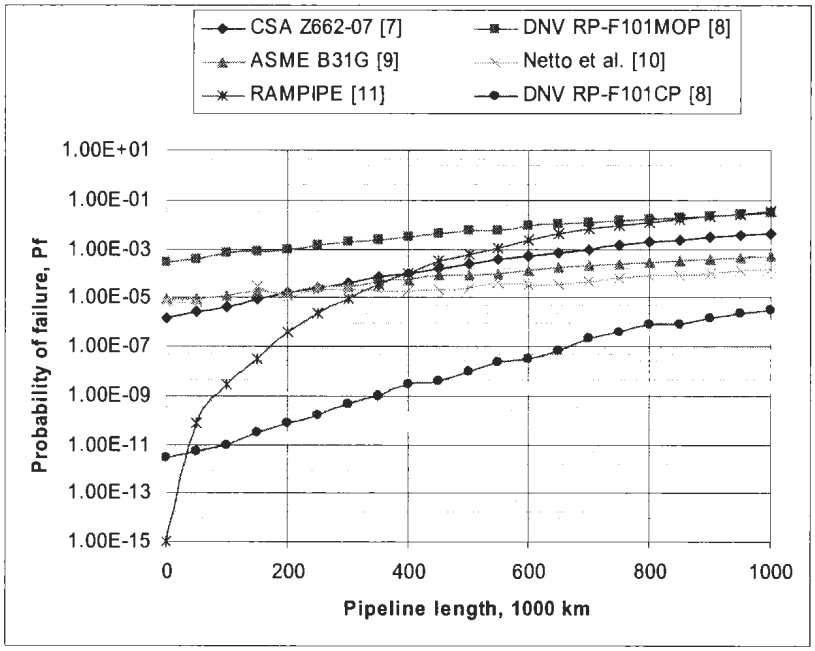

b)

Figure 4.6: Failure probability P_f for different standards and models using burst and critical depth in the limit state equation a) normal graph b) Semi-logarithmic graph excluding Kale et al. [14]

Table 4.4: Results obtained for different codes/standards

Codes/Standard	FOSM		Monte Carlo	
	P_f	β	P_f	β
Kale et al. [14]	$1.4*10^{-28}$	-	-	-
DNV RP-F101 CP [8]	$3.1*10^{-6}$	4.51	$2.0*10^{-5}$	4.10
Netto et al. [10]	$1.4*10^{-4}$	3.63	$3.0*10^{-5}$	4.01
ASME B31G [9]	$4.8*10^{-4}$	3.29	$7.5*10^{-4}$	3.17
CSA Z662-07 [7]	$4.2*10^{-3}$	2.63	$2.4*10^{-3}$	2.82
DNV RP-F101 MOP [8]	$2.7*10^{-2}$	1.92	$1.8*10^{-2}$	2.09
RAM PIPE [11]	$3.4*10^{-2}$	1.82	$3.17*10^{-2}$	1.85

The failure probability estimate for ASME B31G [9] and Netto et al. [10] models are consistent and exhibit limited relative variations along the pipeline length. Netto et al. [10] concluded that ASME B31G [9] and DNV RP-F101 [8] are conservative models, which is consistent with the findings of this study. The analysis of Netto et al. [10] indicated DNV RP-F101 MOP [8] failure probability in Figure 4.6, which considered maximum operating pressure. It could be more accurate if they compared their model with the DNV RP-F101 CP [8] burst capacity equation. However, in Figure 16 of their study they compared the result obtained from Netto et al. [10], ASME B31G [9] and DNV RP-F101 MOP [8] with the experimental result. If the present probabilistic study is compared with the Netto et al. [8] study, it can be safely said that the codes/models that calculate greater failure probability compared to Netto et al. [8] are overly conservative.

A relative ranking of conservatism in the candidate models is illustrated in Figure 4.7, where H denote the load (operating pressure), and F and C denote bursting pressure of the RAM PIPE [11] and Netto et al. [10] model, respectively. The remaining strength or bursting pressure calculated by RAM PIPE [11] model is closest to the load;

that's why its failure probability is highest. As C is far away from H, this is why Nettto et al [10] calculate less failure probability. The other codes/standards in Figure. 4.7 lie in between C and F except DNV RP-F101 CP [8]. To define over conservative or under conservative, the position of A is important, which denotes the experimental remaining strength. According to the Netto et al. [10] model the position of C is below the position of A. The position of A denotes the true remaining strength, evaluated by experimental study. Again, the results of the present study (Table 4.4) suggest that the location point of DNV RP-F101 CP [8], B, in Figure. 4.7 must be located closest to A since DNV RP-F101 CP [8] calculates the least failure probability among the burst models. Therefore the capacity equation developed by DNV RP-F101 CP [8] can be considered as the best estimator of the remaining strength. Finally, it can be stated that the codes and standards which calculate less remaining strength than actual (experimental) remaining strength (line A) can be assumed as over conservative. The relative position presented in Figure 4.7 is also supported by the experimental data studied by Freire et al., [25]. In their analysis they have demonstrated that ASME B31 [9] is over conservative compared to DNV-RP-F101 CP [8]. A deterministic analysis of remaining strength (burst pressure) for different codes and standards in Figure 4.8, shows that the relative conservatism scale remains true for $0.15 \leq \frac{d}{t} \leq 0.42$.

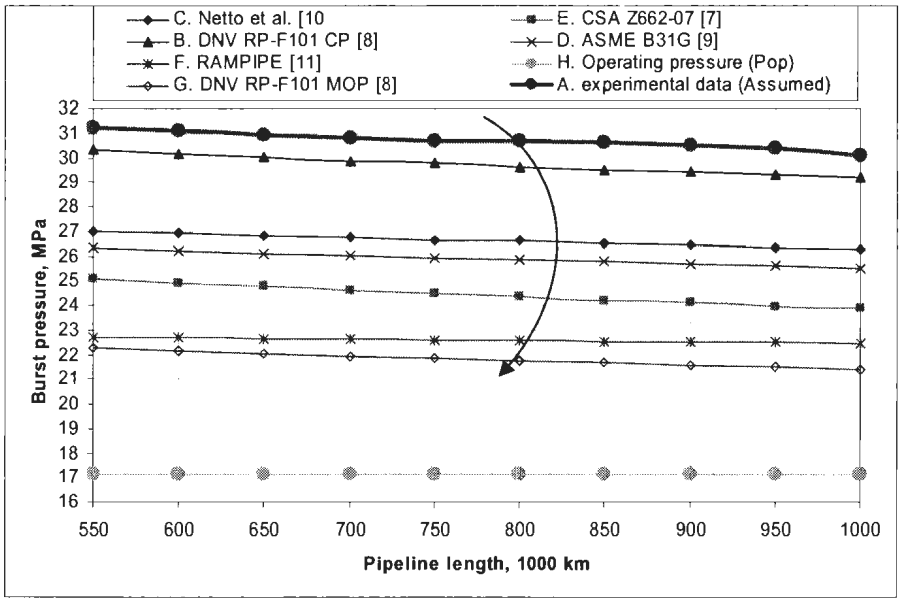

Figure 4.7: Relative position of the codes/standards in 'Conservative Scale' considering remaining strength (burst pressure) and operating pressure.

The conservatism of failure or burst pressure estimated by the codes depends on the geometry of the pipe, the geometry of the defect, and the material. Past research concentrated on the behavior of sharp defects (machined V-shaped notches and slits), but subsequently the work was extended to consider artificial and real corrosion defects.

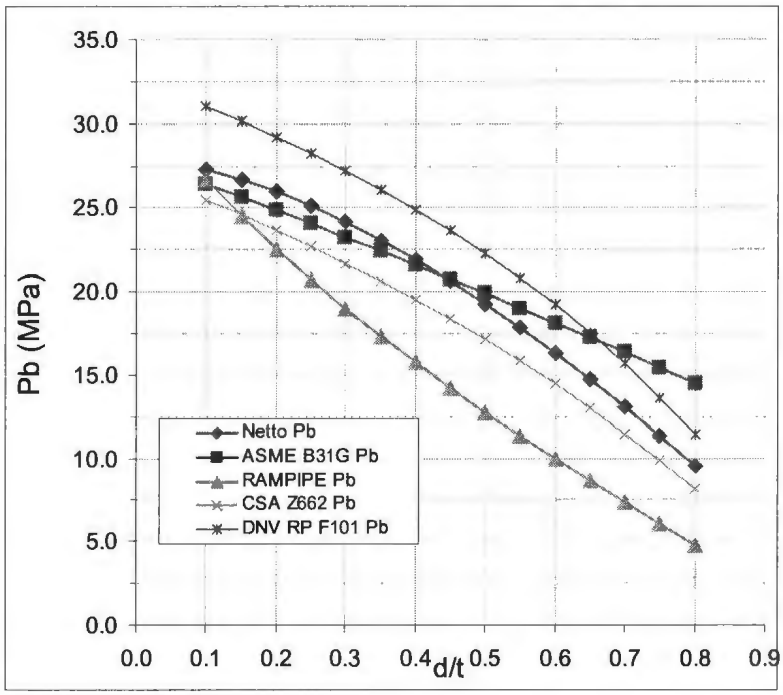

Figure 4.8: A deterministic approach of remaining strength calculation shows that the conservatism scale remains true for $0.15<d/t<0.42$

Many failure criteria such as ASME B31G [9], DNV-RP-F101 [8], CSA Z662-07 [7] etc. are originally based on the flow stress dependent failure criteria of the NG-18 equations [26] and have been assumed as plastic collapse failure criteria. In many tests, failure was preceded by significant amounts of ductile tearing and some of the steels had low toughness. The geometry term was empirical and the flow stress was adjusted to fit the test results. This leads to an empirical definition of the flow stress which is conservative, since it is biased towards the behavior of older steels [27]. The NG-18[26] equations were developed from tests of V-shaped notches, not blunt, part-wall defects.

Therefore, many methods for assessing the corrosion based on the NG-18 [26] equations have a conservative bias when applied to tests of blunt, part-wall defects.

Efforts have been made to develop the accuracy of failure criteria by better describing the effects of reference stress and geometry. DNV-RP-F101 [8] have used finite element analyses of blunt, part-wall defects to determine the form of the geometry, and have considered the form of the reference stress in more detail. The failure criteria has been validated against burst tests of modern pipeline steels containing blunt, part-wall defects or real corrosion defects. Modern pipeline steels have a higher toughness than older steels, so that the failure of blunt part-wall defects is controlled by plastic collapse (where plastic collapse is defined in terms of the ultimate tensile strength), and hence the scope of toughness can be better accounted in burst models.

DNV RP-F101 MOP [8] has a constraint for the standard deviation of defect depth to the wall thickness (StD (d/t)) ratio. When the standard deviation exceeds 0.16, it cannot calculate partial safety factor, γ_d. For the normal safety class, γ_d equals $1+4.6a-13.9a^2$, where a = StD [d/t]. The analysis confirmed that the standard deviation does not exceed the boundary condition within the pipeline design specification for this study for the DNV RP-F101 [8] code.

The Kale et al. [14] model is not a failure model. Rather, it is a model which calculates probability of defect depth (d) exceeding the critical depth, (d_c). In this study it was assumed that defect depth represents a failure state when it exceeds critical depth. There is a limitation in this assumption, but for simplicity it is nonetheless assumed in this analysis. In their analysis Kale et al. [14] assumed the critical depth is 80% of wall

thickness for oil and gas pipelines. The other feature in the Kale et al. [14] model is that, this model considers only depth of defect (d), and does not consider the length of defect (l). The length of defect (l) has due importance in the failure probability of gas pipelines. Another feature in the limit state equation of the Kale et al. [14] model is that the resistance (critical depth (d_c)) is constant, and the load (depth of defect (d)) is variable; the opposite observation is noticed in other models/standards.

The sensitivity for internal corrosion can be studied by considering any codes and standards. If the function g () is considered for sensitivity analysis, the analysis will reveal the parametric affect on the failure function. Gardner et al. [28] recommend simple correlation coefficients, derived from Monte Carlo simulations, as a reasonable way to rank model parameters. Pearson's product moment correlation coefficient is denoted by r and is defined as

$$r_{x_j y} = \frac{\sum_{i=1}^{N}\left(x_{ij} - \bar{x}_j\right)\left(y_i - \bar{y}\right)}{\left[\sum_{i=1}^{N}\left(x_{ij} - \bar{x}_j\right)^2\right]^{1/2}\left[\sum_{i=1}^{N}\left(y_j - \bar{y}\right)^2\right]^{1/2}} \qquad (4.36)$$

The CSA Z662 07 [7] and DNV RP F101 [8] model have been considered for sensitivity analyses in this study. The sensitivity, in terms of dimensionless parameters, was analyzed ($W = \frac{d}{t}, X = \frac{D}{t}, Y = \frac{\sigma_h}{\sigma_y \text{ or } \sigma_u}$ and $Z = \frac{l}{D}$) of the failure functions g () using the Monte Carlo approach. The analysis considered the data given in Table 4.5 for the dimensionless parameter in the g() function. The analysis also assumed remaining

parameters (other than dimensionless) constant in the failure function. The result is presented in Figure 4.9. The sensitivities for the dimensionless parameter $X = \frac{D}{t}$ are found very insignificant for the codes and standards in Figure 4.9. This suggests that a change in either D or t has very little effect on the g() function. The other dimensionless parameters ($W = \frac{d}{t}, Y = \frac{\sigma_h}{\sigma_y \text{ or } \sigma_u}$ and $Z = \frac{l}{D}$) are observed to be highly sensitive in the codes and standards. This means that a small change in W, Y, or Z has a significant effect on the failure function g(). Dimensionless parameter Y has the most significant effect on the failure function g(). It is followed by W and Z. The negative values indicate the dimensionless parameters inversely affect the failure, g(), function.

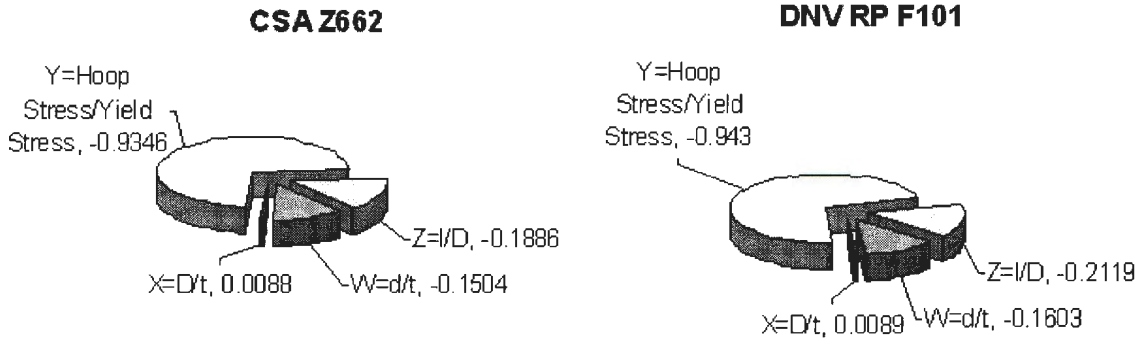

Figure 4.9: Sensitivity analysis of internal corrosion failure probability considering CSA Z662 07 [7] and DNV RP F101 [8]

Table 4.5: Probabilistic models of dimensionless parameters.

Dimensionless Parameter	$W=\frac{d}{t}$	$X=\frac{D}{t}$	$Y=\frac{\sigma_s}{\sigma_y \text{ or } \sigma_u}$	$Z=\frac{l}{D}$
Type	Lognormal	Normal	Weibull	Weibull
μ	0.2135	35.22	0.5695	0.4717
CoV	0.2519	0.0014	0.1077	0.5030

4.7 Conclusion

In this chapter, an approach has been developed and demonstrated to calculate the burst pressure of internally corroded pipeline. The burst pressure and operating pressure are then used to develop the limit state equation. The failure probability of the pipeline was determined by different codes, standards and models, and comparisons were made. The results revealed that RAM PIPE [11] and DNV RP-F101 MOP [8] calculate a greater failure probability, which is followed by a successive decreasing failure probability estimated by CSA Z662-07 [7], ASME B31G [9], Netto et al. [10], DNV RP-F101 MOP [8] codes and standards and the Kale et al. [14] model.

The present study observed that the RAM PIPE [11] model calculates the highest failure probability; therefore, it can be assumed as the most conservative model. The reason for this conservative behavior might be the defect length (l), which was not accounted in this model; due importance is only given to defect depth (d). Next to the RAM PIPE [11] model, DNV RP-F101 MOP [8] calculates greater failure probability.

The reason is that the equation estimates allowable maximum operating pressure, not the capacity of the defected pipeline. However, among the burst models, DNV RP-F101 CP [8] calculates the least failure probability. This is because of its capacity equation, which calculates the maximum remaining strength among all codes and standards. At the same time there observed much sophistication in the DNV RP-F101 CP [8] equation and it has been validated by extensive finite element analysis and experimental full scale burst test results. The study also supports the claim of Cosham et al. [27] that considering the basis of the various criteria and a comparison with full scale test data, DNV RP-F101 [8] is proven for moderate to high toughness steels, whilst ASME B31G [9] is applicable to low, moderate and high toughness steels (assuming upper shelf behavior). Therefore, designing pipelines where the material is tough steel, DNV RP-F101 [8] is a good choice. A design using older pipeline steel, the design code DNV RP-F101 [8] might not be a good selection. As Netto et al. [10] also calculates greater remaining strength and least failure probability (the range of 10^{-5}) after the design life of 20 years, this model may also be considered for pipeline design using new pipe. Considering irrespective of pipeline material toughness, the other standards like CSA Z662 07 [7] and ASME B31G [9] are always good selection for design since they calculate in the safe domain and closely match the failure probability of Netto et al. [10] and DNV RP-F101 CP [8] models. A scale of conservatism for codes and standards developed in Figure 4.7 and 4.8 may be used for prior conception of conservatism of the codes and standards in the design if the design scenario is based within the bounds of $0.15 \leq \frac{d}{t} \leq 0.42$.

4.8 References

[1] Law, M., & Bowie G. (2007). Prediction of failure strain and burst pressure in high yield-to-tensile strength ratio linepipe. *International Journal of Pressure Vessels and Piping*, Vol 84, pp 487-492.

[2] Chiodo, M., Ruggieri C. (2009). Failure assessments of corroded pipelines with axial defects using stress-based criteria: Numerical studies and verification analyses. *International Journal of Pressure Vessels and Piping*, Vol 86, pp 164-176

[3] Zhu, X. -K., & Leis B. N. (2006). Average shear stress yield criterion and its application to plastic collapse analysis of pipelines. *International Journal of Pressure Vessels and Piping*, Vol 83, pp 663-671.

[4] Teixeria, A. P., Soares C. G., Netto T. A., & Estefen S. F. (2008). Reliability of pipelines with corrosion defects. *International Journal of Pressure Vessels and Piping*, Vol 85, pp 228-237.

[5] Lee, Y. K., Kim Y. P., Moon M. –W., Bang W. H., Oh K. H., & Kim W. –S. (2005). The prediction of failure pressure of gas pipeline with multi corroded region, *Trans Tech Publication*, Vols 475-479, pp 3323-3326.

[6] Lee, O. S., & Pyun J. S. (2002). Failure probability of corrosion pipeline with varying boundary condition. *KSME International Journal*, Vol 16, No. 7, pp 889-895.

[7] CSA Z662-07, (2007). Limit state equation for burst of large leaks and rupture for corrosion defect. *Oil and Gas Pipeline Systems*, Canadian Standards Association. pp 554-555.

[8] DNV RP-F101 (2004). *Recommended Practice Corroded Pipelines*. Det norske Veritas

[9] ASME B31G (1995). *Manual for determining the remaining strength of corroded pipelines*. A supplement to ANSI/ASME B31 code for pressure piping.

[10] Netto T. A., Ferraz U. S., & Estefan S. F. (2005). The effect of corrosion defect on the burst pressure of the pipeline. *Journal of Constructional Steel Research,* Vol 61 pp 1185-1204

[11] Bea R., Xu T. (1999). Corrosion Effects on Burst Pressures RAM PIPE REQUAL. *Pipeline Requalification Guidelines Project Report 1*, University of California at Berkeley, pp 103-104.

[12] Kiefner, J. F., Maxey, W. A., Eiber, R. J. & Duffy, A. R. (1973). Failure stress levels of flaws in pressurized cylinders. *American Society for Testing and Materials*, ASTM STP 536, pp. 461 - 48 1.

[13] Shannon, R. W. E. (1974). The failure behavior of line pipe defects. *International Journal of Pressure Vessel and Piping*, Vol. 2, pp. 243 - 255.

[14] Kale A., Thacker B. H., Sridhar N., Waldhart J. C. (2004). A probabilistic model for internal corrosion of gas pipeline. *International Pipeline Conference*, Alberta, Canada. IPC 04-0483.

[15] Nesic S. (2007). Key issues related to modeling of internal corrosion of oil and gas pipeline. *Corrosion Science* 49 (2007) 4308-4338

[16] NORSOK Standard M-506 (1998). *CO_2 Corrosion rate calculation model*, Rev. 1.

[17] Gratland P. O., Johnsen R., Ovstetun I. & (2003). Application of internal corrosion modeling in the risk assessment of pipelines. *Corrosion*, Paper No 03179.

[18] Waard, C. de., & Milliams D.E. (1975). Carbonic acid corrosion of steel. *Corrosion* 31, (5), 177-181.

[19] Waard, C. de., & Lotz, U. (1993). Prediction of CO2 corrosion of carbon steel. *Corrosion*/93, Paper 69. Houston, TX. NACE International.

[20] Amirat A., Benmoussat A., & Chaoui A. (2009). Reliability assessment of underground pipelines under active corrosion defects. *Damage and Fracture Mechanics: Failure Analysis of Engineering Materials and Structures*, 83–92. Springer Science

[21] Zimmerman TJE, Hopkins P., Sanderson N. (1998). Can limit states design be used to design a pipeline above 80% SMYS. *In: Proceedings of the 17th international conference on offshore mechanics and Arctic engineering* (OMAE 1998), ASME

[22] Kiefner J. F., Vieth P. H. & (1990a). Evaluating pipe 1: new method corrects criterion for evaluating corroded pipe. *Oil & Gas Journal*, 88(32):56-9.

[23] Kiefner J. F., Vieth P. H., (1990b). Evaluating pipe conclusion: PC program speeds new criterion for evaluating corroded pipe. *Oil & Gas Journal*, 88(34):91-3.

[24] EN 1990, (2001) . *Basis of structural design*. Brussels.

[25] Freire J. L. F., Vieira R. D., Castro J. T. P. & Benjamin A. C. (2006). Part 3: Burst tests of pipeline with extensive longitudinal metal loss. *Experimental Techniques*, November 2006. pp 60-65.

[26] Kiefner JF., Maxey WA., Eiber RJ., & Duffy AR., (1973). The failure stress levels of flaws in pressurized cylinders. *ASTM STP*, vol. 536. Philadelphia, pp. 461–81.

[27] Cosham A., Hopkins P., & Macdonal K. A. (2007). Best practice for the assessment of defect in pipelines- Corrosion, *Engineering Fatigue Analysis* 14, pp 1245-1265.

[28] Gardner, R.H., O'Neill, R.V., Mankin, J.B. & Carney, J.H. (1981). A Comparison of Sensitivity Analysis and Error Analysis Based on a Stream Ecosystem Model. *Ecol. Modelling.* 12, 173-190.

Chapter 5

Identification of the Cause of Variability of Probability of Failure for Burst Models Recommended by Codes/Standards*

Preface

Chapter 4 provides failure probability assessment of internal corrosion defect whereas this chapter provides failure assessment for external corrosion defect. The chapter further provides an extensive analysis for the identification of the cause of variability of probability of failure for recommended burst models. The chapter has been published in the *Journal of Pressure Vessels Technology*.

The principal author conducted sensitivity analysis for the recommended models to identify the cause of the variability of failure. The co-authors, Dr. Khan and Dr. Kenny supervised and critically reviewed the approaches and provided valuable comments and corrections to improve the work and the manuscript.

An important point may be noted that the codes and standards considered in this chapter are also considered in *Chapter 4*. However, to keep the integrity of the published paper the codes and standards were repeated and kept as it was published in the paper.

*this paper has been published in International Journal of Pressure Vessels and Piping. The reference is provided below.

Hasan, M., Khan, F., Kenny, S., (2011). *Identification of the Cause of Variability of Probability of Failure for Burst Models Recommended by Codes/Standards*, Journal of Pressure Vessel and Technology, vol. 133, n. 041101, August, 2011

Abstract

Failure probability of oil and gas pipelines due to external corrosion defects can be estimated using the corrosion growth model and the evaluation of remaining strength. Codes/Standards have been developed for the assessment of the remaining strength of corroded pipeline. The remaining strength and the operating pressure were considered to develop the limit state equation and consequently the failure probability of the burst models recommended by codes/standards. In the present paper, comparative analyses of the failure probability estimated by the codes/standards were conducted, using Monte Carlo simulation and First Order Second Moment (FOSM) methods. The analysis revealed that the failure probability of the burst models recommended by codes/standards varies significantly for the same size of defects. The study further explored the cause of variability in failure probabilities. The study observed that different defect shape specification (rectangular, parabolic etc.) and different stress concentration factor derivation (different contribution of I) for burst pressure estimation are responsible for high variability in the probability of failure. It is important to reduce variability to ensure a unified risk-based design approach considering any codes/standards.

Key words: External corrosion, First Order Second Moment, Monte Carlo, Probability of failure, limit state function etc.

Nomenclature

σ_u	specified minimum tensile strength of pipe material, SMTS
σ_y	specified minimum yield strength of pipe material, SMYS
σ_{hip}	hoop stress of intact pipe
σ_{xip}	axial stress of intact pipe
σ_{hdp}	hoop stress of defected pipe
σ_f	flow stress
D	outside diameter of pipeline
t	thickness of pipeline
l	length of external corrosion defect
l_c	characteristic length of external corrosion defect
d	depth of external corrosion defect
c	width of external corrosion defect
F	design factor

5.1 Background

The Offshore oil and gas production and distribution involves a complex process system, complex piping system and various other equipment systems necessary for process operations. The process components are subjected to continuous deterioration from the date of operation to the date of design life. Therefore, identification of the risk

sources responsible for deterioration of strength, quantification of remaining life, and an incorporation of them in the design is necessary to avoid a catastrophic failure of the process system.

The aim of this study is to develop a risk-based design framework for a process system. Hence, the scope of this work is comprised of time dependent failure scenarios, i.e, internal corrosion, external corrosion, stress corrosion cracking, fatigue failure due to start up/shut down, and corrosion defects caused by combined loading (combined pressure and axial load) for specific process components. An algorithm of the conceptual risk-based design framework is given in Figure 5.1.

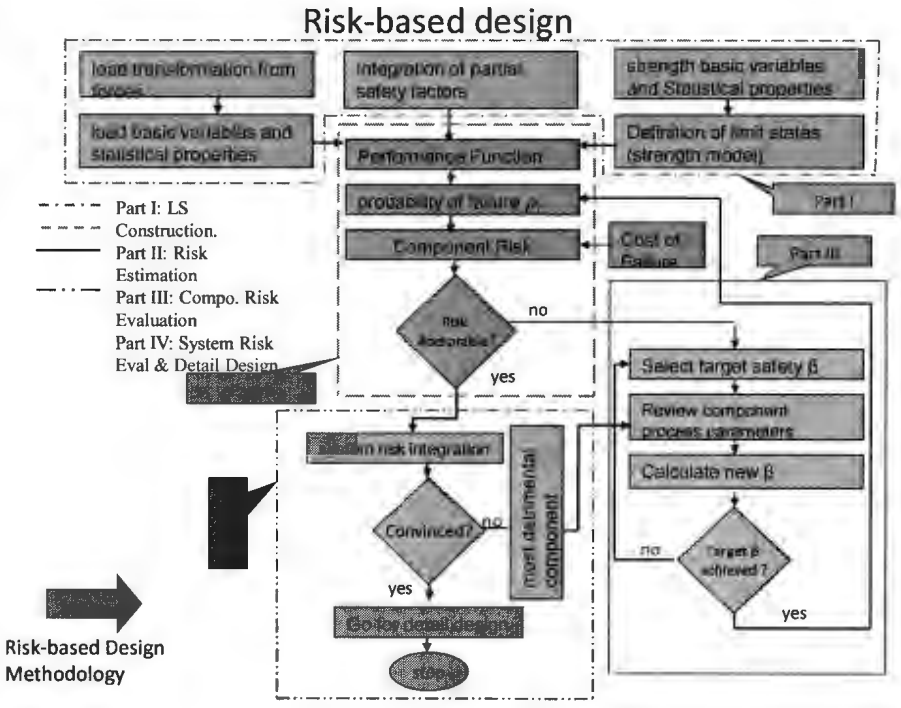

Figure 5.1: Risk-based design of process system

As external corrosion is one of the dominant cause of failure observed in offshore oil and gas work, this study investigates the probability of failure due to external corrosion. It may be noted that the failure probability can be evaluated considering models recommended by codes/standards developed by classification societies or models developed by individuals. For the risk-based design framework, the codes/standards should calculate identical failure probability/remaining strength since the reliable prediction of remaining strength is crucial in engineering design and integrity assessment of process components [1]. However, in practice it is observed that codes/standards calculate different failure probability and remaining strength. Hence this paper extended its study to investigate the cause of variability in failure probabilities estimated by the codes/standards, and the pipeline is considered as the illustrated example.

The study will considerer the First Order Second Moment (FOSM) method and Monte Carlo (MC) approach for the analysis. An analytic method like FOSM requires an extensive background in probability and statistics, which might be tedious. A simplistic tool is the MC approach which calculates the same probability but with not much background in probability and statistics [2]. The results obtained by FOSM are difficult to verify experimentally, hence MC is the alternative technique to verify the accuracy of the results [3].

5.2 External Corrosion

External corrosion is an oxidation process on external surfaces which are normally exposed to subsea water. It is a two step reaction process in which the loss of metal and production of electrons occurs at the anodic area, and the consumption of these electrons occurs at the cathodic area. Hence, the overall external corrosion rate is dictated by the ratio of the anodic area to the cathodic area, the concentration of the cathodic reactant and, to a lesser extent, the resistivity of the local environment, which determines the volume of ion transformation between the anode and cathode [4]. For the corrosion to continue, the electrons remaining on the metal surface must be removed by a cathodic reaction. Typical cathodic reactions are hydrogen evolution and oxygen reduction.

The higher the availability of oxygen to the metal surface, the higher the potential rate of corrosion. Oxygen access to the bare metal surface increases as the temperature of the water decreases, or as the flow rate over the surface increases. The splash zone of offshore process components, like risers, is, therefore, at the highest risk of corrosion in cold water moving at a high velocity [4].

5.3 Defect Growth Model

The growth of external corrosion defects on the process component (i.e, pipeline) surface is time dependent and the trajectory of the growth may be in the radial, circumferential and axial directions. In most studies [5,6,7,8], the shapes of these defects have been characterized by rectangular geometry defects or parabolic defects. Both types of defects have been characterized as two parameters ($l \times d$), discussed later in this section.

Knowledge of the remaining hoop strength of the defected pipeline is required to assess the safe mode of operation. Different codes/standards have been developed to calculate the remaining hoop strength or the bursting pressure of the defected pipeline. These codes/standards were developed and validated by laboratory test data or finite element (FE) simulation [7, 9,10].

5.3.1 Pressure calculation of defect free pipe

Considering a defect free circular pipe, as shown in Figure 5.2, the outside diameter is specified by D and wall thickness by t. Depending on the D/t ratio the pipe may be generally classified as either a thin walled ($D/t \geq 20$) or thick walled pipe. In the case of a thin walled pipe, at any point of the pipe material two stresses are present: hoop stress, σ_{hip}, acts in the circumferential direction and longitudinal or axial stress, σ_{xip}, acts along the length or axis of the pipe. Since hoop stress σ_{hip} is twice the axial stress σ_{xip}, hoop stress is assumed to be the controlling stress that is governed by the pipe wall thickness (t).

In Figure 5.2 the tangential or hoop stress σ_{hip} in the pipe wall is:

$$\sigma_{hip} = \frac{PD}{2t} \qquad (5.1)$$

where P is the internal pressure, D is the external diameter of the pipe and t is the pipe wall thickness. In the above equation, if σ_{hip} is replaced by yield strength σ_y and a

design factor F is introduced, then the yield pressure for a defect free intact pipe (P_{yip}) is [11,12]

$$P_{yip} = \frac{2\sigma_y t}{D} F \qquad (5.2)$$

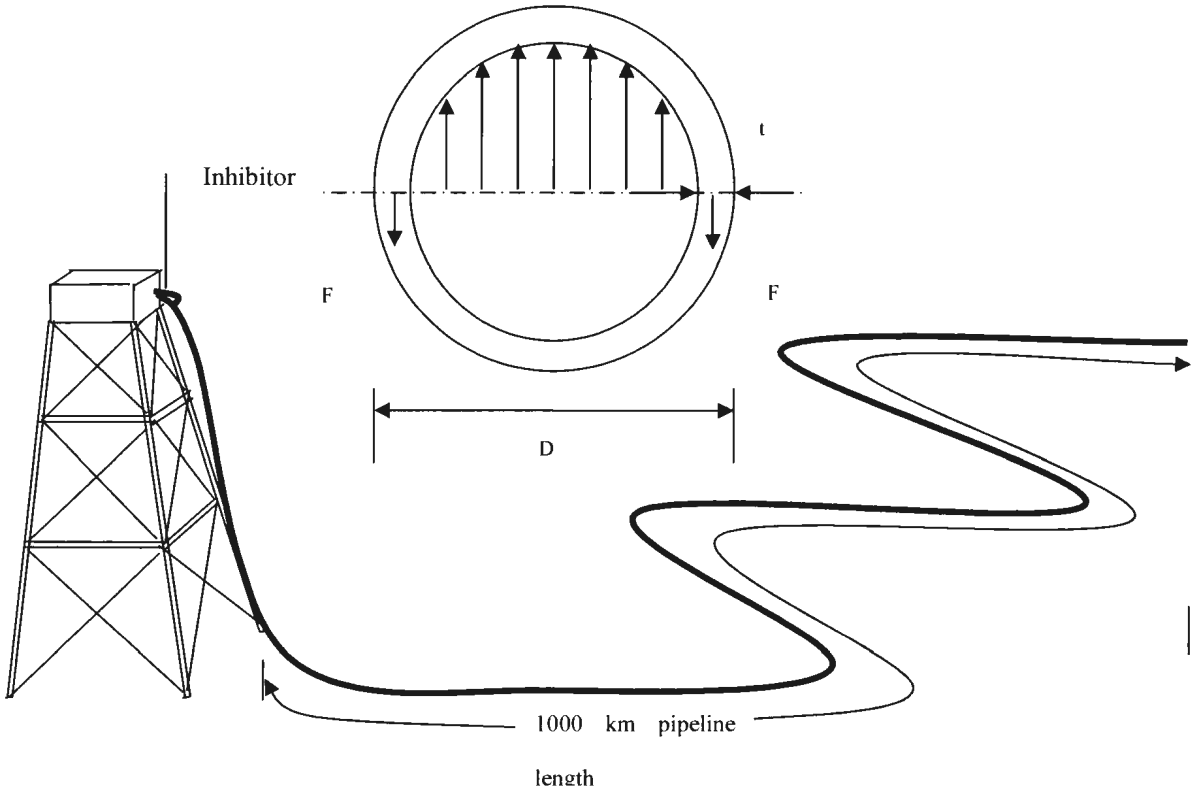

Figure 5.2: Force Equilibrium in a pressurized thin pipe

This is the burst pressure equation for an intact pipe (defect free) that is considered by most of the codes/standards [6,7,8] and models [5,13], with some minor adjustment. The value of F in equation (5.2) is adjusted to the design condition. For example, ASME B31G [8] assumes the value of F is 1.1, whereas DNV RP-F101 [7] assigns different values of F in relation to the safety class or design condition. An

allowable stress design method considers ultimate strength instead of yield strength for intact pipe burst pressure estimation. This is based on flow stress approximation of an intact pipe design.

5.3.2 Pressure calculation for defected pipe

The strength of a pipeline deteriorates due to corrosion damage, and generally a pipeline becomes weaker with increasing age. Hence, the remaining strength of the pipeline must be estimated by adopting a suitable method.

Kiefner et al. [14] and Shanon [15] have developed the following semi-empirical model to calculate the remaining strength. This basic approach is considered by most of the codes/standards. The remaining hoop stress at failure (σ_{hdp}), with a longitudinally oriented corrosion defect is estimated by equation (5.3)

$$\sigma_{hdp} = \sigma_f \left[\frac{1 - \frac{A_c}{A_o}}{1 - \frac{A_c}{A_o M}} \right] \tag{5.3}$$

where σ_{hdp} is the hoop stress of the defected pipe, σ_f is the flow stress, A_c is the actual longitudinal corroded area, A_o is the original area, and M is the Folias factor. The bracketed term can be considered as the reduction factor.

The corroded area can be approximated by a parabola

$$\frac{A_c}{A_o} = \frac{(2/3)ld}{lt} = \frac{2d}{3t} \tag{5.4}$$

and the Folias factor is defined as

$$M = \sqrt{\left[1 + \frac{0.8l^2}{Dt}\right]} \tag{5.5}$$

Equations (5.4) and (5.5) are a basic approach to design the ratio of the corroded area to the original area and the stress concentration factor. The codes/standards and models developed by individuals have defined the above mentioned two terms (ratio of areas and stress concentration factor) in their own way. The basic approach is considered by ASME B31G.

The burst pressure of a defected pipe is therefore,

$$P_{bdp} = \sigma_{hdp}\frac{2t}{D} = \sigma_f\left[\frac{1-\frac{A_c}{A_o}}{1-\frac{A_c}{A_o M}}\right]\frac{2t}{D} \tag{5.6}$$

where the flow stress (σ_f) is usually expressed in specified minimum yield stress or specified minimum tensile stress times the design factor F.

For corrosion studies, the depth of the defect (d) and length of the defect (l) are important factors to be considered. A typical longitudinally oriented, rectangular shaped external corrosion defect, as sketched in Figure 5.3, is considered for this study. It is assumed that this defect occurs at a discrete location and that it is discontinuous throughout the pipeline length. The effect of defect width (c) has been found to have a

comparatively insignificant effect on the burst pressure, as indicated by Netto et al. [5], while defect depth (d) has the most significant effect and defect length (l) has a moderate effect on the pipeline burst pressure. Therefore, the defect depth (d) and length (l) parameters are considered for the prediction of burst pressure (P_{bdp}) for external corrosion. Since the orientation of defect depth (d) and defect length (l) are important considerations in the structural analysis, the defect depth is considered through thickness (radial direction) and defect length is longitudinally oriented (axial direction) in this study. This represents the worst case scenario with respect to the applied hoop stress.

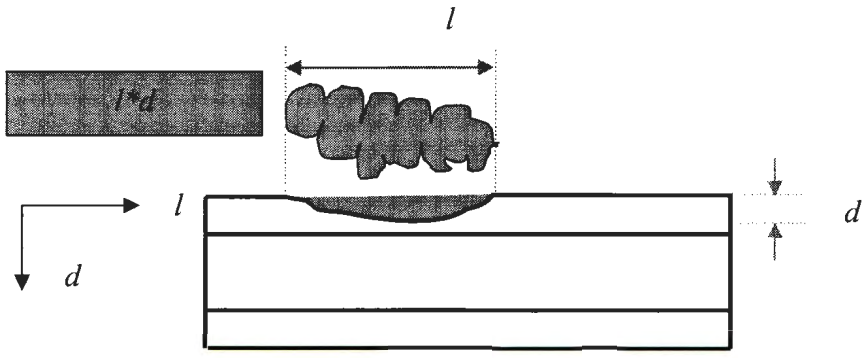

Figure 5.3: A simplified externally corroded surface flaw in pipeline

In this Chapter, an approach has been developed that calculates the burst pressure for internal corrosion considering a rectangular/parabolic shaped defect ($l \times d$) and the corresponding failure probability of the pipeline is assessed using the available codes/standards [6,7,8] and models proposed by Netto et al. [5] and Bea et al. [13]. Among the models/standards considered in the present study, the Bea et al. [13] models account for the defect depth (d) only.

5.3.3 Defect variables specification

The reliability analysis of corroded pipeline requires the probabilistic specification of the basic variables d and l, which define the corrosion defect. It may be noted that there is no correlation between the depth of defect (d) and length of defect (l); instead, it is observed that for a given depth of defect (d), there is a range of associated length of defect (l) [16]. For example, for a depth of 20% wall thickness, the length varied (l) from 8 to 608 mm. However, depth of defect (d) and length of defect (l) can be assumed to be Weibull distributed with a CoV of 0.50, suggested by Zimmerman et al [17]. Thus the probability of defect depth (d) greater or equal than its characteristic value (d_c) is expressed by

$$P(d \geq d_c) = 1 - F(d) = e^{-\left(\frac{d}{\theta}\right)^{\beta'}} = \int_{d_c}^{\infty} f(d)dd \qquad (5.7)$$

where $F(d)$ is the cumulative distribution of defect depth (d), (β') is the shape parameter and (θ) is the scale parameter of the distribution and dd is a small change in defect depth. In the same way the probability of defect length (l) is greater than or equal to its characteristic value (l_c) and is expressed by

$$P(l \geq l_c) = 1 - F(l) = e^{-\left(\frac{l}{\theta}\right)^{\beta'}} = \int_{l_c}^{\infty} f(l)dl \qquad (5.8)$$

The CoV 0.50 means the shape parameter (β') of the Weibull distribution for defect depth (d) and defect length (l) in equations (5.7) and (5.8) are both 2.1. The scale parameters (θ) for defect depth (d) and defect length (l) were calculated using equations (5.7) and (5.8). The calculation considered cumulative distribution F(d)=F(l)=0.90 and characteristic depth (d_c) as 1.5% of the thickness (t) of the pipeline for each year. Similarly, the characteristic length (l_c) was considered as 4% of the diameter (D) of the pipeline for each year. The mean defect depth (d) is thus 0.1807 mm/yr and the defect length (l) is 17 mm/yr. The study also assumed the linear addition of defect depth (d) and defect length (l) for each year. These reflect that after the design life of T=20 years, the mean defect depth (d) and mean defect length (l) would be 3.61 mm and 340 mm respectively. Table 5.1 shows the probabilistic data for the defect depth (d) and defect length (l).

Table 5.1: Probabilistic data for the random variables- depth of defect (d) and length of defect (l)

Variables	d-defect depth (mm/yr)	l-defect length (mm/yr)
Type	Weibull	Weibull
μ	0.1807	17
CoV	0.50	0.50

5.4 Burst Models and Standards

A defected pipe's burst pressure is considered as the resistance in this analysis. The equations developed by different codes/standards for pipeline burst pressure

estimation for defects are discussed below. It may be noted that the codes and standards are based on closed end conditions and considered hoop stress. The codes/standards have not considered axial (the other load in the biaxial plane), radial or combined loads such as thermal or bending load. Each burst model was discussed with the same notations for the parameters (burst pressure of defected pipe, yield/burst pressure of defect free intact pipe etc.) as they were originally developed by the codes/standards or individuals. The notations maintained by the codes/standards were not repeated in the nomenclature provided at the beginning of the paper. The notation for defect length is specified by l in some codes/standards [5,6] where others [7, 8] specified it by L.

5.4.1 CSA Z662-07 [6]

CSA Z662-07 standard is defined, for large leaks and ruptures, as the limit state function g_2 for plastic collapse at a surface corrosion defect with total axial length l (in mm), and average defect depth d_a (in mm) and is given as

$$g_2 = r_a - p \tag{5.9}$$

where r_a = the estimated pressure resistance including model error, MPa

$= e_1 r_c + (1 - e_1) r_o - e_2 \sigma_u$ for SMYS > 241 Mpa $= e_3 r_c + (1 - e_3) r_o - e_4 \sigma_y$ for SMYS $\leq$ 241 MPa

r_c = the calculated pressure resistance, MPa

$$= r_o \left(\frac{1 - \frac{d_a}{t}}{1 - \frac{d_a}{m \times t}} \right)$$

r_o = the pressure resistance for perfect pipe, MPa

$= 1.8\frac{t\sigma_u}{D}$ for SMYS > 241 MPa $= 2.3\frac{t\sigma_y}{D}$ for SMYS $\leq$ 241 MPa

m = the Folias factor

$= \sqrt{1 + 0.6275\frac{l^2}{D \times t} - 0.003375\frac{l^4}{D^2 \times t^2}}$ for $l^2/Dt <= 50$ $= 0.032\frac{l^2}{D \times t} + 3.3$ for $l^2/Dt > 50$

SMYS=Specified Minimum Yield Strength and $d_a = d$, the depth of defect

e_1 = a deterministic multiplicative model error term that equals 1.04, e_2 = an additive model error term, defined by a normally distributed random variable with a mean of –0.00056 and a standard deviation of 0.00146, e_3 = a deterministic multiplicative model error term that equals 1.17 and e_4 = an additive model error term, defined by a normally distributed random variable with a mean of –0.00765 and standard deviation of 0.00650.

5.4.2 DNV RP-F101 [7]

In DNV-RP-F101, the maximum operating pressure for a pipeline with a corrosion defect is given by

$$P_{corr} = 1.05\frac{2t\sigma_u(1-\gamma_d(d/t))}{(D-t)\left(1-\frac{\gamma_d(d/t)}{Q}\right)} \qquad (5.10)$$

where $Q = \sqrt{1 + 0.31\left(\frac{L}{\sqrt{Dt}}\right)^2}$, L is length of defect and σ_u is designed Specified Minimum Tensile Strength.

It may be noted that DNV-RP-F101 [7] proposed two equations for burst estimation: one is to estimate capacity (CP) considering a rectangular defect and the other is to estimate allowable maximum operating pressure (MOP). The MOP equation is not demonstrated here, but is considered in the analysis. In the present analysis, allowable maximum operating pressure (MOP) is referred to as DNV-RP-F101 MOP [7] and capacity pressure is referred to as DNV-RP-F101 CP [7]. In reality, the DNV-RP-F101 MOP [7] equation is more conservative than DNV-RP-F101 CP [7].

5.4.3 ASME B31G [8] CODE

Among the existing criteria for evaluating the residual strength of the corroded pipeline, the ASME B31G code is still the most widely used criterion. Kiefner et al. [18,19] observed that the ASME B31G code is over-conservative for specific defects. They modified the code to develop what is known as the 0.85 *dL* method. Like the original, the defect length and the defect depth are the only parameters required to define the defect.

The burst pressure defined by ASME B31G is

$$P_b^{B31G} = \frac{2t}{D}\left(1.1\sigma_y\right)\left[\frac{1-(2/3)(d/t)}{1-(2/3)(d/t)M^{-1}}\right] \qquad (5.11)$$

where $M = \sqrt{1+0.8\left(\frac{L}{D}\right)^2\left(\frac{D}{t}\right)}$

5.4.4 Netto et al. [5] model

Netto et al. [5] developed a burst pressure equation for external corrosion, considering the depth of defect, length of defect, width of corrosion, pipeline wall thickness and pipeline diameter. The effect of external corrosion defects was investigated through a series of small-scale experiments and non linear numerical models based on the finite element method. The experimental and numerical results were then used to calibrate the equation. The burst pressure equation for defected pipe is given by equation (5.12). In this equation, P_b is the burst pressure for the defected pipe, P_{bi} is the burst pressure for the intact pipe, l is the corrosion defect length, d is the corrosion defect depth, t is the pipeline wall thickness and D is the pipeline diameter. This equation was developed with limiting conditions of corrosion defect depth to wall thickness ratio ($0.1 \leq d/t \leq 0.8$) and corrosion defect length to pipeline diameter ($l/D \geq 0.5$) ratios. The approach is not valid for narrow defects ($c/D \leq 0.0785$).

$$\frac{P_b}{P_{bi}} = 1 - 0.9435\left(\frac{d}{t}\right)^{1.6}\left(\frac{l}{D}\right)^{0.4} \tag{5.12}$$

where $P_{bi} = \dfrac{1.1\sigma_y 2t}{D}$

5.4.5 Bea et al., [13] model

The Pipeline Requalification Guidelines Project [13] developed an equation for burst pressure as

$$P_b = 2.2(t-d)\frac{SMTS}{(D-t)\times SCF} \qquad (5.13)$$

where $SCF = 1 + 2\sqrt{\frac{d}{R}}$, SMTS is the Specified Minimum Tensile Strength and SCF is the Stress Concentration Factor. The burst equation, equation (5.13), does not consider the corrosion defect length (l). This may be a significant issue where aspect ratio plays an important role in biaxial stress states.

5.5 Failure Models

As mentioned earlier, all codes/standards [6, 7, 8] consider defect length and defect depth $(l \times d)$ and not the defect width (c). The main considerations in the present study are:

1. The growth of defect depth (d) and defect length (l) were assumed to be linearly additive for the design life of T=20 years.
2. The defect length (l) is not directly correlated with defect depth (d). The length (l) and depth of the defect (d) is considered to be Weibull distributed with a CoV of 0.50 [17].
3. The orientation of the corrosion defect($l \times d$) parameters is assumed to have the length (l) in the longitudinal direction and depth (d) through the wall thickness or radial direction. The circumferentially oriented corrosion defect width (c) is not considered in this study.

4. In this study the minimum value of the reliability index is assumed to be zero, which corresponds to the highest failure probability 0.50 for the limit state analysis.

The limit state function for externally corroded pipelines can be written as follows:

$$g(X) = P_{bdp} - P_{op} \tag{5.14}$$

where P_{bdp} is the burst pressure of the defected pipe, and P_{op} is the operating pressure. The burst pressure of the defected pipe, P_{bdp}, is considered as the resistance, and operating pressure, P_{op}, is considered as the load in the limit state function defined by equation (5.14). The burst pressure of the defected pipe, P_{bdp} is calculated using respective codes/standards or individual models.

The reliability index β is obtained from load and resistance variables

$$\beta = \frac{\mu_{P_{bdp}} - \mu_{P_{op}}}{\sqrt{\sigma^2_{P_{bdp}} + \sigma^2_{P_{op}}}} \tag{5.15}$$

Using equation (5.15) reliability index, β may be calculated for any codes and standards. Once the reliability index, β, is calculated for any codes/standards or models, the failure probability (P_f) can be calculated using equation (5.16). One can calculate the risk (R) if the consequence (C) is known for a specific material and a specific location considering equation (5.17).

$$P_f = \varphi(-\beta) = 1 - \varphi(\beta) \quad (5.16)$$

$$R = P_f \times C \quad (5.17) \text{ infuse}$$

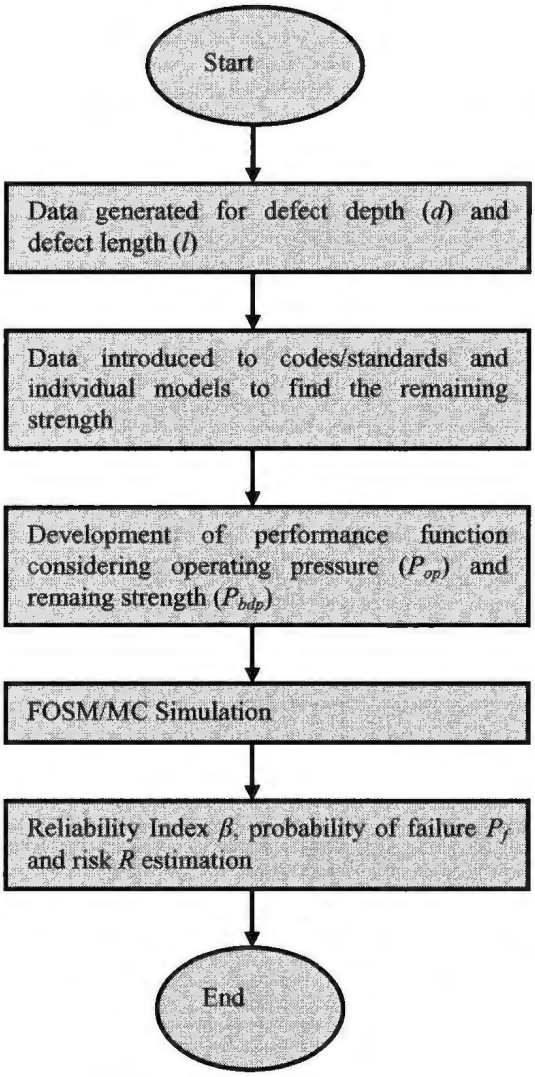

Figure 5.4: The flow chart depicts the calculation procedure followed in this study

A flow chart of calculation procedures is shown in Figure 5.4.

5.6 Failure Analysis

For the external corrosion model CSA Z662-07 [6], DNV RP-F101 [7], ASME B31G [8] code, the Netto et al. [5] model and the Bea et al. [13] model were considered for analysis.

The failure analysis was carried out considering the generalized limit state equation, equation (5.14) for all codes/standards and models [5, 6, 7, 8, 13]. It may be noted that equation (5.14) is a burst limit state, which considers burst pressure and operating pressure. Once a burst limit state was considered, equation (5.15) and equation (5.16) were considered for failure probability estimation.

For example, the ASME B31G code is considered to calculate the burst pressure of the defected pipe. The burst pressure is now represented by equation (5.18). This burst pressure is considered by a generalized limit state equation (5.14).

$$P_{b\,dp} = P_b^{B31G} = \frac{2t}{D}\left(1.1\sigma_y\right)\left[\frac{1-(2/3)(d/t)}{1-(2/3)(d/t)M^{-1}}\right] \tag{5.18}$$

where $M = \sqrt{1+0.8\left(\frac{L}{D}\right)^2\left(\frac{D}{t}\right)}$

The new burst limit state equation (5.19) is derived for the ASME B31G code using equation (5.14). The limit state function for the ASME B31G code is, therefore

$$g_i(X) = \frac{2t}{D}\left(1.1\sigma_y\right)\left[\frac{1-(2/3)(d/t)}{1-(2/3)(d/t)M^{-1}}\right] - P_{op} \tag{5.19}$$

All the basic variables in equation (5.19), are available in Table 5.1 (for d and l) and Table 5.2 (for D, t, σ_y/σ_u and P_{op}). There is less uncertainty observed in pipeline diameter D and thickness t, compared to yield and ultimate strength. This is because of uncertainty in material composition, chemistry and the manufacturing process. This fact is captured in the coefficient of variance reported in Table 5.2. The uncertainty of defect depth d and defect length l have already been discussed in section 5.3.3.

Table 5.2: Probabilistic models of the basic variables for material- API 5L X 65

Variables	σ_u/ MPa	σ_y/MPa	D/mm	t/mm	P_{op}/MPa
Type	Lognormal	Lognormal	Normal	Normal	Gumbel
μ	530	447	713	20.24	17.12
CoV	0.05	0.07	0.001	0.001	0.08

The procedure specified above to develop the limit state equation and calculation of the probability of failure (P_f) is the same for every code/standard. The probability of failure (P_f) is calculated using equation (5.15) and equation (5.16) by the FOSM method. The failure function g() may be considered for the direct evaluation of probability of failure (P_f) by the Monte Carlo method which will verify the result obtained by the FOSM method.

In Table 5.2, the mean value of the operating pressure (P_{op}) was calculated from characteristic operating pressure (p_{cop}), which again was calculated from the yield pressure (P_{yip}) of defect free intact pipe. The characteristic operating pressure (p_{cop}) was considered as 72% of the yield pressure (P_{yip}). The characteristic values for load (P_{op})

were calculated considering the EURO Code EN 1990 [20] recommendation that the characteristic values should correspond with 95% upper and 5% lower values, respectively, for load and resistance variables.

Therefore, $p_{cop} = P_{yip} \times 0.72 = \frac{2 \times 447 \times 20.24}{713} \times 1.1 \times 0.72 = 20.10$ MPa.

The characteristic value of operating pressure (P_{cop}) was considered to calculate the Gumbel mean and standard deviation. It may be noted that operating pressure can be characterized by Gumbel distribution as per CSA Z662-07's [6] recommendation. The equations (5.20) - (5.23) were considered to calculate Gumbel parameters.

$$F_{P_{op}}(p_{cop}) = \exp\left[-e^{-\alpha_{op}(p_{cop}-u_{op})}\right] \tag{5.20}$$

$$P(P_{op} \geq p_{cop}) = 1 - F_{P_{op}}(p_{cop}) \tag{5.21}$$

$$\alpha_{op} = \frac{1}{\sqrt{6}}\left(\frac{\pi}{\sigma_{P_{op}}}\right) \tag{5.22}$$

$$u_{op} = \mu_{P_{op}} - \frac{0.5772}{\alpha_{op}} \tag{5.23}$$

where $\mu_{P_{op}}$ is the Gumble mean, $\sigma_{P_{op}}$ is the Gumble standard deviation and P_{op} is the operating pressure considered as an extreme random variable. The parameters u_{op} and α_{op} are related to the Gumbel mean and standard deviation.

Once the failure probabilities are determined for different codes and standards, the next question that needs to be answered is about the consistency of failure probabilities (P_f) calculated by different methods. Because variability is observed in the probability of failures (P_f), identification of the cause of variability is an important area of research for

this study. Sensitivity analysis of the parameters in the failure function, g(), would help to identify the cause of variability in the probability of failures (P_f).

5.7 Sensitivity Analysis

The sensitivity of the failure function can be studied by a differential approach and a Monte Carlo approach. The differential approach to sensitivity requires the transformation of the parameters distribution to equivalent normal distribution if the distribution is not normal. The transformation calculates the equivalent normal mean and standard deviation at the design point. This approach is rather tedious. A readily available solution may be available considering only mean and standard deviation; however, this is obviously not a good choice. The differential analysis of sensitivity evaluates sensitivity at a specific point. The Monte Carlo approach can be applied when all the parameters of distribution are known. In the present study, the Monte Carlo simulation approach is considered for the sensitivity analysis.

Monte Carlo Approach

A quantitative estimate of linear correlation can be determined by calculating a simple correlation coefficient on the parameter values of input and output. Gardner et al. [21] recommend using simple correlation coefficients, derived from Monte Carlo simulations, as a reasonable way to rank model parameters according to their contribution to predict uncertainty. Pearson's correlation coefficient denoted by r is used in the present study for sensitivity analysis.

$$r_{x_j y} = \frac{\sum_{i=1}^{N}\left(x_{ij} - \bar{x}_j\right)\left(y_i - \bar{y}\right)}{\left[\sum_{i=1}^{N}\left(x_{ij} - \bar{x}_j\right)^2\right]^{1/2}\left[\sum_{i=1}^{N}\left(y_j - \bar{y}\right)^2\right]^{1/2}} \qquad (5.24)$$

5.8 Results and Discussion

The failure probability of different burst models recommended by codes/standard was calculated and compared for external corrosion analysis. The analysis used the First Order Second Moment (FOSM) and Monte Carlo (MC) simulation method and considered 20 years design life. The results obtained by two solution approaches are closely matching as noticed in Table 5.3. This expresses the accuracy of the results. The analytic (FOSM) result of the analysis is presented in Figure 5.5. Analyzing Figure 5.5, a significant difference is noted in the value of P_f for different burst models recommended by codes/standards and that developed by individuals. The highest value of probability of failure 5.5×10^{-2} is observed for the Bea et al [13] model while the lowest probability of failure 5.3×10^{-5} is observed for DNV RP-F101 CP [7] model.

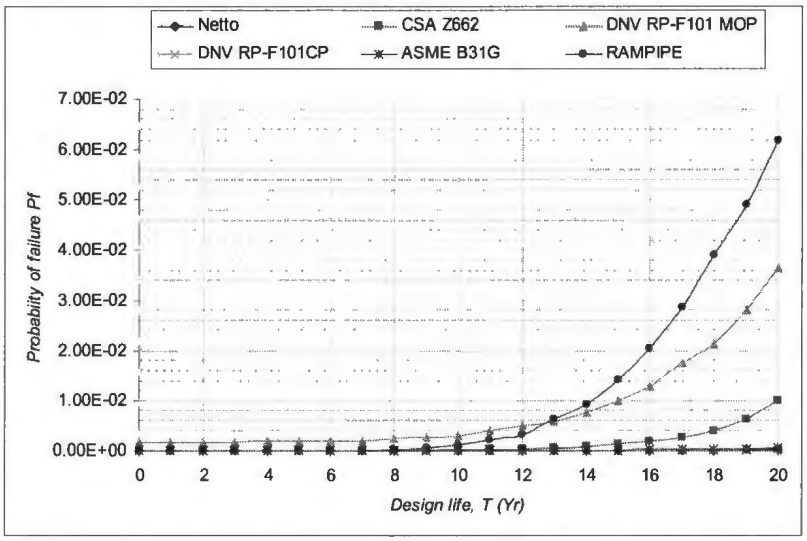

(a)

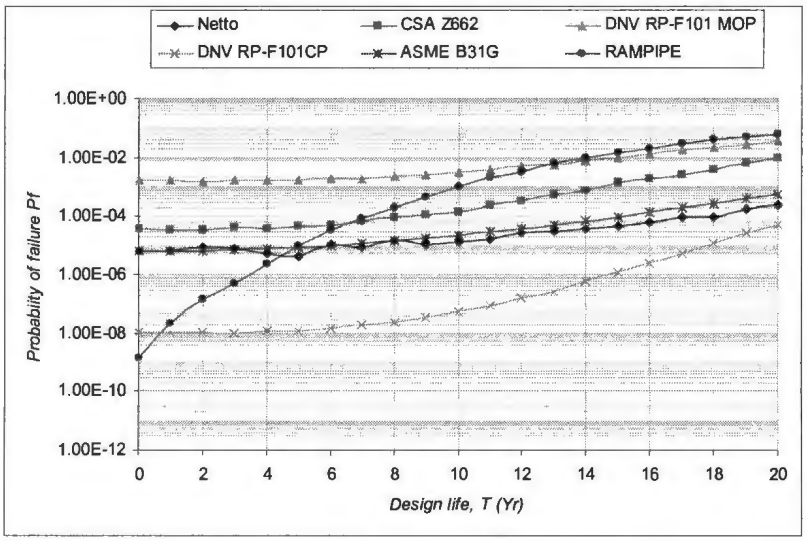

(b)

Figure 5.5: Failure probability P_f for different codes/standards using burst in the limit state equation a) normal graph b) Semi-logarithmic graph

Table 5.3: Probability of failure (P_f) obtained for different codes/standards at the end of the design life, T=20 yrs.

Codes/Standard	FOSM		Monte Carlo	
	P_f	β	P_f	β
DNV RP-F101 CP	$5.3*10^{-5}$	3.87	$1.5*10^{-4}$	3.62
Netto et al. 2008	$2.4*10^{-4}$	3.48	$1.9*10^{-4}$	3.55
ASME B31G	$5.3*10^{-4}$	3.27	$1.9*10^{-4}$	3.55
CSA Z662-07	$9.9*10^{-3}$	2.33	$7.6*10^{-3}$	2.42
DNV RP-F101 MOP	$3.6*10^{-2}$	1.80	$2.6*10^{-2}$	1.93
Bea et al., 1999	$5.5*10^{-2}$	1.59	$5.8*10^{-2}$	1.56

The cause of variability may be determined by sensitivity analysis of the failure functions g() for different codes/standards.

The sensitivity is analyzed in terms of dimensionless parameters ($W=\frac{d}{t}, X=\frac{D}{t}, Y=\frac{\sigma_h}{\sigma_y \text{ or } \sigma_u}$ and $Z=\frac{l}{D}$) of the failure functions g () using the Monte Carlo approach. The analysis considered the data given in Table 5.4 for dimensionless parameters in the g() function. The analysis considered the remaining parameters (other than dimensionless) constant in the failure function. The results are presented in Figure 5.6. The sensitivities for the dimensionless parameter $X=\frac{D}{t}$ are observed to be insignificant for all codes/standards. This suggests that a change in either D or t has little effect on the failure g() function. It may be noted that the failure g() function for the Netto et. al. model does not truly contain any $\frac{D}{t}$ ratio, whereas the other

codes/standards contain $\frac{D}{t}$ ratio in the stress concentration factor, M or Q. The other dimensionless parameters ($W = \frac{d}{t}, Y = \frac{\sigma_h}{\sigma_y \text{ or } \sigma_u}$ and $Z = \frac{l}{D}$) are observed to be sensitive in each of the codes/standards. This means a small change in (W, Y, or Z) has a significant effect on the failure function g(). Dimensionless parameter Y has the most significant effect on the failure function g(), followed by W and Z. The sensitivity for Y is rather consistent for all codes/standards, and does not vary significantly from one code to another. This indicates that it is not a significant issue whether yield or ultimate strength are considered in the burst models. It seems the dimensionless parameters W and Z are most responsible for the significant variation in failure probability (P_f). The sensitivity of dimensionless parameters, W and Z, corresponds to the sensitivity of d and l respectively. It may be noted that the effects of the parameters t and D in $W = \frac{d}{t}$ and $Z = \frac{l}{D}$ are already identified as insignificant in the failure g() function.

Table 5.4: Probabilistic models of dimensionless parameters

Dimensionless Parameter	$W = \frac{d}{t}$	$X = \frac{D}{t}$	$Y = \frac{\sigma_h}{\sigma_y \text{ or } \sigma_u}$	$Z = \frac{l}{D}$
Type	Weibull	Normal	Normal	Weibull
μ	0.1792	35.22	0.6794 (Netto et al., ASME B31G) 0.5730 (CSA) 0.5558 (DNV)	0.4717
CoV	0.5050	0.0014	0.1130 (Netto et al., ASME B31G) 0.1157 (CSA) 0.1123 (DNV)	0.5030

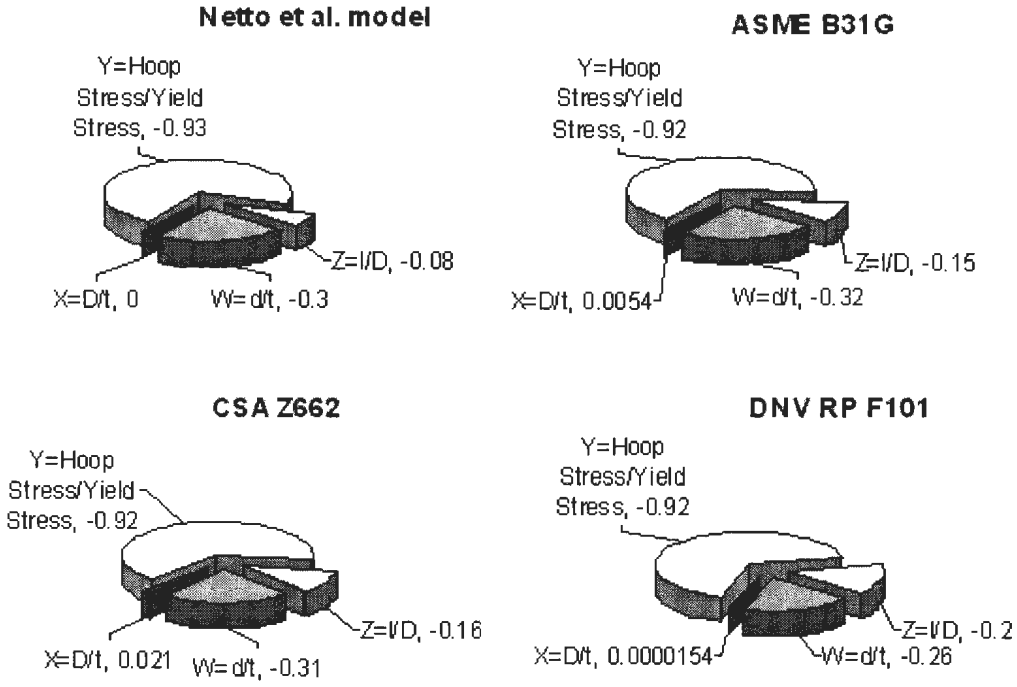

Figure 5.6: Graphical representation of sensitivity analysis of dimensionless parameter by Monte Carlo method.

Considering equation (5.18), the burst pressure of the defected pipe is a function of intact pressure and the reduction factor.

$$P_{dp} = f\{\text{Intact burst, 'reduction factor' Pb}_i\}$$
$$= f\{\text{Intact burst } f(F,t,\sigma_y,D), \text{'reduction factor' } f(d,t,l,D)\}$$

As it is observed that parameters in the intact burst pressure are not responsible for variation in remaining strength estimation of corroded pipe for different codes and standards, a further sensitivity analysis of the reduction factor, *Pbi*, reveals the cause of variability in the remaining strength. Figure 5.7 shows the sensitivity analysis of the *Pbi*

factor. According to Figure 5.7, the contribution of *d* and *l* in the burst model equation are responsible for variation in the calculated remaining strength. Table 5.5 further illustrates the importance of the dimensionless parameters in the failure function. The contribution of the parameter *d* in the reduction factor *Pbi* is found to be most significant, which is followed by *l*. According to Table 5.5, the basic variable *d* contributes 76% in the Netto et. al. model while 59% is contributed in the DNV-RP-F101 model. A similar observation was noticed for the basic variable *l*, in which 21% was contributed in the Netto et. al. model, while 59% was contributed in the DNV-RP-F101 model. The insignificant contribution is again observed for *D* and *t*.

Table 5.5: Importance factor in the reduction factor *Pbi*.

Individual Parameter (*i*)	Importance factor (in % contribution) in reduction factor, *Pbi*			
	Netto et al model	ASME B31G	CSA Z662	DNV RP F101
d	76	64	63	59
l	21	34	35	41
Other parameters (*D* & *t*)	3	2	2	0

In the present study significant variation is observed in probability of failure (P_f) for different burst models recommended by codes/standards and also by individuals. The variation in probability of failure is due to differences in remaining strength estimation of the different models. The cause of variability in remaining strength is contributed by *d* and *l* in the burst models recommended by codes/standards.

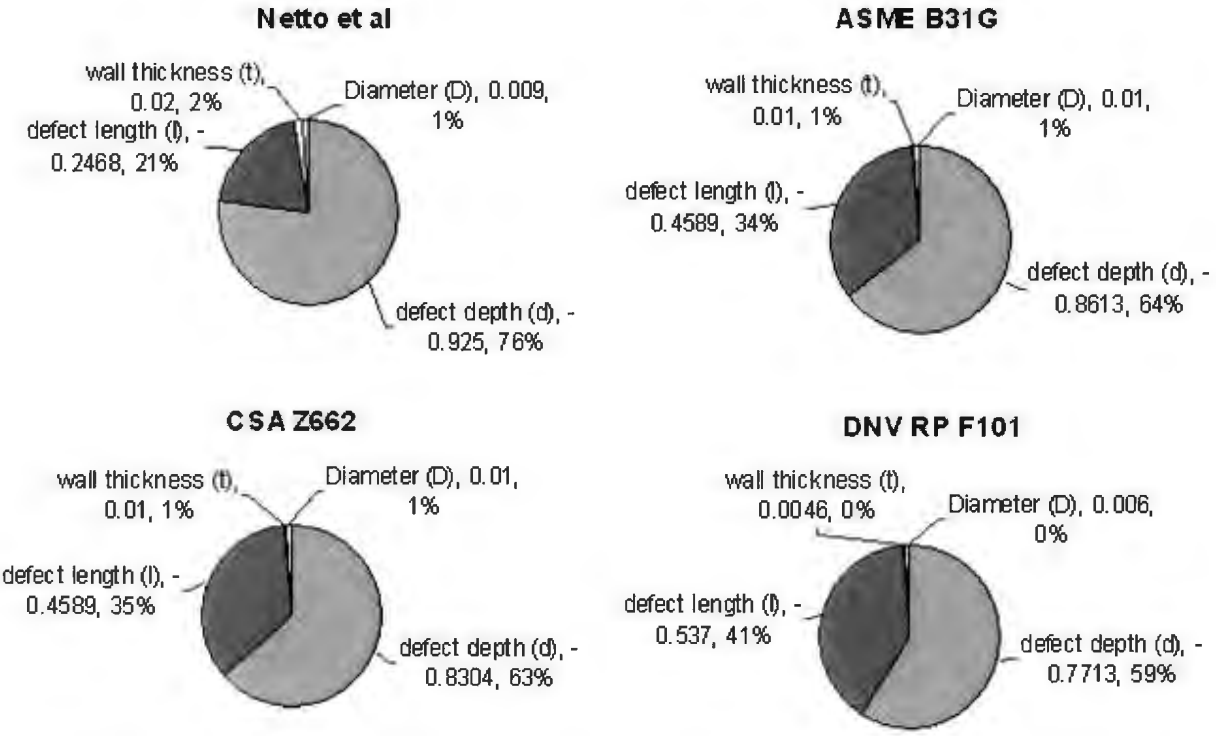

Figure 5.7: Graphical representation of sensitivity analysis of *Pbi* factor by Monte Carlo method.

The Bea et al. [13] model is not considered in this analysis as it considers only defect depth, *d* for *Pbi* factor estimation. The DNV-RP-F101 MOP [7] model is also not considered in the sensitivity study, since this equation is not for designing the pipeline, but is rather intended to evaluate the maximum operating pressure in the system.

5.9 Conclusion

The validation of failure probability, calculated by FOSM with experimental tests, is difficult to obtain since it requires significant test data to get a standard deviation of burst pressure. However, Monte Carlo simulation verifies the results obtained by the FOSM method. As the result obtained by the two methods closely match, therefore the accuracy of the result is ensured. This paper further investigated the cause of variability in probability of failure that must be minimized for a risk-based design approach. It is observed that different ways of accounting for the defect geometry in the burst models is responsible for variation in estimated remaining strength. This variation is highly responsible for significant variability in probability of failure. It is therefore recommended that the modelers or classification societies should concentrate on the reduction factor, *Pbi* for a unified risk-based design approach. This will provide an identical probability of failure (P_f) of the burst models recommended by codes/standards.

5.10 Acknowledgements

The authors gratefully acknowledge the financial support provided by Petroleum Research Atlantic Canada (PRAC) and Natural Science and Engineering Research Council (NSERC) of Canada.

5.11 References

[1] Zhu, X. -K., & Leis B. N. (2006). Average shear stress yield criterion and its application to plastic collapse analysis of pipelines. *International Journal of Pressure Vessels and Piping*, Vol 83 pp 663-671.

[2] Haldar A., & Mahadevan S. (2000). *Probability, Reliability and Statistical Methods in Engineering Design*. John Wiley & Sons, Inc.

[3] Lee, O. S., & Kim D. H. (2006). The reliability estimation of pipeline using FORM, SORM and Monte Carlo simulation with FAD. *KSME Int. J.*, **20** (12), pp. 2124-2135.

[4] Palmer A. C., & King R. A. (2008). *Subsea Pipeline Engineering*. 2nd Edition, PennWell.

[5] Netto T. A., Ferraz U. S., & Estefan S. F. (2005). The effect of corrosion defect on the burst pressure of the pipeline. *Journal of Constructional Steel Research,* Vol 61 pp 1185-1204

[6] CSA Z662-07, (2007). Limit state equation for burst of large leaks and rupture for corrosion defect. *Oil and Gas Pipeline Systems*, Canadian Standards Association. pp 554-555.

[7] DNV RP-F101 (2004). *Recommended Practice Corroded Pipelines*. Det norske Veritas

[8] ASME B31G (1995). *Manual for determining the remaining strength of corroded pipelines*. A supplement to ANSI/ASME B31 code for pressure piping.

[9] Lee, O. S., & Pyun J. S. (2002). Failure probability of corrosion pipeline with varying boundary condition. *KSME International Journal*, Vol 16, No. 7, pp 889-895.

[10] Lee, Y. K., Kim Y. P., Moon M. –W., Bang W. H., Oh K. H., Kim W. –S., 2005, "The prediction of failure pressure of gas pipeline with multi corroded region," Trans Tech Publication, **475-479**, pp. 3323-3326.

[11] Menon E. S. (2005). *Piping Calculations Manual*. McGrawhill

[12] McLamb M., Hopkins P., Marley M., & Nessim M. (2002). A justification for designing and operating pipelines up to stresses of 80% SMYS. *4th International Pipeline Conference*, IPC2002-27007, Calgary, Alberta, Canada.

[13] Bea R., Xu T. (1999). Corrosion Effects on Burst Pressures RAM PIPE REQUAL. *Pipeline Requalification Guidelines Project Report 1*, University of California at Berkeley, pp 103-104.

[14] Kiefner, J. F., Maxey, W. A., Eiber, R. J. & Duffy, A. R. (1973). Failure stress levels of flaws in pressurized cylinders. *American Society for Testing and Materials*, ASTM STP 536, pp. 461 - 48 1.

[15] Shannon, R. W. E. (1974). The failure behavior of line pipe defects. *International Journal of Pressure Vessel and Piping*, Vol. 2, pp. 243 - 255.

[16] Amirat A., Benmoussat A., & Chaoui A. (2009). Reliability assessment of underground pipelines under active corrosion defects. *Damage and Fracture Mechanics: Failure Analysis of Engineering Materials and Structures*, 83–92. Springer Science

[17] Zimmerman TJE, Hopkins P., Sanderson N. (1998). Can limit states design be used to design a pipeline above 80% SMYS. *In: Proceedings of the 17th*

international conference on offshore mechanics and Arctic engineering (OMAE 1998), ASME.

[18] Kiefner J. F., Vieth P. H. (1990a). Evaluating pipe 1: new method corrects criterion for evaluating corroded pipe. *Oil & Gas Journal*, 88(32):56-9.

[19] Kiefner J. F., Vieth P. H., (1990b). Evaluating pipe conclusion: PC program speeds new criterion for evaluating corroded pipe. *Oil & Gas Journal*, 88(34):91-3.

[20] EN 1990, (2001) . *Basis of structural design*. Brussels.

[21] Gardner, R.H., O'Neill, R.V., Mankin, J.B. & Carney, J.H. (1981). A Comparison of Sensitivity Analysis and Error Analysis Based on a Stream Ecosystem Model. *Ecol. Modelling*. 12, 173-190.

Chapter 6

Probabilistic Transgranular SCC Analysis for Oil and Gas Pipelines*

Preface

Where *Chapter 4* and *Chapter 5* discussed failure assessment of internal and external corrosion defects respectively; this chapter provides a stress corrosion crack (SCC) analysis for oil and gas pipeline. This chapter is published in the *Journal of Pressure Vessel Technology*. It may be noted that the result obtained from *Chapter 4-7* is integrated using FTA in *Chapter 8*

The principal author did the literature review and identified codes/standards for the analysis. The principal author characterized the SCC crack probabilistically and calculated failure probability considering stress/strain based approaches. The co-authors provided directions and recommendations to develop validation approaches. The co-authors monitored the progress, and reviewed the output results.

The principal author prepared the manuscript, which was consecutively revised and improved based on the co-author's comments and corrections.

*this paper has been published in Journal of Pressure Vessel and Technology. The reference is provided below.

Hasan, M., Khan, F., Kenny, S., (2012). Probabilistic Transgranular Stress Corrosion Cracking Analysis for Oil and Gas Pipelines, Journal of Pressure Vessel and Technology, Vol. 134 / 051701-1. October, 2012

Abstract

The crack morphology of Transgranular stress corrosion cracking (TGSCC) suggests that the mechanism of growth and the condition at which TGSCC occurs are different than that of intergranular stress corrosion cracking (IGSCC). Several attempts have been made to characterize IGSCC probabilistically; however, a limited effort has been dedicated for TGSCC. This paper attempts to analyze TGSCC probabilistically. The study includes assessment of the probability of failure for low pH, transgranular SCC by the R-6 approach/BS 7910 approach/API 579 approach which considers plastic yielding and linear elastic fracture mechanics, CSA Z 662-07 burst model approach and the author's proposed strain based approach. The paper observes that failure assessment diagram (FAD) based approaches (R-6 ,BS 7910, API 579) calculate least failure probability compared to burst model approaches such as CSA Z 662-07 etc. burst model approaches. The authors also observed that their proposed hoop strain based approach calculates closely to the CSA Z 662-07 burst model approach. Finally the authors justified the rationality of the results obtained by their approach.

Keywords: Transgranular SCC, failure assessment diagram (FAD), strain based design, limit state etc.

6.1 Introduction

Environmentally assisted cracking (EAC) is a generic term that describes all types of cracking in a pipeline where the surrounding environment, the pipe material and stress act together to reduce the strength or load-carrying capacity of the pipe. Transgranular SCC is one form of EAC; the other forms are corrosion fatigue (CF), hydrogen induced cracking (HIC) and hydrogen embrittlement etc. SCC and CF depend on the loading and environmental conditions. If a deleterious environment is present with cyclic loading, then CF is the time dependent mode of failure; otherwise, it is SCC when static loading is working. The work of Parkins et al. [1, 2] suggests that the loading condition considered in their work is cyclic but at the same time it closely matches the static loading condition as mostly an average stress was maintained with a high R value.

SCC is categorized in two forms: near neutral pH SCC (mostly TGSCC) and high pH SCC (mostly IGSCC). High pH SCC occurs only in a relatively narrow cathodic potential range in the presence of a carbonate/bicarbonate environment and at a pH greater than 9. A thin oxide protective film is formed on the pipe surface from the electrochemical reaction in the presence of cathodic potential and the potent environment. This protective film acts as a barrier to SCC and the corrosion process can not initiate unless the film is broken. Hence the microplastic strain rate, related to the rate at which the pressure in the pipe changes, acts as a driving force to initiate and expand the crack [3]. Though the mechanism of near neutral pH SCC (pH in the range of 5.5-7.5) is not well understood, a convincing explanation is made by Parkins [4,5]. He suggested that the mechanism of crack growth involves dissolution and ingress of hydrogen into steel,

facilitating crack growth by promoting reduced ductility. This view is supported by Beavers , Leis , Wilmot and Jack , and Lambert and Plumtress [3]. In the present study, Parkin's et al. [1, 2] work is taken as the basis for probabilistic analysis of failure for API X 65 steel.

It may be noted that three basic conditions must be satisfied for the occurrence of near neutral pH SCC :

a) A potent environment

b) Tensile stress and

c) Susceptible pipe material.

The susceptibility of pipe material to near-neutral pH SCC depends on a couple of factors which include the pipe manufacturing process, type of steel, grade of steel, cleanliness of the steel, steel composition, plastic deformation characterstics of the steel (cyclic softening characterstics), steel temperature and pipe surface condition. Pipe grades from 241 MPa to 483 MPa from a range of manufacturers have been found to be susceptible to near neutral pH SCC.

Internal operating pressure is the primary source of stress in the pipe both in the axial and circumferential directions and is considered in this study. Residual stress created during pipe manufacturing, bending stress resulting from ovalization, or local stress resulting from soil settlement or land slides might be other sources of secondary stress, but these stresses are not considered in this study. The choice of circumferential or axial stress in the pipeline failure analysis is subjected to crack orientation. If the crack is

longitudinally oriented, circumferential stress or hoop stress is selected for subsequent remaining stress analysis. The reverse is true for a circumferentially oriented crack. Considering the criticality of stress in the hoop direction as twice that of axial direction, hoop stress and the longitudinal crack are considered for subsequent failure analysis. Figure 6.1 depicts a longitudinal crack for general presentation.

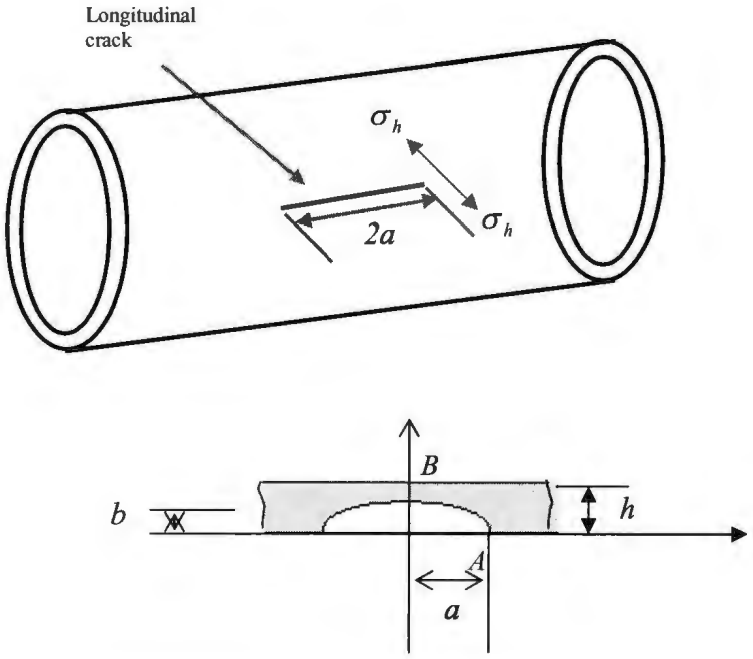

Figure 6.1: Cracks and stresses in pipeline

Figures 6.2 and 6.3 depict the crack response for a sustained load and cyclic loading respectively. Figure 2 reflects the true case of SCC where the loading is sustained and Figure 6.3 reflects the true case of crack fatigue (CF) where the loading is cyclic. In both cases the environment is deleterious. In the cyclic loading the stress range varied with $\Delta K = K_{max} - K_{min}$ or stress ratio $R = \frac{K_{min}}{K_{max}}$. As the operating condition resembles the

slow cyclic loading condition, and material is exposed to hydrogen embrittlement [6], the work of Parkings et al . [1, 2] has been chosen to extract the basic data for this study. Parkings et al . [1, 2] created the test environment with cyclic loading associated with slow strain rate technique (SSRT) and ensured the test was conducted with liquid solutions that closely match to the field. As the stress ratio R is not too low in the operating condition and in the test environment mostly an average stress is maintained with higher R value in the Parkings et al . [1, 2] experiment. Therefore, for simplicity it is assumed there is 'no cyclic loading condition' or sustained loading condition for subsequent analysis.

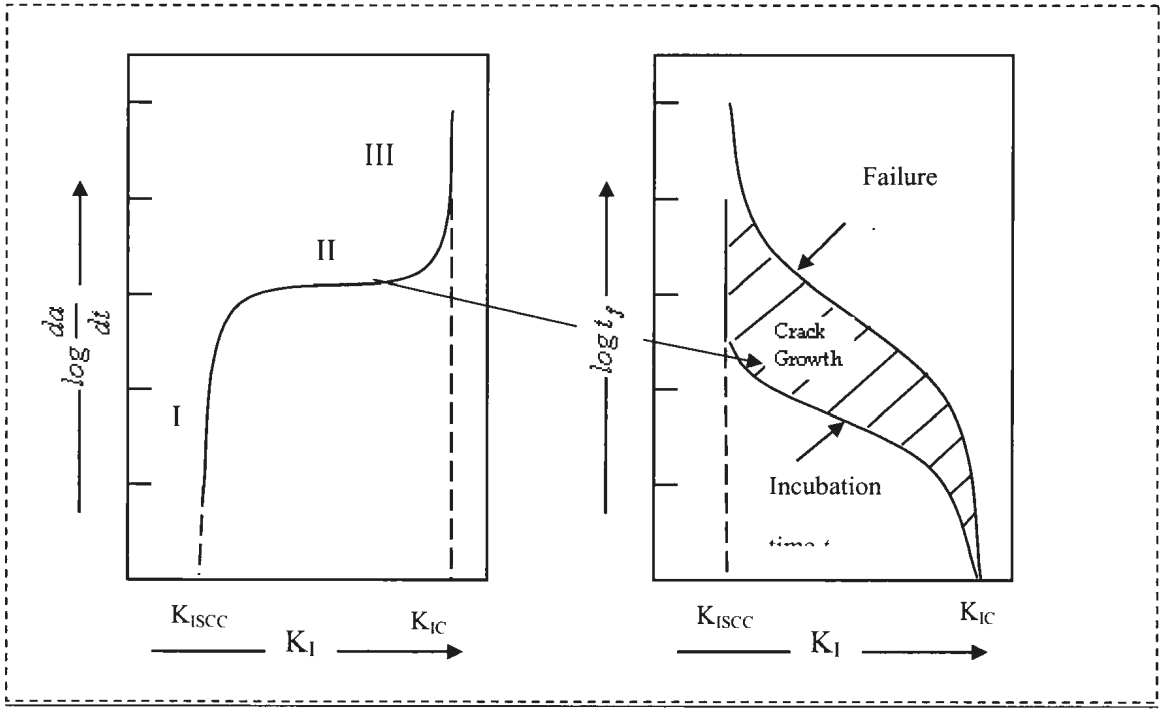

Figure 6.2: Typical sustained load (stress corrosion) cracking response in terms of steady state crack growth rate (left) and time (right) [7]

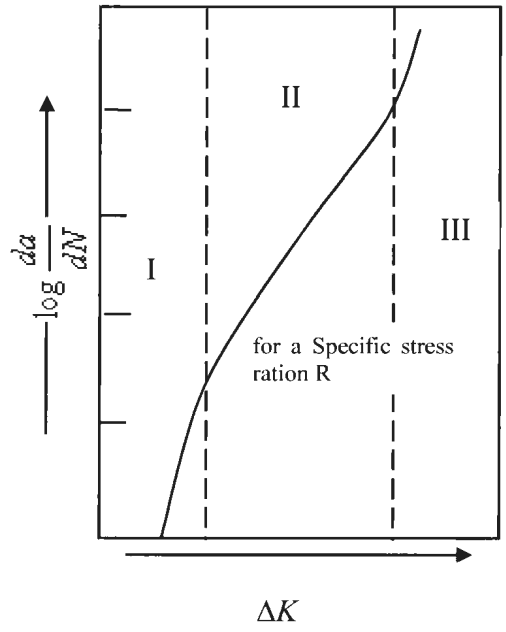

Figure 6.3: Fatigue crack growth phenomenon indicating three regions of crack propagation [7]

The following assumptions were made for this study:

1) The test environment of Parkings et al [1] suggests that it is a case of CF with cyclic loading but the result of Parkings et al [1] suggests that SCC has been assumed. This might be due to the fact that the cyclic loading variation is very small with higher R values. Again it is also stated in Figure 12 of Parkings et al [1] that the stress was mostly maintained as an average stress. Hence the data from Parkings et al [1] is assumed for SCC crack growth rate as that of a near plateau crack growth rate of phase II of Figure 6.2 and the data from Parkings et al [2] is assumed for crack initiation time as the time to initiate as in phase I of Figure 6.2 for TGSCC evaluation.

2) The data is considered for Figure 12 (a) of Parkings et al [1] with the assumption that the stress level <414 MPa, but mostly 345 MPa is the closest combination of 17.12 MPa operating pressure considered in this analysis.
3) Two limits were imposed for crack length and crack depth as suggested by CEPA [8] that the maximum length of the crack is 400 mm and the depth of the crack does not exceed 80% of the wall thickness.

6.2 Model Formulation

6.2.1 Related Research Background

The flaw growth due to SCC is a function of the material condition, environment, the stress intensity factor due to sustained loading, and the total time that the flaw is exposed to the environment under sustained loading. The procedure for computing SCC flaw growth for nuclear power plant components is based on experimental data for sustained load stress intensity factor K_I proposed by ASME [9]. It may be noted that ASME [9] also suggested the flaw size determination for the combination of fatigue and SCC by adding the increment of flaw size caused by fatigue to the regular SCC flaw size.

$$\dot{a} = \exp\left[-\frac{Q_g}{R}\left(\frac{1}{T}-\frac{1}{T_{ref}}\right)\right]\alpha\left(K_I - K_{th}\right)^{\beta} \tag{6.1}$$

where

$\dot{a}$ = crack growth rate at temperature T in m/s

Q_g = thermal activation energy for crack growth = 130 KJ/mole

R = universal gas constant = 8.314×10^{-3} KJ/mole ^{o}K

T= absolute operating temperature at location of crack, ^{o}K

T_{ref}= absolute reference temperature used to normalize data = 598.15 ^{o}K

α = crack growth rate coefficient = 2.67×10^{-12} at 325 ^{o}C for $\dot{a}$ in units of m/s and K_I in units of MPa $\sqrt{m}$

K_I = crack tip stress intensity factor, MPa $\sqrt{m}$

K_{Ih} = crack tip stress intensity factor threshold for SCC= 9 MPa $\sqrt{m}$

β = exponent = 1.16

The above formula is mainly devised for nuclear power plant components maintenance and might not be suitable for oil and gas pipelines flaw evaluation.

Attempts also have been made to characterize the truly mechanical fatigue crack growth. Paris, Gomez and Anderson [10] suggested that for a cyclic variation of an imposed stress field the linear elastic fracture mechanics characterization of the rate of fatigue crack growth should be based on the stress intensity factor range.

Paris, Gomez and Anderson [10] showed that fatigue crack growth rate da/dN is related to the stress intensity factor range by the power law relationship.

$$\frac{da}{dN} = A(\Delta K)^p \qquad (6.2)$$

where A and p are empirical constants, and the equation (6.2) is called the Paris or Paris-Erdogan equation. The constants are influenced by material microstructure, cyclic load frequency, waveform, environment, test temperature and stress ratio R.

Besides the simple Paris-Erdogan equation other detailed equations were proposed by researchers [11-12]. However, the Paris-Erdogan equation is the most desirable one due to its simplicity. These equations characterize the fatigue crack behavior of material; however not SCC or CF where a deleterious environment is active.

Harris, Dedhia, and Lu [13] developed the probabilistic fracture mechanics code that has recently been modified to evaluate the probability of welds in a nuclear power plant piping system. The PRAISE computer code was originally developed by Lawrence Livermore National Laboratory (LLNL), in United States of America. PRAISE is an acronym for piping reliability analysis including seismic events, and has been significantly expanded in recent years to allow consideration of both crack initiation and growth in a variety of piping materials in a pressurized and boiling water reactor. PRAISE has a deterministic basis in fracture mechanics. PRAISE provides a comprehensive summary of the deterministic basis along with the description of statistical distribution of random variables. However, again, this code is limited to application in nuclear power plants.

To predict the corrosion fatigue (CF) crack growth behavior of metals the superposition model was proposed by Wei and Lands [14] and was modified by Wei and Gao [15]. This model recognizes the fact that mechanical (or pure) fatigue and cycle dependent corrosion fatigue proceed by different micro mechanisms and occur

concurrently. Modeling was based on the proposition that the rate of crack growth in a deleterious environment, $(da/dN)_e$ is composed of the sum of three components given in equation (6.3)

$$\left(\frac{da}{dN}\right)_e = \left(\frac{da}{dN}\right)_r (1-\phi) + \left(\frac{da}{dN}\right)_c \phi + \left(\frac{da}{dN}\right)_{SCC} \qquad (6.3)$$

In this equation, $(da/dN)_r$ is the rate of fatigue crack growth in an inert environment, $(da/dN)_{SCC}$ is the contribution by sustained load crack growth; $(da/dN)_c$ represents the cycle dependent contribution which requires the synergistic interaction of fatigue and environmental attack and ϕ is the fractional area of the crack that is undergoing pure corrosion fatigue.

Due to complexity of the model where individual components are not available, the author's motive is to find a simpler approach where experimental data are used to evaluate TGSCC in API X 65 steel.

It has been indicated by researchers, for example, Mollan et al. [16] and Bulloch [17] that SCC might be possible in an offshore pipeline but many researchers ruled out the idea of true SCC in offshore for HSLA steel, or carbon manganese steel. Instead, they have suggested the possibility of CF with SSRT in an offshore pipe line. Cigada et al [18] stated that SCC has not been identified as a cause of failure of low alloy and carbon steels with yield strength below 700 MPa in seawater even under cathodic protection. However, it has been observed on steels with yield strength exceeding 1250 MPa. On lower strength steels SCC has been observed starting from the heat affected zone of welding

with high hardness (above 46HRc). It is recognized that SCC may be active on lower strength steels in the presence of a sharp defect or under slow straining. Under slow straining, cracking in seawater is reported even on steels with 500 MPa yield strength [18]. It may be noted that cracking starts when plastic deformation is reached.

Recognizing the fact that limited data are available for SCC in offshore oil and gas pipeline the authors decided to choose the data of low pH transgranular SCC with cyclic loading and SSRT as the closest combination of offshore pipelines. The results obtained by Parkins et al. [1, 2] were chosen for the analysis of low pH transgranular SCC. The data obtained by Parkins et al [1] for crack growth rate suggest a relatively constant crack growth rate which permits the assumption of sustained load (stress corrosion) cracking response model as explained in Figure 6.2. A simplistic model is therefore developed in the present study to calculate the probability of failure for low pH transgranular SCC. In this model the SCC crack is characterized and subsequently the probability of failure is analyzed by a different stress/strain based approach. Figure 6.4 shows the process diagram of the predictive study.

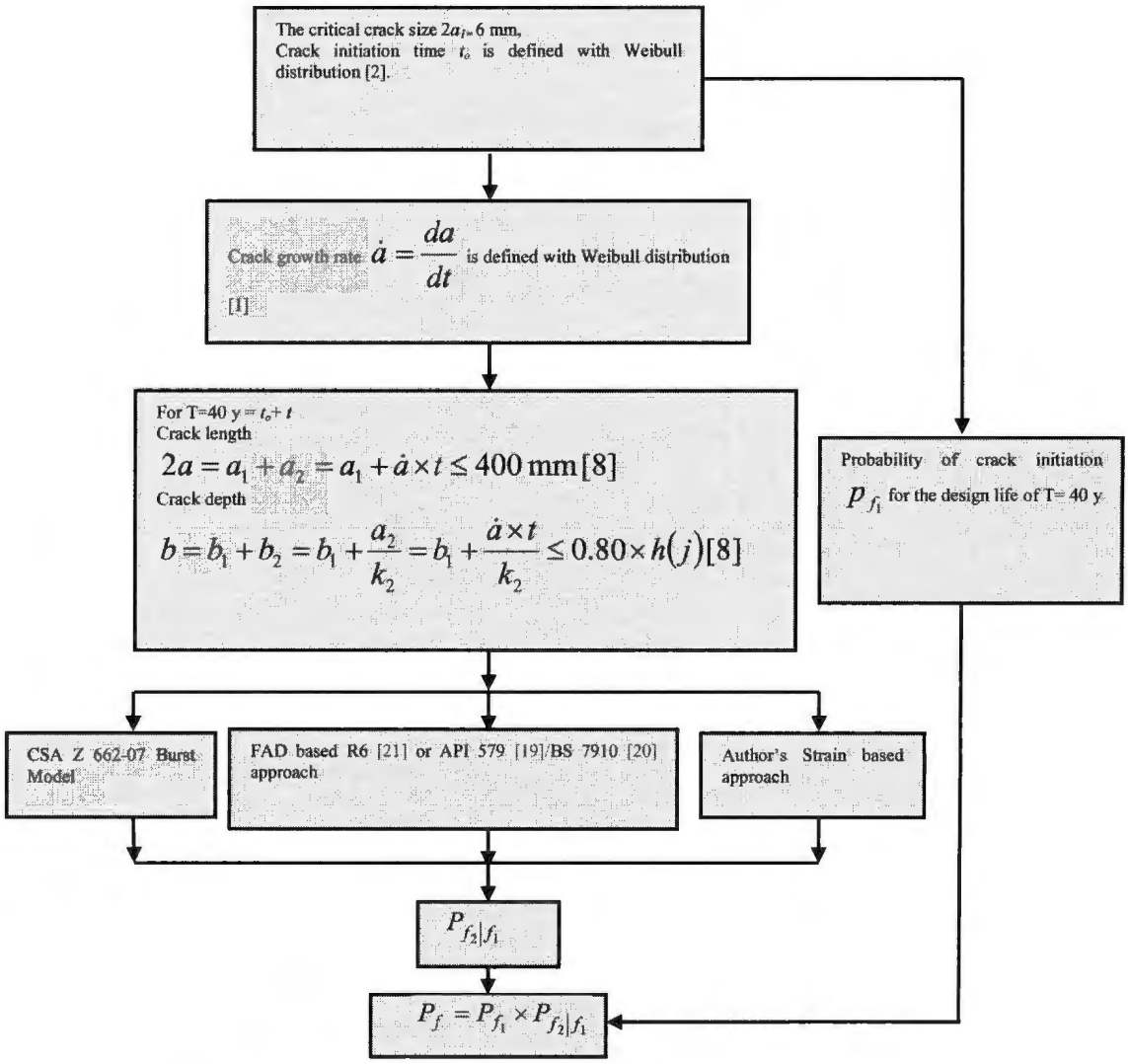

Figure 6.4: Process diagram of the predictive model for SCC analyis

6.2.2 SCC Crack Characterization

Let the period after the crack initiation time, t_o, when the stress intensity factor K approaches threshold stress intensity factor K_{ISCC}, the crack length is a_1 and the crack

depth is b_1. The ratio of crack length to crack depth is $k_1 = \frac{a_1}{b_1}$. Now the crack is subjected to growth. After the growth time t, the crack length is a_2 and the crack depth is b_2. The ratio of crack length to crack depth is $k_2 = \frac{a_2}{b_2}$. Therefore considering the crack growth rate in the length direction $\dot{a} = \frac{da}{dt}$ the crack length ($2a$) and crack depth (b) for the design life of $T = (t_o + t)$ years are

$$\text{Crack length } 2a = a_1 + a_2 = a_1 + \dot{a} \times t \tag{6.4}$$

$$\text{Crack depth } b = b_1 + b_2 = b_1 + \frac{a_2}{k_2} = b_1 + \frac{\dot{a} \times t}{k_2} \tag{6.5}$$

In the above equations the crack initiation t_o and the distribution of crack growth rate $\dot{a}$ are two important parameters. Once the crack is characterized in terms of its length $2a$ and depth b, the next step is to evaluate the crack criticality.

6.2.3 SCC Evaluation

6.2.3.1 SCC Stress Based Evaluation

SCC stress based evaluation determines the failure pressure of SCC flaws. Several analytical models were developed to determine SCC failure pressures. These models rely on the relationship between the applied stress, the material properties, and the resultant tolerable SCC size. Some of the models allow a rupture or leak as the SCC mode of

failure. The axial propagation of the leak may or may not occur depending on the applied stress, toughness of the steel and axial length of the steel; however, rupture is assumed as the normal mode of failure. Most of the failure pressure models have been developed based on the extensive work performed by the Battelle Memorial Institute in the 1970s. Other failure criteria have been developed that incorporate elastic-plastic fracture mechanics. Available failure pressure methods are:

- Log-Secant
- Pipe axial flaw failure criterion (PAFFC)
- CorLAS^{TM}
- API 579 [19] & BS 7910 [20]
- R-6 Procedure [21]

PAFFC and CorLAS^{TM} have shown improved correlations to SCC burst test results compared to the Log-Secant method [8]. The API 579 [19], BS 7910 [20], and R-6 [21] approaches provide similar results while assessing SCC-like flaws using the failure assessment diagram (FAD). The FAD is based on the principle of fracture mechanics. CSA Z662-07 [22] also developed a stress based approach for longitudinal defects and hence this approach is considered for the present analysis.

6.2.3.1.1 A. R 6 Approach or API 579 & BS 7910

API 579 [19]/BS 7910 [20] or R6 approach [21] are stress based approaches and take into account elastic fracture as well as plastic collapse. The flaw is evaluated by the

failure assessment diagram (FAD). The FAD diagram is shown in Figure 6.5 which provides a schematic illustration of the FAD methodology that determine the failure condition in terms of load ratio (L_r^A) and fracture ratio (K_r^A). The acceptable boundary is defined by the failure assessment curve expressed by equation (6.6). According to the FAD failure criterion, if the assessment point A falls inside the failure assessment line, it is considered safe. If the point lies outside the curve, it is considered a failure.

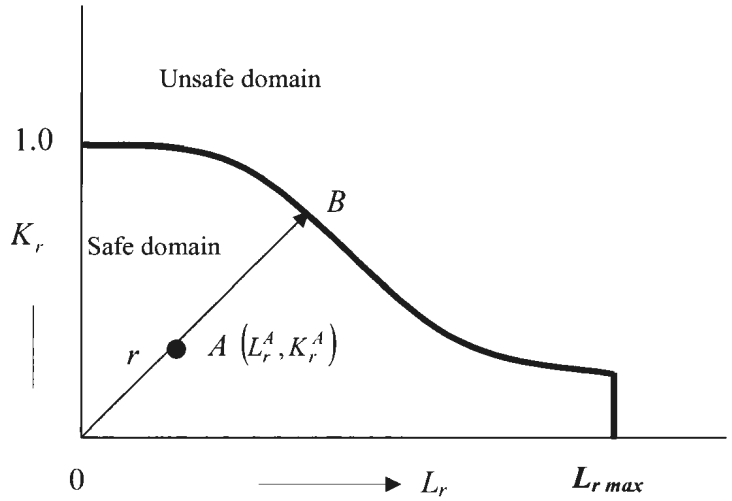

Figure 6.5: Failure assessment diagram (FAD) according to R6 approach [21] or API 579 [19]/BS 7910 [20]

$$K_r = \left\{1 - 0.14L_r^{\,2}\right\}\left\{0.3 + 0.7\exp\left(-0.65L_r^{\,6}\right)\right\} \tag{6.6}$$

The safety margin corresponding to assessment point $A\left(L_r^A, K_r^A\right)$ is given by

$$g = r - \sqrt{\left(L_r^A\right)^2 + \left(K_r^A\right)^2} \tag{6.7}$$

where L_r^A and K_r^A are coordinates of the assessment point A and r is the distance OB as shown in Figure 6.5. The values of L_r^A and K_r^A are determined as

$$K_r^A = \frac{K}{K_{IC}} \tag{6.8}$$

$$L_r^A = \frac{\sigma_{ref}}{\sigma_y} \tag{6.9}$$

K is the stress intensity factor at any time, K_{IC} is the material fracture toughness, σ_{ref} the applied stress. The maximum value of L_r is given by $L_{r_{\max}} = \frac{\sigma_f}{\sigma_y}$ and for $L_r > L_{r_{\max}}, K_r = 0$, where σ_f is the flow stress of the material.

The flow stress, $\sigma_f = \frac{1}{2}\left(\frac{\sigma_u + \sigma_y}{\sigma_y}\right)$ and σ_{ref} may be calculated considering API 579 [23], $\sigma_{ref} = M_s \sigma_o$ where M_s is the Folias bulging factor and σ_o is the applied primary stress. The bulging factor is defined as

$$M_s = \frac{1}{[1-(b/t)+(b/t)M_t^{-1}]}$$

with the parameter M_t expressed by

$$M_t = \left(\frac{1.02 + 0.4411\lambda^2 + 0.006124\lambda^4}{1.0 + 0.02642\lambda^2 + 1.533\times10^{-6}\lambda^4}\right)^{0.5}$$

where the shell parameter λ is defined as

$$\lambda = \frac{1.818a}{\sqrt{D/2b}}$$

For more detailed information the readers are encouraged to see references [8, 19, 20, 21].

6.2.3.1.2 B. Stress Based Approach (CSA Z 662-07)

For large leaks and ruptures, the burst pressure P_b at a surface corrosion defect with total axial length ($2a$) in mm, and average defect depth b (in mm) is given by the CSA Z662-07 [22] standard.

CSA burst equation $$P_b = 1.8\frac{h\sigma_u}{D}\left(\frac{1-\frac{b}{h}}{1-\frac{b}{m\times h}}\right) \qquad (6.10)$$

The model error is also considered in the analysis. For detailed information the readers are encouraged to review the reference CSA Z 662-07 [22]

Considering burst pressure P_b and operating pressure P_o in the hoop direction, the limit state equation representing the failure state is

$$P_b \leq P_o \qquad (6.11)$$

6.2.3.2 SCC Strain Based Evaluation

Strain based design (SBD) encompasses both strain demand (applied strain) and strain capacity (strain limit). SBD can be cost effective and sometimes necessary when

displacement controlled loading is expected. Such loading may arise from seismic activity, slope instability, frost heave or mine subsidence for onshore pipelines. For offshore pipelines, displacement controlled loading can occur during pipe laying and in service. In conventional stress based design, the applied stress is kept below the specified minimum yield stress (SMYS). The SMYS is typically defined as the yield strength measured at 0.5% total strain. Therefore, stress based design limits the longitudinal strain to less than 0.5%.

A number of recent developments of strain-based fracture assessment approaches, including proposals by Budden [24] for a strain-based failure assessment diagram (FAD) related to the conventional stress based FAD have been found in the open literature. However, recent comparisons with finite element (FE) data have shown that this proposed strain-based FAD can be non-conservative in some cases, particularly for deeper cracks (b/h>0.20) and materials with little strain hardening capacity [25].

Therefore, in this paper the existing strain-based FAD or modified proposed FAD by Budden et al. [25] have not been considered for analysis since b/h<0.20 is a shallow crack and particularly not of interest for this study. Hence the author proposed a strain based approach in the hoop direction for defected pipe.

It may be noted that efforts have been made by some individuals [26] to develop hoop failure strain criteria for defect free pipe. However, when the reference is cross checked no such formula is seen in the referred papers. Again these formulas calculate hoop failure strain for defect free pipe whereas defected pipe is of interest in this study.

6.2.3.2.1 C. Proposed Strain Based Approach

In this study the Ramberg-Osgood equation is considered for developing a strain based approach. Burst pressures of intact pipe and defected pipe are converted to equivalent strain. After simplification equations, (6.14) or (6.15) or (6.16) may be considered for strain based analysis.

Burst strain of intact pipe

$$\varepsilon_1 = \varepsilon_1^{'} + \varepsilon_1^{''} = \frac{P_1 D}{2tE} + \left(0.005 - \frac{\sigma_y}{E}\right)\left(\frac{P_1 D}{2t\sigma_y}\right)^n \tag{6.12}$$

Burst strain of defected pipe

$$\varepsilon_2 = \varepsilon_2^{'} + \varepsilon_2^{''} = \frac{P_2 D}{2tE} + \left(0.005 - \frac{\sigma_y}{E}\right)\left(\frac{P_2 D}{2t\sigma_y}\right)^n \text{ where } P_2 = FP_1 \tag{6.13}$$

Dividing equation (6.13) by equation (6.12)

$$\Rightarrow \frac{\varepsilon_2 - \frac{P_2 D}{2tE}}{\varepsilon_1 - \frac{P_1 D}{2tE}} = \frac{\left(0.005 - \frac{\sigma_y}{E}\right)\left(\frac{P_2 D}{2t\sigma_y}\right)^n}{\left(0.005 - \frac{\sigma_y}{E}\right)\left(\frac{P_1 D}{2t\sigma_y}\right)^n}$$

$$\Rightarrow \frac{\varepsilon_2 - \frac{P_2 D}{2tE}}{\varepsilon_1 - \frac{P_1 D}{2tE}} = \left(\frac{P_2}{P_1}\right)^n$$

$$\Rightarrow \varepsilon_2 - \frac{P_2 D}{2tE} = \left[\varepsilon_1 - \frac{P_1 D}{2tE}\right] F^n$$

$$\Rightarrow \varepsilon_2 = \varepsilon_1 F^n + \frac{P_2 D}{2tE} - \frac{P_1 D}{2tE} F^n$$

$$\Rightarrow \varepsilon_2 = \varepsilon_1 F^n + \frac{P_1 D}{2tE} F - \frac{P_1 D}{2tE} F^n$$

$$\Rightarrow \varepsilon_2 = \varepsilon_1 F^n + \frac{P_1 D}{2tE}\left(F - F^n\right) \quad (6.14)$$

$$\Rightarrow \varepsilon_2 = \varepsilon_1 F^n + \frac{1.1\sigma_y}{E}\left(F - F^n\right) \quad (6.15)$$

$$\Rightarrow \varepsilon_2 = \varepsilon_1 F^n + \varepsilon_1^{'}\left(F - F^n\right) \quad (6.16)$$

where,

ε_2 is the burst strain of defected pipe which would be considered ε_h in the subsequent equation

ε_1 is the burst strain of intact pipe

$\varepsilon_1^{'}$ is the elastic part of the burst/flow strain of intact pipe in Ramberg-Osgood equation

F is the defect factor from stress based design code (CSA Z 662-07 considered in this case) $= \left(\dfrac{1-\dfrac{b}{h}}{1-\dfrac{b}{m \times h}}\right) = \dfrac{P_2}{P_1}$

n is the hardening parameter in the Ramberg-Osgood equation and is assumed 25 in the analysis.

This strain based design is strictly reserved for longitudinal defects. The parameter ε_1 may be considered as having uniform distribution with min 1.0% to 2.5%

[27] and ε_1' may be considered 0.0023 for X 65 steel. The following table, Table 6.1, may be considered for other steel for ε_1'.

Table 6.1: Elastic strain property of different steel grade

Steel	σ_y MPa	1.1 σ_y MPa	Elastic strain part of Ramberg-Osgood equation $\frac{P_1 D}{2hE} = \frac{1.1\sigma_y}{E}$
X52	359	395	0.0019
X60	414	456	0.0022
X65	448	493	0.0023
X70	483	531	0.0025
X80	551	606	0.0029

The predicted burst capacity, normalized with the tensile strength hoop pressure P_b/P_i, as a function of the corrosion length is shown in Figure 6.6*a* for a yield strength - tensile strength ratio of 0.91 using the ASME B31G code. The same kind of failure strain capacity, $\varepsilon_2 / \varepsilon_1$, against normalized corrosion length is shown in Figure 6.6*b* for the same API X 65 steel. In Figure 6a with a higher order of *d/t* ratios the burst capacity reduces gradually and maintains a consistent distance of burst to intact pressure ratios among *d/t* ratios for a given normalized corrosion length. In Figure 6b the burst capacity reduces with the higher order of *d/t* ratios but demonstrates a sharp fall of failure strain at a shorter normalized corrosion length (say less than 5). This signifies that the trend of failure by strain follows the similar trend of stress (with n=25) but with a higher response (sharp decline in strain capacity) at the very beginning of corrosion length. It may be

noted that with hardening parameter n=5, the response in Figure 6.6b closely match with response in Figure 6.6a.

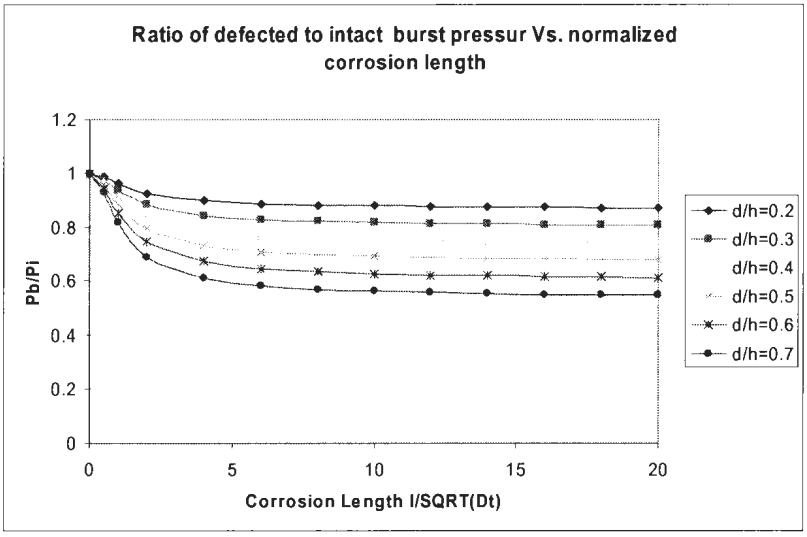

a)

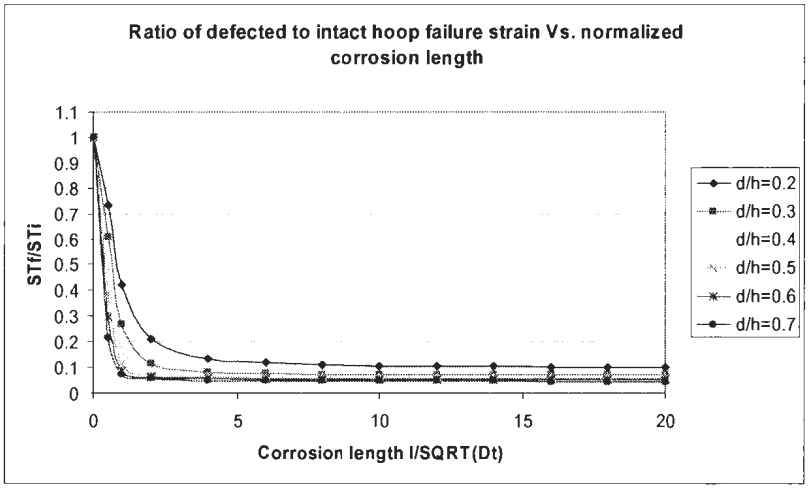

b)

Figure 6.6: Burst-pressure/failure-strain capacity of defected pipe depending on extent of corrosion a) burst pressure ratio, P_b/P_i b) failure strain ratio, $\varepsilon_2 / \varepsilon_1$ as function of normalized corrosion length.

In probabilistic analysis, equation (6.13) is considered for equivalent hoop strain for operating pressure to maintain the same level of reference with stress based design. Equation (6.17) is the new form of equation (6.13)

$$\varepsilon_o = \frac{P_o D}{2tE} + \left(0.005 - \frac{\sigma_y}{E}\right)\left(\frac{P_o D}{2t\sigma_y}\right)^n \tag{6.17}$$

The failure limit state may be considered as

$$\varepsilon_h = \varepsilon_2 < \varepsilon_o \tag{6.18}$$

6.3 SCC stress/strain based rupture evaluation

The rupture failure probability, p_f, may be evaluated for SCC growth over time. If p_{f_1} is the probability of crack initiation and $p_{f_2|f_1}$ is the probability of failure due to growth given that the crack has been initiated the total probability of failure is a conditional probability

$$p_f = p_{f_1} \times p_{f_2|f_1} \tag{6.19}$$

6.4 Data Considerations

As stated in section 6.2.2 regarding crack initiation time t_o and crack growth rate $\dot{a}$, this section discusses the parameters of the distribution for t_o and $\dot{a}$ as per the understanding and results of Parkins and his coworkers [1, 2].

6.4.1 Crack Initiation Time, t_o

Parkins et al. [2] developed a generalized probabilistic model for crack initiation time considering the power law equations for different steels. The critical crack size adopted for the crack simulation runs was 6 mm in length. That size was based upon laboratory data that showed 6 mm corresponding to the size where the threshold stress intensity factor (K_{ISCC}) is reached. The time to failure either by the crack penetrating a wall thickness and creating a leak or by the crack coalescing to achieve the size for fast fracture is relatively short compared to the time occupied in reaching that condition. A Weibull plot of the average times to achieve the critical crack size for the various values of the constants was demonstrated in the works of Parkins et al [2]. Examining Figure 22 of Parkins et al [2] suggests that the average time to reach the critical crack size is Weibull distributed with $\beta : \hat{\beta} = 1.416$ and $\theta : \hat{\theta} = e^{-a/\beta} = e^{-(-4.012/1.416)} = 17.002$

6.4.2 Crack Growth rate $\dot{a} = \frac{da}{dt}$

The transgranular crack velocity with the best approximation of field operating conditions is obtained from Parkins et al. [1]. The best approximation of the field scenario is necessary since SCC is dependent on many variables. Examining Figure 12 a) of Parkins et al [1] suggests that the average time to reach the critical crack size is Weibull distributed with $\beta : \hat{\beta} = 0.7066$ and $\theta : \hat{\theta} = e^{-a/\beta} = e^{-13.32/0.7066} = 6.50E-9$.

Now the crack length (mm) and crack depth (mm), $2a$ and b respectively are determined considering equations (6.4) and (6.5). The other basic variables given in Table 6.2 are considered from previous work [28] of the authors for external corrosion for API 5L X 65 pipes. It may be noted that for simplicity, crack depth, b, is calculated from aspect ratio, $b/2a = 0.1 \sim 0.2$ which is in line with the work of [29-31].

Table 6.2: Probabilistic models of the basic variables for material- API 5L X 65

Variables	σ_u/ MPa	σ_y/MPa	D/mm	h/mm	P_{op}/MPa
Type	Lognormal	Lognormal	Normal	Normal	Gumbel
μ	530	447	713	20.24	17.12
CoV	0.07	0.07	0.001	0.001	0.08

6.5 Failure Modes and Analysis

6.5.1 Design by Current Stress/Strain Based Approach

An SCC crack is defined in terms of defect length and defect width. At this stage the failure modes can be considered for probability of failure given by equation (6.19).

Two distinct modes of failure were considered for the analysis: stress based and strain based. Table 6.3 summarized the factors considered in the study.

The probability of failure P_f for the design life of T=40 years is estimated and given in Table 6.4 for each fracture analysis mode. Note that the results in Table 6.4, are calculated considering the stress due to operating pressure P_o.

Table 6.3: Modes of failure/rupture, crack orientation and stress/strain assumed.

Name of the Failure /Rupture Modes	*Orientation of Crack*	*Driving Stress/Strain*	*Limit load*
Case A: R6 [21, 32] approach (close to API 579 [19] & BS 7910 [20])	longitudinal crack	Applied stress $\sigma_{ref} = M_s \sigma_0$ considered case *A*	Operating pressure, P_o Standard procedure is Newton-Raphson method to calculate intersection point, B (the point of intersection between option 1 curve and line joining assessment point and origin). But due to complexity, here, the y distance $\left(K_r^A\right)$ is compared for assessment point A with y distance $\left(K_r\right)$ of assessment point B for the same x distance $\left(L_r^A / L_r\right)$
Case B: CSA Stress based (CSA Z 662-07 [22])	Longitudinal crack	Hoop stress $0.9\sigma_y F$ Considered the case of *B*	Operating pressure, P_o
Case C: Author's strain based approach	Longitudinal crack	Hoop strain $\varepsilon_h = \varepsilon_y F^n + \varepsilon_y^n (F - F^n)$ Considered the case of *C*	Equivalent operating strain from operating pressure

Table 6.4: Failure probabilities for the design life of T=40 years and stress due to operating pressure P_o

Name of the Failure /Rupture Modes	*Total probability* $p_f = p_{f_1} \times p_{f_2\|f_1}$
Case A: R6 [3, 24] approach (close to API 579 [22] & BS 7910 [23])	2.98E-5
Case B: CSA Stress based (CSA Z 662-07 [6])	1.15E-3
Case C: Author's proposed strain-based approach	8.5E-4

It may be noted that the Log-secant method is not considered since it is a bit conservative [33]. Some commercially available software is also available, such as PAFFC or CorLAS^{TM} [33] but these are not used in this study. The R6 approach is basically the same approach, based on API 579 & BS 7910 [19, 20]. The severity category of SCC recommended by CEPA [33] is examined in this study. The maximum operating pressure (MOP) as suggested by DNV RP-F101 [34] and the probabilistic SCC failure pressure, $SCC_{fp}=P_b$, for CSA Z 662-07 [22] have been calculated and found to be in agreement with category IV of Table 4.1 of CEPA [33] which indicates imminent failure.

6.6 Results and Discussion

The failure probability is assessed for the transgranular SCC defect once defect depth and defect length are defined for a particular design life. Two distinct failure limit

modes (stress/strain) were considered for the assessment of the defect. In strain based design the strength of the intact pipe can be assumed to be more than SMYS at 0.5% offset strain value or 0.9 SMTS, which is usually assumed in conventional stress based design. The authors therefore suggested a revised approach of the strain based design which is demonstrated in section 6.2.3.2. The longitudinal crack is considered both in stress based design (case *A*, *B*) and strain based design (case *C*). Table 6.4 summarizes the result for approaches *A*, *B*, and *C*. The objective is to check the strain based method *C*, for how it calculates failure probability compared to stress based approaches *A* and *B*.

The result indicates *A*, *B* and *C* closely calculate the probability of failure. Approach *A* considers linear elastic fracture mechanics and plastic yielding. Probably, for that reason, the probability of failure calculated by *A* is found to be the least. In the estimation of failure probability by approach *A* or by R6/ API 579 / BS 7910 approach [19, 20, 21] the fracture toughness, $K_{IC} = 180\,\text{MPa}\sqrt{\text{m}}$, is considered for oil and gas pipelines as suggested by the API RP-579 [23] code. The stress intensity factor, F=1.715 is considered in the analysis. In deterministic selection of F the priority is given to the long defect depth and length which closely match with the last chapter of Table 16 of the ASM handbook [35]. Approach *B* considered flow stress, which accounts strain hardening and plastic flow by means of a single hardening parameter [27]. The identical calculation of probability of failure calculated by *C* as that of *B* indicates the integrity of the author's proposed strain based approach, which is simple but rational. The strain-based calculation depends on the burst strain of the intact pipe, ε_1; the elastic part of the

burst/flow strain of intact pipe in the Ramberg-Osgood equation, ε_1', the defect factor, F and the hardening parameter, n, in the Ramberg-Osgood equation.

The strain based design is strictly restricted to the longitudinal defect. The parameter ε_1 may be considered as uniform distribution with min 1.0% to 2.5% as suggested by Zimmerman [27]. In real life design a strain based approach requires true judgment of the approximation of strain capacity and strain load.

In the deterministic analysis using Excel the burst strain ε_1, calculated by the Ramberg-Osgood equation, shows 2.88% strain capacity (with σ_f = 490 MPa) for intact pipe which is in reasonable agreement with the following table, Table 6.5 [36]. The experimental result of 3.29% strain corresponds to 492 MPa which only has a 2 MPa margin. The elastic part of the burst/flow strain of intact pipe in the Ramberg-Osgood equation, ε_1' remains almost constant 0.23-0.24% for load variation.

Table 6.5: Failure Strain results and predictions % [36]

	X42	X65 aged	X70 aged	X80 ex mill	X80 aged	Average discrepancy (%)	Standard error (%)
Test result	**9.09**	**3.29**	**2.53**	**2.56**	**1.01**	—	—
Gaessler–Voght	8.37	3.39	2.39	4.70	2.62	34.7 (18.0)	53.3 (44.6)
Half uniform strain	10.70	4.40	2.93	4.60	3.45	62.2 (36.4)	63.2 (30.1)
Liessem-Graef	6.10	3.49	3.01	4.07	2.27	25.0 (12.6)	43.2 (38.1)
Zhu–Leis	7.59	3.51	3.01	4.24	2.42	32.0 (18.4)	42.9 (34.9)
CIS-full	9.07	2.87	1.98	3.03	2.66	17.4 (-4.4)	51.0 (17.3)
CIS-A	9.87	3.36	2.41	2.77	2.64	23.2 (3.2)	45.0 (5.9)
CIS-B	9.52	2.71	2.00	2.61	2.71	15.1 (−8.3)	53.4 (12.8)

Another exciting work [37] supports the work of this current study. Though the study [37] is carried out for X52 steel, it is closely related to X 65 steel. In a probabilistic defect length of $2a$= 252 mm=9.92 inch, and the defect depth b= 12 mm the percent wall

thickness, %wt= 59.28%, the pipe fails at MOP =72% SMYS. Figure 6.7 shows the work of Limon-Tapia et al. [37]. It may be noted that in the whole analysis it is confirmed that the random value of $2a$ satisfies the condition $2a \leq 400mm$ and b satisfies the condition $b \leq 16mm$ which is 80% of wall thickness. The $2a$ and b values which do not satisfy the condition, were not included in the analysis.

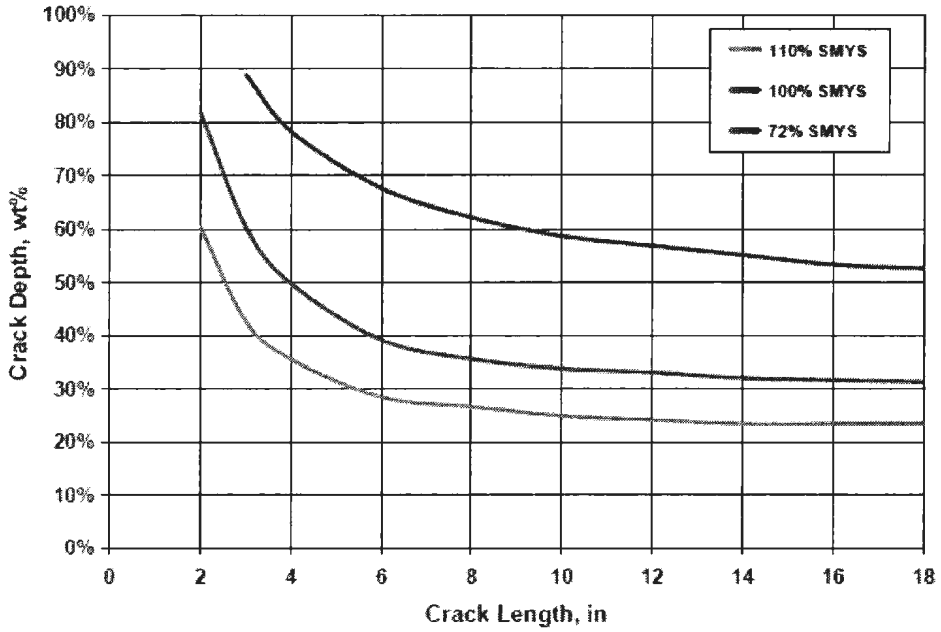

Figure 6.7: Limiting Acceptance Curve for Crack-like Indications (based on Level III FAD) [37]

The strain based approach of Case *C* is equivalent to the burst model approach of Case *B* where linear elastic fracture mechanics or plastic yielding is not considered as that of Case *A*. Naturally it is expected that the probability of failure calculated by Case *C* would not be as sound as that of Case *A*. However, the approach still calculates closely with less than two orders of magnitude. It may be noted that strain based FAD, which is

closely related to stress based FAD, is recently found to be non-conservative with FE analysis for deeper cracks (b/h>0.20) and for little strain hardening capacity [25]. Again it may be noted that the hoop strain of defected pipe is a function of $\varepsilon_h\left\{\varepsilon_1, \varepsilon_1', F, n\right\}$ in which $\varepsilon_1, \varepsilon_1'$ are constants for this particular kind of steel. F can be considered from any standard or codes and n is the strain hardening parameter that is also constant for any kind of steel. The proposed hoop strain failure model considers strain hardening parameter, n, which is not considered in the burst model.

6.7 Conclusion

The present study characterized TGSCC flaws in terms of length and depth and evaluated the failure probability. The failure probabilities were found to be identical for the same crack growth rate and crack initiation time. The result shows that case *C*, the strain based approach, calculates failure probability between *A* & *B*.

In short the novelty of the work is two fold: a) failure assessment of TGSCC of X65 steel and b) demonstration of the strain based approach which calculates failure probability close to, or lower than the CSA Z 662-07 [22] burst model.

6.8 Acknowledgements

The authors gratefully acknowledge the financial support provided by Petroleum Research Atlantic Canada (PRAC) and Natural Science and Engineering Research Council (NSERC) of Canada.

6.9 References

[1] Parkins R. N., Blanchard W. K., & Delanty B. S. (1994). Transgranular Stress Corrosion Cracking of High-Pressure Pipelines in Contact with Solutions of Near Neutral pH. *Corrosion Engineering*, NACE International.

[2] Parkins R. N., Blanchard W. K., & Belhimer E. (1993). Stress Corrosion Cracking Characterstics of a Range of Pipeline Steels in Carbonate-Bicarbonate Solutions. *Corrosion* Vol 49 No 12, NACE International.

[3] Report of the Inquiry (1996). *Stress Corrosion Cracking on Canadian Oil and Gas Pipelines*. National Energy Board, MH-2-95

[4] Parkins R. N. (2000). A review of stress corrosion cracking of high pressure gas pipelines. *Corrosion* 2000, Houston, Texas, USA. Paper No 00363

[5] CEPA, 1996. *Proceeding MH-2-95 Vol. 2*, Submission to National Energy Board.

[6] Torres-Islas A., Salinas-Bravo V. M., Albarran J.L., & Gonzalez-Rodriguesz J. G. (2005). Effect of hydrogen on the mechanical properties of X-70 pipeline steel in

diluted NaHCO3 solutions at different heat treatments. *International Journal of Hydrogen Energy* 30(2005) 1317-1322.

[7] Wei R. P., 2010. *Fracture Mechanics*, Cambridge University Press.

[8] Recommended Practice (2007). *Stress Corrosion Cracking*. CEPA

[9] ASME boiler and pressure vessel code (2004). *Rules for in-service inspection of nuclear power plant components*. An international code, ASME, New York.

[10] Paris P. C., Gomez M. P., & Anderson W. E. (1961). *A rational analytic theory of fatigue*. The trend in Engineering at the University of Washington, 13, 1, 9–14.

[11] Hall, L. R., Shah R. C., & Engstrom, W. L. (1974). *Fracture and Fatigue crack growth behavior of surface flaws and flaws originating at fastener holes*. AFFDL-TR-74-47, Air force dynamic laboratory, WPAFB, Ohio.

[12] Collipriest, J. E., Jr., & Ehret, R. M. (1972). *Computer modeling of part through crack growth*. SD72-CE-15

[13] Harris D. O., Dedhia D. D., & Lu S. C. (1992). *Theoretical and user's manual for pc-PRAISE, A probabilistic fracture mechanics computer code for piping reliability analysis*. NUREG/CR-5864, UCRL-ID-109798.

[14] Wei R. P., & NS Lands, J. (1969). Correlation between sustained load and fatigue crack growth in high strength steels. *Material research and standards*, 9, 25-27.

[15] Wei R. P. & Gao M. (1983). Reconsideration of the superposition model for environmentally assisted fatigue crack growth. *Scripta Metallurgica*, 17, 959-962.

[16] Mollan R., Eliasesen S., Holt T., & Ratkje S. K. (1982). Possibility of stress corrosion cracking in submarine pipelines. *Material performance, Corrosion/82*

[17] Bulloch J. H., 1991. *Stress corrosion cracking of low alloy steels in natural seawater environment- the influence of carbon level*, Theoretical and Applied Fracture Mechanics 16(1991) 1-17, Elsavier.

[18] Cigada A., Pastore T., Franzoso G., Kopliku A., & Tarenzi M. (1992). SCC of high strength steel in deep sea water under cathodic protection. *Proceedings of ISOPE conference*, San Francisco, USA

[19] API 579-1/ASME FFS-1, (2007). *Fitness-For-Service*. American Petroleum Institute and the American Society of Mechanical Engineers.

[20] BS 7910:2005, (2005). *Guide to methods for assessing the acceptability of flaws in metallic structures*. British Standards Institute, London, England.

[21] R6, (2005). *Assessment of the integrity of the structure containing defects.* Revision 4, Amendment 4, British Energy, Gloucester.

[22] CSA Z662-07, (2007). Limit state equation for burst of large leaks and rupture for corrosion defect. *Oil and Gas Pipeline Systems*, Canadian Standards Association.

[23] API RP-579, (2000). *Recommended practice for fitness-for-service*, American Petroleum Institute.

[24] Budden P. J. (2006). Failure assessment diagram methods for strain-based fracture. *Eng. Fract. Mech.*; 73:537-552.

[25] Budden PJ, & Ainsworth RA (2011). The shape of a Strain-based failure assessment diagram. *International Journal of Pressure Vessels and Piping*, doi: 10.1016/j.ijpvp.2011.09.004

[26] Law M., & Bowie G. (2007). Prediction of failure strain and burst pressure in high yield-to-tensile strength ratio linepipe. *International Journal of Pressure Vessels and Piping* 84 (2007) 487–492

[27] Zimmerman T. J. E., Chen Q., & Pandey M. D. (1997). *Limit State and Reliability based Pipeline Design*, PRCI

[28] Hasan M., Khan F., Kenny S. (2011). Identification of the Cause of Variability of Probability of Failure for Burst Models Recommended by Codes/Standards. *J. of Pressure Vessel Technology*, V 133 Issue 4.

[29] Miyazaki K., & Mochizuki, M. (2011). The Effects of Residual Stress Distribution and Component Geometry on the Stress Intensity Factor of Surface Cracks. *Journal of Pressure Vessel Technology*, Vol. 133.

[30] Chen W., King F., & Vokes E. (2002). Characterization of Near-Neutral-pH Stress Corrosion Cracks in an X-65Ppipelines. *Corrosion*- Vol. 58, No. 3.

[31] Fang B., Han E-H., Elboujdaini M., Zheng W., Li J., & Revie R. W. (2006). *Stress-Corrosion Crack Initiation of High-Strength Pipeline Steel in Near-neutral pH Environments. International Journal of ISSI*, Vol. 3, No. 1, pp. 20-25.

[32] Priya C., Rao K. B., Anoop M. B., Lakshmanan N., Gopika V., Kushwaha H S., & Saraf R. K. (2005). Probabilistic Failure Analysis of Austenitic Nuclear Pipelines Against Stress Corrosion Cracking. *Proc. IMechE Vol. 219 Part C: J. Mechanical Engineering Science*. DOI: 10.1243/095440605X31526

[33] Recommended Practice (2007). *Stress corrosion cracking*. Canadian Energy Pipeline Association (CEPA).

[34] DNV RP-F101 (2004). *Recommended Practice Corroded Pipelines*. Det norske Veritas

[35] ASM Handbook (1996). *ASM Handbook Fatigue and Fracture*, Vol. 19, ASM International. USA

[36] Law, M., & Bowie G. (2007). Prediction of failure strain and burst pressure in high yield-to-tensile strength ratio linepipe. *International Journal of Pressure Vessels and Piping,* Vol 84, pp. 487-492.

[37] Limon-Tapia S., & Katz D. (2008). *A framework for managing the threat of SCC and other forms of cracking in pipelines using in-line inspection tools.* IPC2008-64090.

Chapter 7

Fatigue Analysis of Weld Defect Crack Subjected to Combined Effect of Variable and Constant Amplitude Loading *

Preface

This chapter presents a manuscript which developed weld defect fatigue damage assessment for corrosion fatigue. The manuscript has been submitted to International Journal of Pressure Vessels and Piping. The manuscript is currently under review. It may be noted that this chapter considered weld defect cracking under cyclic loading whereas the previous chapters, *Chapter 4-6*, considered defects or cracks under sustained loading.

The principal author formulated the approaches for developing fatigue damage for the combined effect of variable and constant amplitude loading with a small weld defect crack in a pipeline. The co-authors supervised the assessment methodology, reviewed the technical aspects and investigated the output results. They also provided the essential corrections and guidelines to improve the quality of the manuscript.

*this paper has been submitted to International Journal of Pressure Vessels and Piping. The reference is provided below.

Hasan, M., Khan, F., Kenny, S., (2012). Fatigue Analysis of Weld Defect Crack Subjected to Combined Effect of Variable and Constant Amplitude Loading - submitted to International Journal of Pressure Vessels and Piping IPVP-D-12-00076

Abstract

Generally it is believed that a pipeline with no defects is not susceptible to failure due to regular pressure fluctuation. Pipeline analysis with defects subjected to pressure fluctuation is not broadly discussed in open literature, except for some particular loading conditions discussed at the introduction section of this paper. This paper examines fatigue damage due to regular pressure fluctuation and start up shut down loading for a small weld crack. The Miner's rule and Paris law are considered for failure evaluation. The analysis does not confirm the general belief that regular pressure fluctuation is not a significant source of failure for weld defect cracks at the end flange of the pipeline operating in uncertain marine condition. The study observed that the failure probability of weld defect crack in pipeline in the marine environment is much higher compared to the non-marine environment. The study also observed that the mixed-mode operation (pressure derating) of a pipeline may extend the design life by at least 2 years, keeping the risk still minimum (below 1.0E-5) while operating for the first 15 years at 17.82 MPa and successively at an 11% reduction of pressure. The safe life could be increased by up to 4 years if an 18% reduction in operating pressure is considered from the 16^{th} year when the design life is considered to be 30 years.

7.1 Introduction

Defects in the structures and components may act as initiation sites for fatigue cracks. Because a fatigue crack grows slowly initially and then accelerates as the crack length and the stress intensity range increase, the initial size and shape of the defect have

a much larger influence on the total fatigue life than the fatigue crack size at which failure occurs.

The oil and gas pipelines made of API 5 L X 65 steel are joined by welding during pipeline construction. The girth weld in the gas pipeline is the most likely site for crack initiation. Girth weld is comprised of base metal, weld metal and a heat affected zone (HAZ). Figure 7.1 depicts the three zones of a typical girth weld of a pipeline. A crack can initiate and propagate in any part of this area or in multiple areas. A crack is considered to be propagating in the radial direction in the weld affected zone.

The fluctuation in operating pressure is considered as the driving force for fatigue in oil and gas pipeline steel and again this is broken down to a) variable amplitude loading, i.e. regular pressure fluctuation and b) constant amplitude loading, i.e. start up and shut down loading.

Different studies indicate fatigue due to pressure fluctuation might cause serious damage to the weld defects [1-7] when a particular condition is considered. Beltrao et al. [1] identified that girth welded joints are prone to initiation and propagation of fatigue cracks that have been observed mainly at stress concentration points such as inclusion and weld defects. Gresnigt et al [2] studied buried pipelines with local buckles and indicated that buckle areas associated with significant strain concentrations in the presence of repeated loading (e.g. variations of internal pressure or temperature), may develop fatigue. Pinheiro et al. [3] studied the failure mode in dented sections [3] in which cyclic loadings may be generated by fluid pressure and temperature changes. Under the alternating stress caused by random loads, a very tiny flaw in the pipeline span

may lead to formation and growth of a fatigue crack [4]. Therefore, the fatigue reliability of a pipeline span in service life is very essential security for an oil and gas transportation pipeline. An FAD based approach is considered for defective pipeline fatigue life prediction by Jinheng et al. [5]. Stress corrosion cracking (SCC) is evaluated by Gamboa et al. [6] in which the combination of the range of pressure stresses is considered.

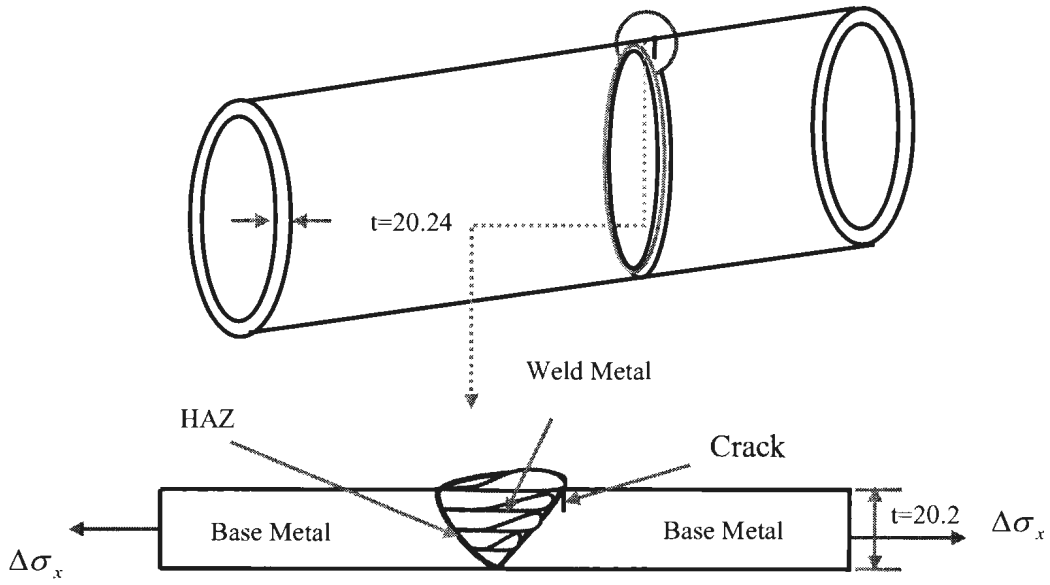

Figure 7.1: Girth weld (Butt) through the thickness in pipeline

Corcoran [7] in 'Corrib Gas Pipeline Design Part 2' reported all typical sources of cyclic stresses which should be considered in the fatigue design of the pipeline. Full stress cycles (start-up to shutdown cycles) and fluctuations in operational (pressure and thermal) cycles are two of them.

The following considerations were made in the analysis:

1) The extreme value distribution (Gumbel, Type I [18]) is considered for the operating pressure because all data points (data from data logger) of pressure fluctuation does not add much value in the analysis. The data logger may record the pressure value every 6 seconds or every 10 seconds, and this is the user's choice. Therefore, instead of considering 5 or 3 values in each 30 seconds the maximum value is used to see the extreme value distribution. Thus, the operating pressure is considered to be an extreme value distribution with a mean of 17.82 MPa and CoV of 0.053. The random number of data points generated in one year is therefore, 1.05×10^6, which includes peaks, valleys and reversals of random operating pressure.
2) The other operating pressure in the pipeline is considered to be 15.82 MPa and 12.825 MPa with the same CoV 0.053. The extreme value data are again generated for every 30 seconds, thus in a year approximately 1.05×10^6 data points are considered.
3) Start up and shut down loading considered that the number of startups and shut downs is 3 for a year, which mainly reflects the start up and shut down for scheduled maintenance. The amplitude is considered the difference between max (full operating pressure) and min (zero operating pressure) value of axial stress. It may be noted that operational shut down may be required for some other reasons and in that case the number of start up and shut down may demand revision.
4) The weld defect is considered at the end flange of the pipeline.

7.2 Mathematical Model

Characteristic resistances are normally given by S-N curves; *i.e.,* stress range versus number of cycles to failure. The S-N curve used must be applicable for the particular material, construction details, state of stress and strain, and the surrounding environment being considered. For constant amplitude loading the number of cycles to failure for a given stress range $\Delta\sigma$ is determined by the SN curve. The analytical expression for the SN curve:

$$\log N = \log \bar{a} - m' \log \Delta\sigma \qquad (7.1)$$

$$\text{or } N = \bar{a}\Delta\sigma^{-m'} \qquad (7.2)$$

where m' = inverse negative slope of the SN curve, $\log \bar{a}$ = the intercept of the log N axis. Values of m and $\bar{a}$ are dependent on different types of welded joints.

However, variable amplitude loading as given in Figure 7.2 cannot be assessed in terms of simply-described stress reversals. The Rainflow-counting algorithm or the rain-flow counting method may be used in the analysis of fatigue data in order to reduce a spectrum of varying stress to a set of simple stress reversals. The Rainflow assessment methodology is discussed in section 7.3.

Where stress fluctuations occur with varying amplitude in random order, the linear damage hypothesis (Miner's rule) may be used to determine the cumulative damage for the life of the structure. In this case the fatigue criteria are based on the limit damage ratio as follows:

$$D = \sum_{i=1}^{s} \frac{n_i}{N_i} \leq \eta \tag{7.3}$$

where D= damage ratio

s= number of stress ranges;

n_i = number of stress cycles in stress range i; (Rainflow)

N_i = number of cycles to failure at constant stress range; (S-N curve)

η = limit damage ratio, dependent on Safety Class and access for inspection and repair

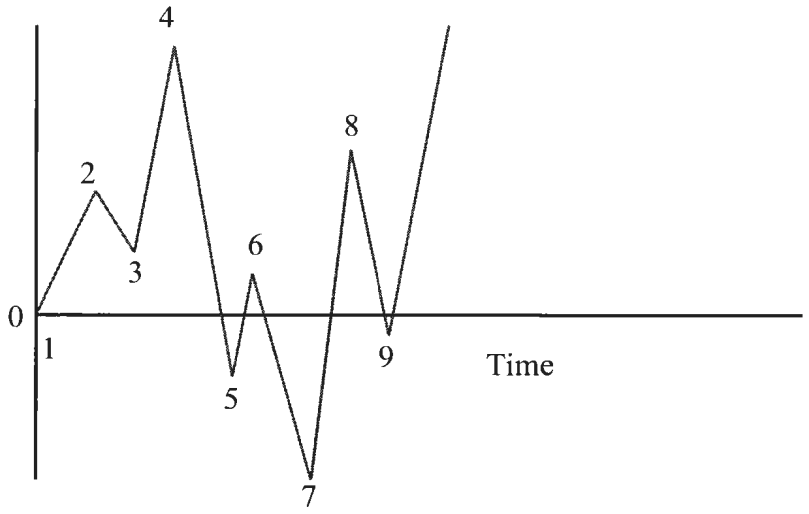

Figure 7.2: Spectrum loading

For variable amplitude loading the long term stress range distribution may be divided into blocks with constant stress range shown, in Figure 7.3. The damage corresponding to the number of cycles within each block is calculated and the summation can be carried out acording to Miner's rule.

The Miner's rule in its current form can not be directly considered to calculate damage for a defected component or a component that develops a crack. The N_i's in

equation (7.3) represents the number of cycles to failure at a constant stress range for a defect free component. If the N_is can be assessed for defected components as well, the Miner's rule still can be considered for damage assessment. Hence the linear elastic fracture mechanics (LEFM) may be considered for N_i's assessment of a defected component.

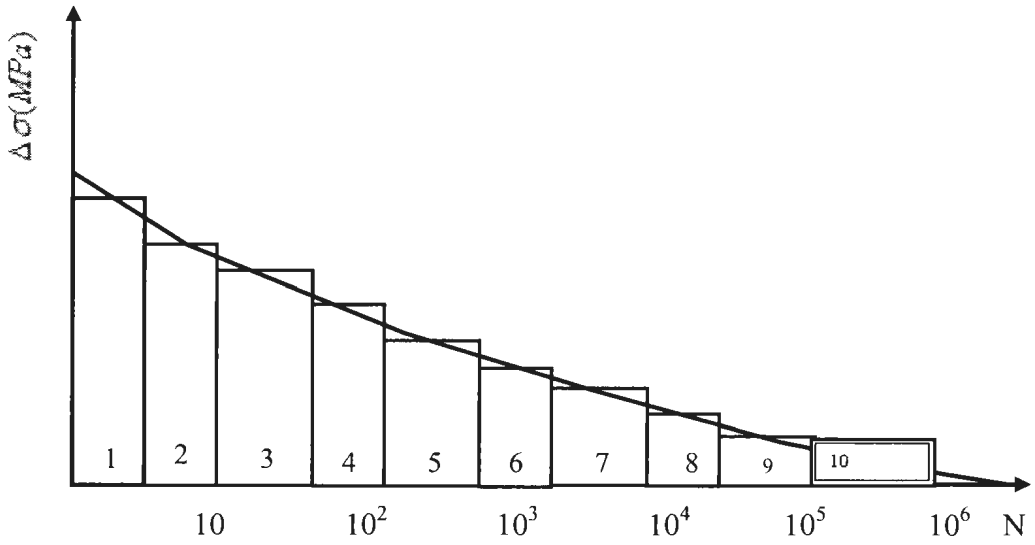

Figure 7.3: Stress distribution divided into stress block

The Paris law in region II of Figure 7.4 is the main region of interest where a crack propagates linearly. In Figure 7.4 the *Y* abscissa represents the crack growth rate, *da/dN*, in *mm* per cycle, while the *X* abscissa represents stress range, ΔK , in MPa$\sqrt{m}$. Paris related fatigue crack growth rate *da/dN* with the stress intensity factor range by the power law relationship.

$$\frac{da}{dn} = C(\Delta K)^m \qquad (7.4)$$

where: a= crack depth

n= number of cycles

C, m= material constants

ΔK = range of stress intensity factor in mode I fracture= $K_{max} - K_{min}$

$K = \sigma\sqrt{\pi a}.F$

σ = nominal stress normal to the crack

F= correction factor depending on the geometry of the member and the crack.

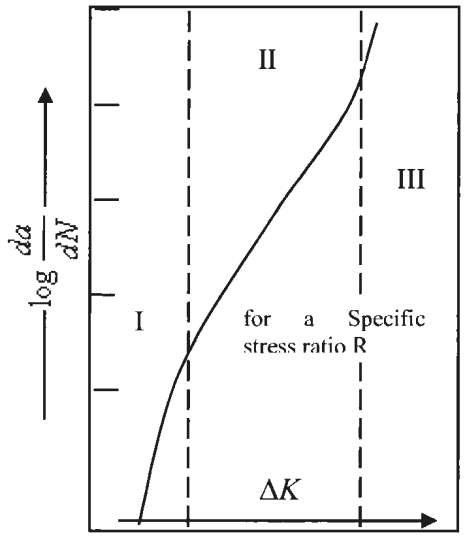

Figure 7.4: Fatigue crack growth phenomenon indicating three regions of crack propagation [8]

The empirical constants, C and m are influenced by material microstructure, cyclic load frequency, waveform, environment, test temperature and stress ratio R. The stress ratio R can be expressed by

$$R = \frac{\sigma_{\min}}{\sigma_{\max}} = \frac{K_{\min}}{K_{\max}} \tag{7.5}$$

Paris suggested that for a cyclic variation of an imposed stress field the linear elastic fracture mechanics characterization of the rate of fatigue crack growth should be based on the stress intensity factor range

$$\Delta K = K_{\max} - K_{\min} \tag{7.6}$$

where K_{max} and K_{min} are the maximum and the minimum values, respectively, of the stress intensity factor during a fatigue stress cycle. For any crack configuration

$$\Delta K = F(\sigma_{\max} - \sigma_{\min})\sqrt{\pi a} \tag{7.7}$$

where F is geometrical factor which depends upon the crack configuration and σ_{max} and σ_{min} are the maximum and minimum values of stress respectively.

If the threshold stress intensity factor ΔK_{th} can be sufficiently documented, a modified formula can be used for the crack growth in region I

$$\frac{da}{dn} = C[\Delta K^m - \Delta K_{th}^m] \tag{7.8}$$

where ΔK_{th} is the stress range intensity factor below which no growth take place. For region III equation (7.9) may be considered

$$\frac{da}{dn} = \frac{C(\Delta K)^m}{(1-R)K_c - \Delta K} \tag{7.9}$$

where K_c is the fracture toughness. The crack growth in region III is of minor importance for the marine structure [9]. Forman et al [16] corrected the simple Paris-Erdogan power by critical cyclic stress intensity K_c

$$\frac{da}{dN} = \frac{A(\Delta K)^p}{(1-R)K_c - \Delta K} \tag{7.10}$$

7.3 Assessment Methodology

Step1: Rain flow counting

For variable amplitude loading as described in Figure 7.2, the Rainflow-counting algorithm allows the application of Miner's rule in order to assess the fatigue life of a structure subjected to variable amplitude loading. Though there are a number of cycle-counting algorithms for such applications, the Rainflow method, described in Figure 7.5, is the most popular one and hence considered for the analysis.

The algorithm

1. Rain will flow down the roof initiating at the inside of each peak or valley. When it reaches the edge it will drip down.

2. The rain is considered to stop, and a cycle is completed, when it meets another flow from above.
3. Starting from the peak, the flow stops when it comes opposite a more positive peak than that from which it started. Starting from a valley, the flow stops when it comes opposite a more negative valley than that from which it started.

Example

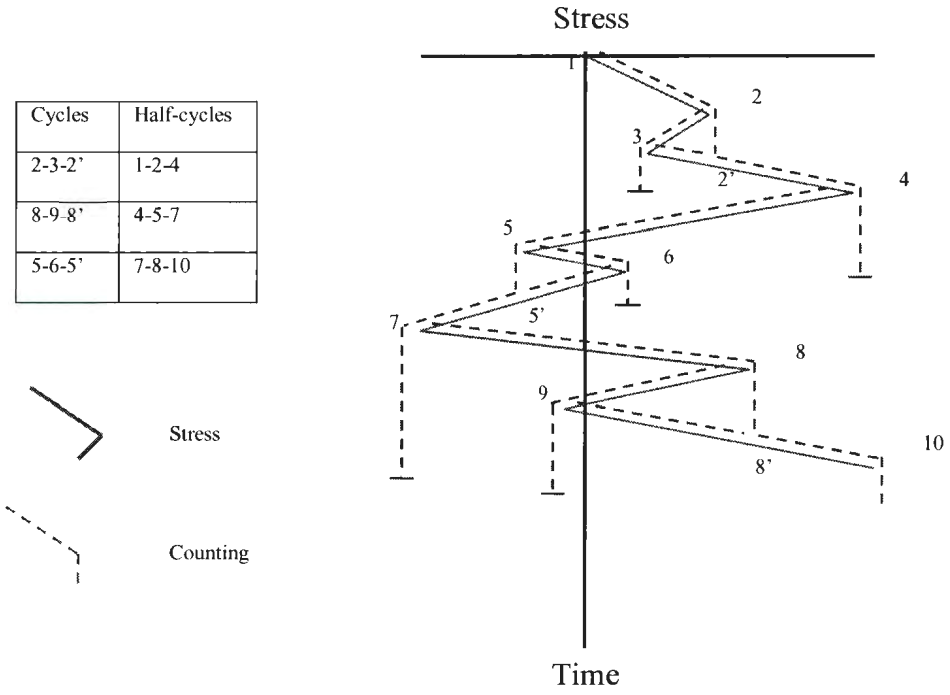

Cycles	Half-cycles
2-3-2'	1-2-4
8-9-8'	4-5-7
5-6-5'	7-8-10

Figure 7.5: Rainflow analysis of variable amplitude loading

From the Rainflow analysis, applied stress cycles n_i, may be constructed as in Table 7.1 given in Figure 7.6.

Random loading considered by extreme value operating pressure, P_o, considered

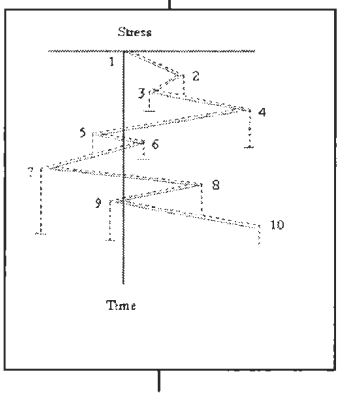

$$\frac{da}{dn} = C(\Delta K)^m$$

$$N_f = \frac{a_f^{1-m/2} - a_i^{1-m/2}}{C.\Delta\sigma^m.\pi^{m/2}.F^m.(1-m/2)} *$$

Table 7.1: Cycles Required for Failure Crack Growth

a_i	a_{i+1}	$(a_i+a_{i+1})/2$	F_{mean}	ΔN
0.5	2.5	1.75	1.15	$3.2*10^3$
2.5	5.5	4.0	1.37	0.291
5.5	9.5	7.5	1.98	0.0523
9.5	14	11.8	3.86	0.0010

Table 7.2: Applied Cycles

Block	$\frac{1}{2}\Delta\sigma_i$	n_i
1	>70	x
2	65-70	x
3	60-65	x
4	55-60	x
5	50-55	x
6	45-50	x
7	40-45	x
8	35-40	x
9	30-35	x
10	25-30	x
11	20-25	xx
12	15-20	xx
13	10-15	xx
14	5-10	xxx
15	0-5	xx

Table 7.3: Required Failure Cycles

Block	$\frac{1}{2}\Delta\sigma_i$	N_i
1	75	xx
2	67.5	xxx
3	62.5	xxx
4	57.5	xxx
5	52.5	xxx
6	47.5	xxx
7	42.5	xxx
8	37.5	xxx
9	32.5	xxx
10	27.5	xxxx
11	22.5	xxxx
12	17.5	xxxx
13	12.5	xxxxx
14	7.5	xxxxxx
15	2.5	xxxxxxx

n_i $\quad D_i = \frac{n_i}{N_i}$ $\quad N_i$

Table 7.4: Damage ratio

Block	n_i	$\Delta\sigma_i$	N_i	n_i/N_i
1	x	>70	xx	0.xx
2	x	65-70	xxx	0.xx
3	x	60-65	xxx	0.xx
4	x	55-60	xxx	0.xx
5	x	50-55	xxx	0.xx
6	x	45-50	xxx	0.xx
7	x	40-45	xxx	0.xx
8	x	35-40	xxx	0.xxxx
9	x	30-35	xxx	0.xxxx
10	x	25-30	xxxx	0.xxxx
11	xx	20-25	xxxx	0.xxxx
12	xx	15-20	xxxx	0.xxxx
13	xx	10-15	xxxxx	0.xxxx
14	xxx	5-10	xxxxxx	0.xxxxx
15	xx	0-5	xxxxxxx	0.xxxxx
n_0=501			D=0.xxxx	

$$D = \sum_{i=1}^{k} D_i \le 20/Yr$$

$$N = N + 1$$

Figure 7.6: Calculation process

• if the threshold stress intensity factor ΔK_{th} is considered as in equation (7.8) the solution may be considered as

$$\int_{a_i}^{a_f} \left\{ \frac{(1-R)}{F\sqrt{\pi a} - \frac{\Delta K_{th}}{\Delta\sigma}} \right\}^m da = C(\Delta\sigma)^m N$$

but the problem with this equation C and m value is defined by considering the simple Paris law equation and not considering ΔK_{th}. Another problem is integration of this formula which is not very straightforward for probabilistic calculation.

Step 2: Geometry factor

For the geometry in Figure 7.1 for $\frac{a}{t} \leq 0.70$ equation (7.11) is considered

F= 1.12-0.23.(a/t)+10.6. $(a/t)^2$-21.7. $(a/t)^3$+30.4. $(a/t)^4$ [7] (7.11)

Step 3a:

To calculate the damage ratio, $D = \sum_{i=1}^{s} \frac{n_i}{N_i}$ as in equation (7.3), n_i (= number of stress cycles in stress range i) is available from Table 7.1 which is obtained from rain flow counting. The N_i (= number of cycles to failure at constant stress range i) values in equation (7.3) need to be obtained. The N_i values may be obtained by solving the Paris law equation, equation (7.4) for crack defects. For constant or variable amplitude loading with stress range $\Delta\sigma$ and constant F equation (4) can be integrated to

$$N_f = \frac{a_f^{1-m/2} - a_i^{1-m/2}}{C.\Delta\sigma_i^{\ m}.\pi^{m/2}.F^m.(1-m/2)} \tag{7.12}$$

where a_i is the initial crack depth and a_f is crack depth at an unstable fracture or yield at remaining section

In Table 7.2 as in Figure 7.6, N_i is the number of cycles required for failure in the stress range blocks $\Delta\sigma_i$ considering equation (7.12).

Step 3b:

Equivalent constant amplitude loading approach (this approach will be considered to validate the result obtained in 3a).

Provided that threshold stress intensity factors are not included in the fatigue analysis, the following equation, equation (7.13), may be considered to convert variable amplitude loading to constant amplitude loading. Then equation (7.14) may be considered to calculate failure cycles

$$\Delta\sigma_{eq} = \left(\frac{\sum_{i=1}^{k} n_i.\Delta\sigma_i^m}{n_o} \right)^{1/m} \tag{7.13}$$

$$D = \sum_{i=1}^{k} \frac{n_i.\Delta\sigma_i^m}{\bar{a}} \tag{7.14}$$

where n_i and $\Delta\sigma_i$ represent the number of cycles and stress range respectively for a particular block i, and n_o represents the total number of cycles applied as depicted in Figure 7.7.

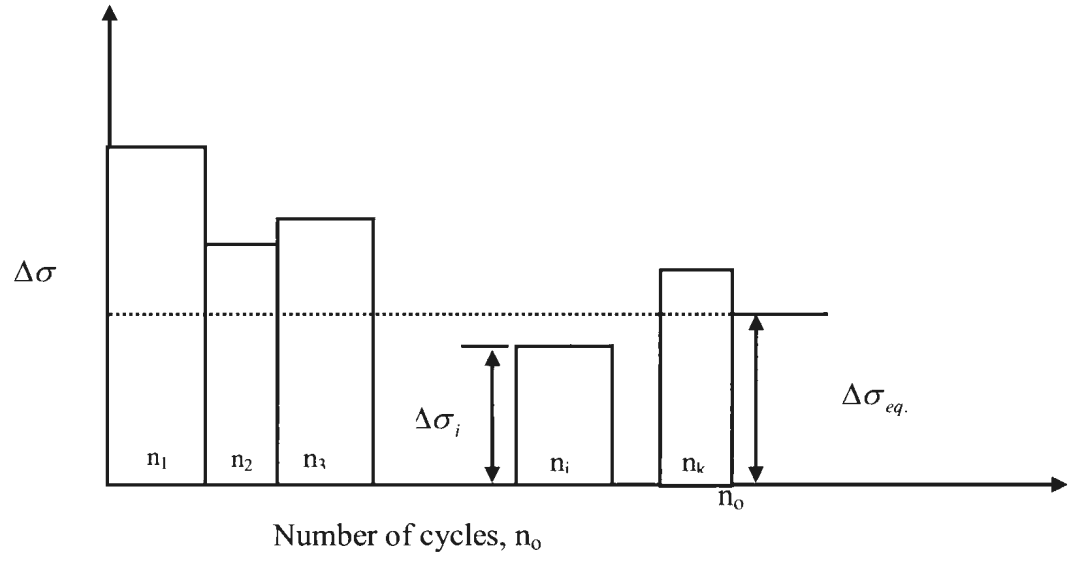

Figure 7.7: Long term stress range distribution divided into histogram

Step 4

Table 7.4 as in Figure 7.6, may be considered for sample damage calculation from direct variable amplitude loading instead of equivalent constant amplitude loading. The damage may be calculated considering Table 7.1, Table 7.3 and equation (7.3).

Step 5

Limit state

The limit state is considered as $D \leq 1$ for 20 years design life and it is a case of survival as suggested by DNV RP C203 [10] for DFF=1

$$D = \sum_{i=1}^{k} D_i \leq 20/Yr \tag{7.14}$$

where *Yr* is the number of years.

7.4 Example Problem

What is the number of stress cycles that the butt connection in Figure 7.1 can endure before it fractures? Consider the member is subjected to variable amplitude loading with a Gumble mean operating pressure and a standard deviation of 17.82 MPa, 15.82 MPa and 12.82 MPa and with CoV 0.053 as given in Table 7.5. Reasonable data may be assumed for loading frequency.

The bilinear model is considered as per the BS7910 [11] guideline. The material property or the Paris law constant may be considered for X65 steel from the guideline BS7910 [11] for a marine/non-marine environment which is given in Table 7.6.

Table 7.5: Operating Pressure Variables

Distribution	Mean, MPa	CoV
Gumble	17.82	0.053
Gumble	15.82	0.053
Gumble	12.82	0.053

Table 7.6: Paris Law constants for marine/non-marine steel

	i stage	m_i	C			
			Distribution	Mean value $b=\frac{mm}{\left(MPa\sqrt{mm}\right)^{m_i}}$		Transition point $c=\left(MPa\sqrt{m}\right)$ or $d=\left(MPa\sqrt{mm}\right)$
BS7910 [11] marine condition	1	3.42	Lognormal	5.37×10^{-14}[b]	1.11	Mean=1098[d] CoV=-0.16[d]
	2	1.11	Lognormal	5.67×10^{-7}[b]	0.158	
BS7910 [11] Non-marine condition	1	5.10	Lognormal	5.37×10^{-14}[b]	2.61	Mean=363[d] StD=-0.13[d]
	2	2.88	Lognormal	5.37×10^{-14}[b]	0.350	

Stress range is calculated considering Rainflow counting with the MATLAB tool developed by Nieslony A. [12] according to the ASTM guideline [13]. All the random values of the data points (1×10^6) of pressure fluctuation are converted to axial stress fluctuations and provided as the input value of the Rainflow counting tool. The Rainflow counting tool constructs cycles and returns the data of cycles amplitude, the cycles mean value and the number of cycles as 0.5 or 1 for each cycle. The cycles are then counted for 15 stress blocks. The stress block ranges are divided into 0-5, 5-10, 10-15, 15-20, 20-25, 25-30, 30-35, 35-40, 40-45, 45-50, 50-55, 55-60, 60-65, 65-70, and >70.

The damage ratio is calculated considering equation (7.3).

with a/t =0.7, F=6.0 maximum.

The maximum stress intensity factor for a/t=0.7

$K = \sigma\sqrt{\pi a}.F = 75 \times \sqrt{\pi \times 0.7 \times 0.02024} \times 6 = 95MPa\sqrt{m}$.

K_{IC} may be considered 180 $MPa\sqrt{m}$

As $K<K_{IC}$ for a/t=0.7, fatigue crack growth according to equation (7.4) may take place up to this depth. The crack depth at failure to a_f = 0.7W= 0.7*20=14 mm will therefore give a safe value for the fatigue life.

In Table 7.2, the crack growth from 0.5 mm to 14 mm has been divided into four intervals and ΔN calculated for each interval considering equation (7.11). For a typical run the result is presented in Table 7.4.

In the First Order Reliability Method (FORM), fatigue damage D follows normal distribution for which the reliability index may be calculated as

$$\beta = \frac{\mu_R - \mu_S}{\sqrt{\sigma_R^2 + \sigma_S^2}} \qquad (7.15)$$

where μ 's are mean and σ 's are standard deviation.

7.5 Resultss and Discussion

In fatigue design of the welded steel structure the use of S-N curves is well established [14]. The S-N curves predict fatigue failure under constant amplitude loading but, by virtue of S-N curve definition, cannot incorporate information related to crack detection and/or a measurement to revise fatigue life. The use of fracture mechanics techniques combined with the S-N curve framework can do the treatment successfully for

this type of problem. The study considered standard Paris law approximation to crack growth using a bi-linear crack growth model presented in BS 7910 [11]. It may be noted that use of the standard linear model can be overly conservative, especially for cases where the loading spectrum contains large numbers of low stress ranges.

The analysis considered BS 7910 [11] recommendation for X 65 steel Paris law constants (C and m) in marine/non-marine environments. The loading phenomena considered regular pressure loading (variable amplitude type) and start up shut down loading (constant amplitude type). The operating pressure loading is considered by extreme value distribution with a different mean (μ) magnitude of 12.82, 15.82, and 17.82 MPa and a standard deviation (σ) of 0.68, 0.84 and 0.94 MPa respectively. The extreme value distribution is considered from extreme values of every 30 seconds for each loading case. This makes the loading cycles consistent. Thus, in each year the number of extreme values of operating pressure is considered to be 1×10^6, which returns on the order of 3.45×10^5 cycles after Rainflow counting. This gives the concept of loading frequency considering extreme values of the operating pressure. A design fatigue factor (DFF=2.50) is also considered in the analysis.

It may be noted that the analysis considered the end cap effect, which is the longitudinal stress in the axial direction, as the primary load influencing fatigue crack propagation. The end cap effect occurs in an end or in blind flanges, 90^o bend, T branches (limited) etc in the pipeline. The pipeline stress state was evaluated with two limiting conditions that included hoop pressure, with a design factor of 0.8 and an incidental overpressure factor of 1.1, and an equivalent stress check with a design factor of 0.9. It

may be noted that the marine environment may be considered for the subsea pipeline with shallow depth where no compressive stress has developed. The subsea pipeline, when approaching the shore with a blind flange, and containing a weld defect, or a pipeline close to the sea with the same features, may be considered as the ideal candidate for this analysis.

The result is given in Table 7.7 and Table 7.8 for the non-marine and marine environment respectively considering design fatigue factors DFF=1 and DFF=2.5. As fatigue loading is highly uncertain DFF=1~10 is recommended by DNV-RP-C203 [10]. Hence, from the analytic result obtained in Table 7.7 and Table 7.8, pressure fluctuation is not a concern for DFF=1 but becomes a concern when DFF=2.5 or higher order are considered, particularly in a marine environment. It may be noted that DFF=1 refers to a certain condition, whereas DFF=2.5 refers to low uncertainty in the loading condition.

A comparison of results for the marine and non-marine environment as presented in Figure 7.8 indicates that the failure probability in the marine environment is much higher than for the non-marine environment, considering an identical loading condition. This depicts the effect of the marine environment on steel by a SN curve with reduced fatigue life and increased crack growth rate. Again the comparison may be made in Table 7.7 for a different operating pressure. The reduction in operating pressure reduces the stress amplitude in the stress blocks while keeping the total number of cycles after rain flow counting apparently the same. For example, if compared in a stress block of $\Delta\sigma$=35 MPa, the number of cycles for 17.825 MPa should be higher than that of 12.825 MPa. Again, if compared in a stress block of $\Delta\sigma$=10 MPa, the number of cycles for 17.825

MPa should be lesser than that of 12.825 MPa. In both cases gross cycles apparently remain the same which is approximately 3.45×10^5 cycles.

Table 7.7: Failure Probability in non-marine environment

DFF	Yr	No of extreme values 1×10^6, Gross cycles $n=3.45\times10^5$, μ=17.82 MPa σ= 0.94 MPa		No of extreme values 1×10^6, Gross cycles $n=3.45\times10^5$, μ=15.82 MPa σ= 0.84 MPa		No of extreme values 1×10^6, Gross cycles $n=3.45\times10^5$, μ=12.82 MPa σ= 0.68 MPa	
		Reliability index, β	Probability of failure (tentative)	Reliability index, β	Probability of failure (tentative)	Reliability index, β	Probability of failure (tentative)
1	25	36.63	0	58.69	0	157.03	0
	30	34.21	0	54.18	0	147.48	0
2.5	25	16.75	0	27.75	0	71.58	0
	30	10.81	0	18.52	0	51.69	0

Table 7.8: Failure Probability in marine environment

DFF	Yr	No of extreme values 1×10^6, Gross cycles $n=3.45\times10^5$, DFF=2.5, μ=17.82 MPa σ= 0.94 MPa		No of extreme values 1×10^6, Gross cycles $n=3.45\times10^5$, DFF=2.5, μ=15.82 MPa σ= 0.84 MPa		No of extreme values 1×10^6, Gross cycles $n=3.45\times10^5$, DFF=2.5, μ=12.82 MPa σ=0.68 MPa	
		Reliability index, β	Probability of failure	Reliability index, β	Probability of failure	Reliability index, β	Probability of failure
1	25	9.68	0 (tentative)	15.06	0 (tentative)	34.02	0 (tentative)
	30	8.63	0 (tentative)	13.68	0 (tentative)	31.16	0 (tentative)
2.5	20	5.27	6.7E-08	9.78	6.5E-23	25.48	0 (tentative)
	25	1.66	4.8E-02	5.05	2.2E-07	16.41	0 (tentative)
	30	-0.70	7.6E-01	2.13	1.6E-02	10.79	0 (tentative)

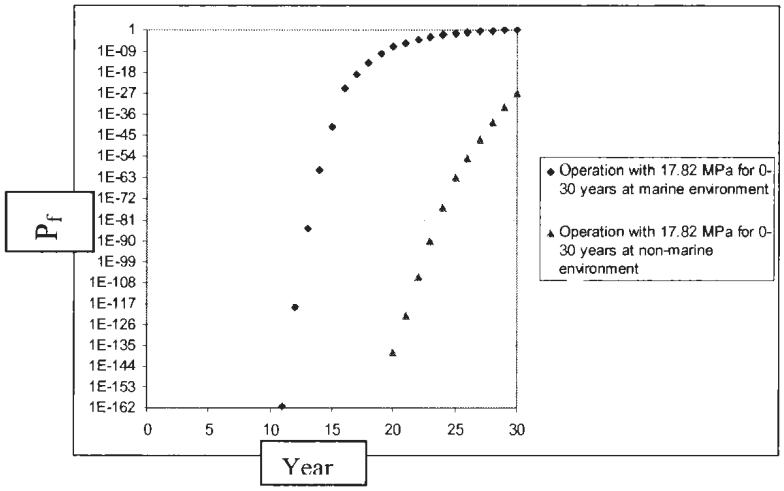

Figure 7.8: Comparison of marine and non-marine environment failure probability for DFF=2.5

The management can therefore take a new strategy of mixed mode operation or 'hybrid operation'. In hybrid operation, initially the pipeline will be operated at high operating pressure, then a reduced operating pressure will be considered for operation.

Careful observation of Figure 7.9 indicates the operators can take an advantage of low operating pressure to keep continue the operation after initial operation of (1-15) yrs. By using the Hybrid operation, with a mean of 17.82 MPa for the first 15 years and then adopting a low operating pressure (15.82 MPa) from 16 years, the operators can keep the risk minimal for up to 24th years, which is 1.1E-4. This adds 2 years of safe life. Again if, 12.82 MPa is selected from the 16th year the operator is safe up to the 26th year which adds 4 years safe life. It may be noted that other issues may be considered as a threat at the same time such as an internal or external corrosion defect, or SCC, which are ignored

in this analysis. The interested reader may go through the author's other papers [16, 17] on probabilistic analysis of the internal and external corrosion defect.

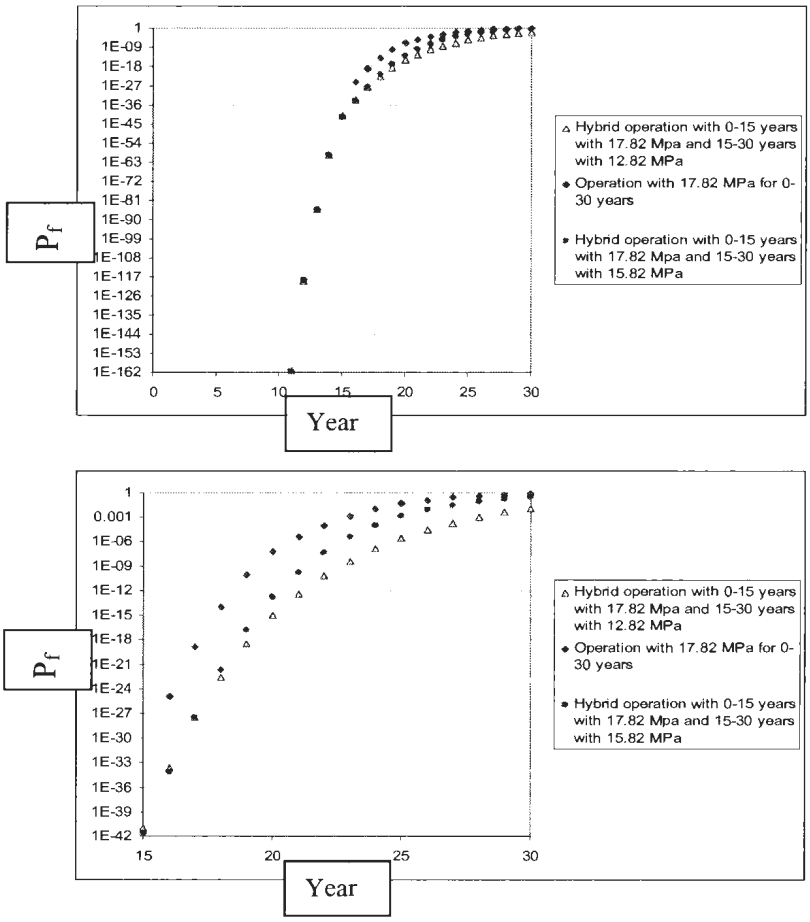

Figure 7.9: Fatigue failure probability of X 65 steel (logarithmic scale)

It may be noted that the damage ratio calculated by the equivalent stress method as specified in step 3b of section 7.3 calculates the identical damage ratio as is calculated by step 3a. Again, in this process of the equivalent stress method, the inverse negative slope of the SN curve m', is calculated for marine and non-marine steel for crack defects. The value of the inverse negative slope of the SN curve, identified as $m' = 2.94$ and $m' =$

5.13 respectively for the marine and non-marine environment is given in the following Figure 7.10. The values become obvious when checked for X as a function of Y as in equation (7.1)

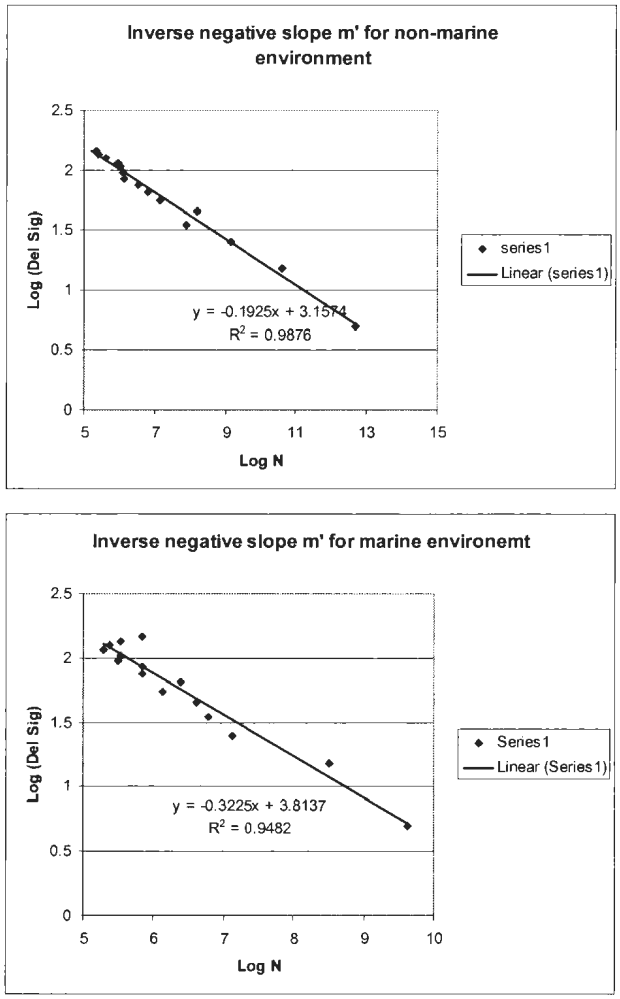

Figure 7.10: Inverse negative slope, *m'*, for marine and non-marine environment

7.6 Conclusion

The analysis considered mainly (other than limited start up and shut down) the effect of variable amplitude loading (pressure fluctuation) on small weld. A model was developed for fatigue damage assessment for defected items for variable amplitude loading. Miner's rule and Paris law are simultaneously considered for failure assessment and the Rainflow counting method is considered for stress block and cycles counting. Thus, the damage is evaluated. The analysis confirm the general believe that non-marine environment is not a significant source of failure where marine environment could be a threat if pressure derating is not adopted for aged pipeline.

7.7 Acknowledgements

The authors gratefully acknowledge the financial support provided by Petroleum Research Atlantic Canada (PRAC) and the Natural Science and Engineering Research Council (NSERC) of Canada.

7.8 References

1. Beltrao M. A. N., Castrodeza E. M., & Bastian F. L. (2010). Fatigue crack propagation in API 5L-X70 pipeline steel longitudinal welded joints under constant and variable amplitude. *Fatigue Frac. Eng. Mater Struc.* 34, 321-328, Blackwell Publishing Ltd.

2. Gresnigt, A. M., Karamanos S. A., Giakoumatos E., Dijkstra O. D., & Kreber J. (2004). Fatigue failure of buckled pipelines. *ASCE conf. proc.*, doi.10.1061/40745(146)20

3. Pinheiro B. de C., & Pasqualino I. P. (2009). Fatigue analysis of damaged steel pipelines under cyclic internal pressure. *International Journal of Fatigue*, 31 (2009) 962–973

4. Han z., Xue S., & Huang X. (2011). Wave-induced Fatigue Reliability Study of Submarine Pipeline Span by First Passage Failure Approach. *ICPTT*, ASCE.

5. Jinheng L, Xinwei Z, Qingren X, & Chunyong H. (2004). Defective pipeline fatigue-life prediction using failure assessment diagram technique. *IPC* 2004-487.

6. Gamboa E., Linton V., & Law M. (2008). Fatigue of stress corrosion cracks in X65 pipeline steels. *International Journal of Fatigue* 30 (2008) 850–860

7. Corcoran L. (2005). *Report on Corrib Gas Pipeline Design*. Part 2: Pressure Cycling

8. Wei R. P. (2010). *Fracture Mechanics*. Cambridge University Press.

9. Almar-Naess A. (1985). *Fatigue Handbook*. Tapir Publisher

10. DNV RP C203 (2010). *Fatigue design of offshore steel structure*. DNV

11. BS7910-2005 (2005). *Guide to methods in assessing the acceptability of flaws in metallic structure*. BSI

12. NIESŁONY A. (2009). Determination of fragments of multiaxial service loading strongly influencing the fatigue of machine components. *Mechanical Systems and Signal Processing*, Vol. 23(8), 2009, pp. 2712-2721

13. ASTM E 1049-85 Reapproved (1997). Standard practices for cycle counting in fatigue analysis. *In: Annual Book of ASTM Standards*, Vol. 03.01, Philadelphia 1999, pp. 710-718

14. BS 5400: Part 10, (1980). *Steel, concrete and composite bridges*. Code of practice for fatigue. London

15. Forman R. G., Kearney V. E., & Engle R. M. (1976). Numerical Analysis of Crack Propagation in Cyclic Loaded Structure. *Journal of Basic Engineering*, 89, 459-464.

16. Hasan, M., Khan, F., Kenny, S. (2011). Identification of the Cause of Variability of Probability of Failure for Burst Models Recommended by Codes/Standards. *Journal of Pressure Vessel and Technology*, vol. 133, n. 041101, August, 2011

17. Hasan, M., Khan, F., Kenny, S. (2011). Probability Assessment of Burst Limit State Due to Internal Corrosion. *International Journal of Pressure Vessels and Piping*, vol 88 pp.48-58

18. Haldar A., & Mahadevan S. (2000). *Probability, Reliability and Statistical Methods in Engineering Design*. John Wiley & Sons, Inc.

Chapter 8

Integration of Failure Probabilities

8.1 General

The transportation pipelines are exposed to extreme operating and environmental conditions. The integrity of aged pipeline can be assessed by fitness for purpose or fitness for service. This is complex, time consuming and expensive procedure. In the alternative way the accidental failure can be minimized or avoided by considering the risk sources in the early stage of design. The risk-based design will consider potential risk sources, quantify them criticality, and finally, incorporate the potential risks in the designing of the process component i.e. pipeline.

It may be noted that codes and standards were developed by classification societies which are currently being used in industry to ensure structural integrity of pipeline. However, this is not a comprehensive approach giving a complete picture of the risks of the process system. In general, the codes/standards suggest rather deterministic approach to ensure critical design parameters are met. Consideration of uncertainty of the risk sources in the design is important to ensure the long-term integrity of the process components.

The present work developed a unique methodology for risk-based design of a process component as described in Figure 3.1. The methodology considered risk to estimate the design parameters at the component level as well as the system level to ensure that the overall risk remains within the limit. Considering the probability and consequence of failure, the risk-based design (not reliability-based) thus, sees the complete picture and determines the design parameters. The scope of the work is comprised of assessing and incorporating different time dependent failure scenarios into the design consideration. The failure scenarios considered are: internal corrosion, external corrosion, stress corrosion cracking, fatigue failure due to start up/shut down and regular pressure fluctuation. It may be noted that time independent failure mechanisms such as third party damage, earth movement and material defects are not considered in the present risk-based design approach.

The failure probability obtained for internal and external corrosion and other degradation mechanisms will be added to the risk-based design framework for overall risk estimation. Subsequently all individual component risks will be integrated using fault tree analysis to obtain overall risk of the system.

The unified risk to individual components will be thus minimized by achieving the target safety level of the system.

8.2 Results Obtained From Degradation Mechanism

The present work focused on four major areas of time dependent degradation:

a) internal corrosion

b) external corrosion

c) stress corrosion cracking (SCC) and

d) Corrosion fatigue (CF) of weld crack defect

Pipe wall thinning due to internal corrosion and loss of pressure containment due to burst (i.e. leak or rupture) is considered a significant operational hazard for pipelines. The failure probability of a pipeline, with longitudinally oriented internal corrosion defects, due to burst from internal operating pressure, is estimated.

Chapter 4 describes internal corrosion defect analysis, and is published in the Journal of Pressure Vessels and Piping [3]. The burst models used by design codes and standards [4-8] are considered for internal corrosion defect analysis. In the analysis, the burst pressure and operating pressure are considered in the limit state of the defected pipe. The defect is characterized in terms of defect depth and defect length. The defect depth is calculated considering the SwRI equation [1]. The defect length is considered as per the suggestion of Zimmerman et al [2]. The corrosion feature geometry is integrated within burst pressure models, which have been adopted by industry standards, codes and recommended practices. The first order second moment method and Monte Carlo simulation are considered for probability analysis. The two alternative methods virtually verify the predicted result.

The results obtained by FOSM and Monte Carlo methods have been compared, and it is found they closely match one another. A relative ranking of conservatism in the

models has also been discussed. Based on the probabilistic assessment, recommendations are provided to assist designers in appropriate model selection.

As external corrosion is one of the dominant failure scenarios observed in offshore oil and gas pipeline, the study in Chapter 5, which has been published [9], investigates the probability of failure for the external corrosion defect. Different burst models were considered for assessment of failure probability. The study identified the cause of variability in probability of failure for the burst models. The variability is studied through sensitivity analysis of the parameters in the burst models. The study observed that different defect shape specifications (rectangular, parabolic) and different stress concentration factor derivations (different contributions of l) for burst pressure estimation are responsible for high variability in the probability of failure. It is important to reduce variability to ensure a unified risk-based design approach considering any codes/standards.

Chapter 6 attempts to analyze transgranular stress corrosion cracking (TGSCC) probabilistically. The study characterized TGSCC flaws in terms of length and depth and evaluated the failure probability. The crack is evaluated by failure assessment diagram (FAD) based approaches: API 579 [10]/BS 7910 [11] or R6 approach [12]. The crack is also evaluated by the CSA Z662-07 [13] stress based approach. The authors also developed a strain based approach and the crack is evaluated with this approach. The considered models calculated the failure probability, which closely match. It may be noted that the R6 [9] approach calculates the least failure probability, which indicates that it is less conservative.

This is because the model assumes linear elastic fracture mechanics (LEFM) or plastic yielding in the resistance part of the limit state equation.

Chapter 7 examines the susceptibility of failure due to fatigue loading for a small weld crack. The fatigue damage due to regular pressure fluctuation and startup shutdown loading were considered to evaluate damage by crack propagation. The Miner's rule and Paris law are considered for failure evaluation. Constant and variable amplitude loading are considered in the analysis with the bi-linear model in the Paris law equation. The developed model is tested for the marine and non-marine environment following the recommendation of BS7910 [11]. The loading is considered as an extreme value of the operating pressure. Therefore, Rainflow counting is employed to count the number of cycles acting in the system. The analysis shows that with the given operating pressure the marine pipeline will cross the safety limit (probability of failure <10^-5) at 21 years with an initial weld defect of 0.5 mm. The analysis confirmed that the safe life of pipeline could be extended with lower operating pressure and hence it is recommended to adopt a lower operating pressure after 15 years of operation with a regular operating pressure.

The individual failure probabilities have been assessed so far as discussed in *Chapter 4* to *Chapter 7*. The individual failure probabilities now require to be integrated as the algorithm discussed in *section 3.4*. To make it simple, the failure events are assumed independent which indicates there exists no correlation between the failure events.

8.3 Integration of Probabilities

For 25 years of operation, the failure probabilities of different degradation mechanisms in pipelines are given in Table 8.1. The combined failure is calculated using the fault tree and is given in Figure 8.1. The top event probability is calculated as 3.97×10^{-3}. The consequence of failure cannot be assessed with any unique method that determines identical value of consequences. Based on the assessment methodology and type of failure, the consequence varies significantly [14-16]. However, the consequence associated with this failure is assumed to be, $500 million considering both direct and indirect costs. The risk of pipeline failure at 25th years is $ 2,000,000.

Table 8.1: Calculated failure probabilities of different degradation mechanisms of X65 pipeline steel.

Degradation Mechanisms	Probability of failures
Internal corrosion	2.6×10^{-4}
External corrosion	3.6×10^{-3}
Stress corrosion cracking	2.98×10^{-7}
Fatigue damage of cracked pipeline (Hybrid operation in marine environment)	1.1×10^{-4}

The risk increases with the increase of consequences. Provided that the maximum allowable risk is $ 1,000,000, the risk of $2,000,000 is unacceptable which means design variables need to change to tighten the risk. It may be noted that the risk of $2,000,000 is calculated with the probability of failure of 3.97×10^{-3}. If the probability of failure is revised to 3.97×10^{-5} by revising the design parameters and assumed the same consequence, the risk would come down to $20,000 which indicates a very low risk.

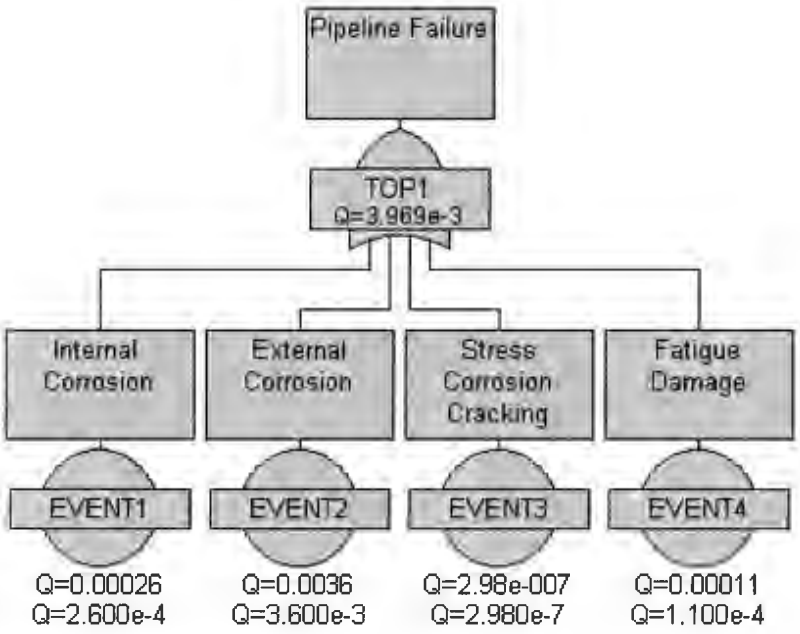

Figure 8.1: Top event of pipeline failure

8.4 Conclusion

The pipeline design with current specification is not safe provided the design is made for 25 years with maximum allowable risk is $ 1,000,000. Revised specification is required to curve down the risk.

8.5 References

[1] Kale A., Thacker B. H., Sridhar N., & Waldhart J. C. (2004). A probabilistic model for internal corrosion of gas pipeline. *International Pipeline Conference*, Alberta, Canada. IPC 04-0483.

[2] Zimmerman TJE, Hopkins P., & Sanderson N. (1998). Can limit states design be used to design a pipeline above 80% SMYS. *In: Proceedings of the 17th international conference on offshore mechanics and Arctic engineering* (OMAE 1998), ASME

[3] Hasan, M., Khan, F., Kenny, S. (2011). Probability Assessment of Burst Limit State Due to Internal Corrosion. *International Journal of Pressure Vessels and Piping*, Piping 89 (2012) 48-58

[4] CSA Z662-07, 2007. Limit state equation for burst of large leaks and rupture for corrosion defect. Oil and Gas Pipeline Systems, Canadian Standards Association. pp 554-555.

[5] Recommended Practice DNV RP-F101 , Corroded Pipelines. 2004

[6] ASME B31G Manual for determining the remaining strength of corroded pipelines, 1995. A supplement to ANSI/ASME B31 code for pressure piping.

[7] Netto T. A., Ferraz U. S., Estefan S. F., 2005. The effect of corrosion defect on the burst pressure of the pipeline. Journal of Constructional Steel Research. Vol 61 pp 1185-1204

[8] Bea R., Xu T., 1999. Corrosion Effects on Burst Pressures RAM PIPE REQUAL, Pipeline Requalification Guidelines Project Report 1. pp 103-104. University of California at Berkeley.

[9] Hasan, M., Khan, F., Kenny, S., (2011). *Identification of the Cause of Variability of Probability of Failure for Burst Models Recommended by Codes/Standards*, Journal of Pressure Vessel and Technology, vol. 133, n. 041101, August, 2011

[10] API 579-1/ASME FFS-1, Fitness-For-Service, 2007. American Petroleum Institute and the American Society of Mechanical Engineers.

[11] BS 7910:2005, 2005. *Guide to methods for assessing the acceptability of flaws in metallic structures*. British Standards Institute, London, England.

[12] R6, 2005. *Assessment of the integrity of the structure containing defects.* Revision 4, Amendment 4, British Energy, Gloucester.

[13] Recommended Practice CSA Z662-07

[14] Hopkins, P., Palmer A., 1994. Pipeline internal inspection - what a pipeline operator needs to know, Penspen, United Kingdom

[15] Simonoff J. S. , Restrepo Carlos E., Zimmerman R., 2010. Risk management of cost consequences in natural gas transmission and distribution infrastructures, Journal of Loss Prevention in the Process Industries 23 (2010) 269-279

[16] Restrepo Carlos E., Simonoff J. S. , Zimmerman R., 2010. Causes, cost consequences, and risk implications of accidents in US hazardous liquid pipeline infrastructure, International Journal of Critical Infrastructure Protection 2 (2009) 38-50

Chapter 9

Contribution and Future Research

9.1 Contributions of the Present Work

The author has made the following original contributions in the present work:

- A risk-based design framework is developed for pipeline design. In the risk-based design the pipeline design parameters are justified based on risk instead of reliability. This is a shift towards a more realistic view of the failure scenario in the processing facility. A risk-based evaluation in the present study is in line with CSA Z 662-11 [1] and ISO 13623 [2] for individual risk assessment of particular degradation mechanisms. In the present study major time dependent degradation mechanisms are considered and integrated using Fault Tree Analysis (FTA). In the risk-based design of the present study the design parameters are directly linked with the end risk. Therefore the design parameters are subjected to adjustment to meet the target risk.
- The key time dependent degradation mechanism of a pipeline is identified. In the non-marine environment internal corrosion and external corrosion are the most crucial degradation mechanisms compared, to stress corrosion cracking and

corrosion fatigue. In the marine environment corrosion fatigue is also a major concern.

- The burst pressure models of recommended codes/standards or individual models are compared. A relative conservatism scale of codes and standards. DNV RP-F101 [8] burst model is a good selection for integrity assessment of higher toughness steel pipeline, whereas other codes (CSA Z662 07 [7] and the ASME B31G [9]) may be considered for integrity assessment of older steel pipeline.

- Dimensionless parameter, hoop to yield/ultimate stress ratio, $Y = \frac{\sigma_h}{\sigma_y \ or \ \sigma_u}$, has the most significant effect on the failure function g(), followed by defect depth to thickness ratio, $W = \frac{d}{t}$, and defect length to pipeline diameter ratio, $Z = \frac{l}{D}$, in the burst models. The sensitivity for Y is rather consistent for all codes/standards, and does not vary significantly from one code to another. This indicates that it is a non-significant issue whether yield or ultimate strength is considered in the burst models. It seems that the dimensionless parameters W and Z are most responsible for the significant variation in failure probability (P_f) as indicated in Figure 5.6. Further investigation identified that the different importance of 'Bulging' or 'Folias' factor is responsible for variation in estimated remaining strength.

- The present study characterized TGSCC flaws in terms of length and depth and evaluated the failure probability. The failure probability is calculated by

considering the failure assessment diagram (FAD) and stress based burst models. The stress based burst model, such as CSA Z 662-11 [1], is not particularly suitable for crack assessment, since originally the model was developed for defect assessment, not for cracks.

- The work proposed a strain based model for defect assessment which predicts better than a stress based model. However, this still remains little conservative compared to the FAD based approach.
- The study observed that weld defect crack in marine environment poses higher risk compared to the non-marine environment. The study also observed that pressure de-rating (mixed-mode operation) of a pipeline extends the design life by at least 2 years, keeping the risk still minimal (below 1.0E-5) while operating for the first 15 years at 17.82 MPa and successively at an 11% reduction in pressure. The safe life could be increased by up to 4 years if an 18% reduction in operating pressure is considered from the 16^{th} years, while the design life is 30 years.

The current industry practice is to keep a corrosion allowance in the design without a detailed estimation of expected corrosion growth in the form of either defects or cracks. The guidance 'fitness for purpose' or 'fitness for service' is considered for the assessment of the integrity of the pipeline when the pipeline ages. The assessment itself is a complex, time consuming and expensive effort which sometimes requires excavation. The repair may require a complete shut-down of the transportation system.

The present study considered the time dependent expected defect or crack within the design life and assessed the reliability of the pipeline and risk of its failure. The design parameters were ascertained based on allowable maximum risk within the design life. In contrast to reliability-based design, the risk-based design surfaces (floats up) with a complete picture of damage by simultaneous consideration of consequence and failure probability.

9.2 Recommendations for Future Research

Based on this work the following recommendations for future research are suggested.

- The quantitative assessment of consequence of failure for a pipeline may be assessed for oil and gas pipelines separately considering different class location, transported fluid and pipeline design variables. The consequence may be multiplied to determine the realistic risk of the pipeline failure.
- A dedicated risk matrix may be constructed for pipeline failure.
- In the present study the corrosion growth rate is assumed constant for the design life. In reality the growth rate might be variable. Therefore, by considering a variable growth rate, the probability may be reassessed.
- Other forms of time dependent failure mechanism may be considered such as time dependent denting or hydrogen induced cracking (HIC) for failure probability assessment.

- The other forms of loading conditions and limit states may be considered for probability assessment. For example, limit states other than the ultimate limit state (ULS) as considered in this study, the leakage limit state (LLS) or the serviceability limit state (SLS) may be considered in conjunction with different loading conditions. The different loading conditions other than the internal pressure, as considered in this study, may be chosen from Table O.1 Annex O of CSA Z662 11 [1]
- Design economics may be considered as an important area of research. The other grades of pipeline steels may be considered and their time dependent degradation mechanisms may be identified. For example, in addition to X 65 steel other available steels X40, X52, X70, X80, X100 may be considered and their failure probability may be calculated. The design decision will be based on the economics of risk. The steel which renders minimal risk will be finally selected for design.
- Component failure may be calculated from complex defects instead of simple defects. Complex defects may be defined by the connection of defects.
- The advancement, qualification, calibration and validation of the mechanistic models and mechanisms used in the study may be considered to provide better confidence and reduce uncertainty, particularly considering high strength high toughness steel.

9.3 References

[1] CSA Z662-07 (2001). *Limit state equation for burst of large leaks and rupture for corrosion defect.* Oil and Gas Pipeline Systems, Canadian Standards Association.

[2] ISO 13623, (2009). *Petroleum and natural gas Industries- Pipeline Transportation Systems*. International Standard, Geneva, Switzerland.

[3] DNV RP-F101 (2004). *Corroded Pipelines, Recommended Practice.* Det Norske Veritas

Electronic Appendix

Please find the attached CD.